FOREWORD

The research work described in this report was performed by Bolt Beranek and Newman Inc., Cambridge, Massachusetts for the Aerospace Dynamics Branch, Vehicle Dynamics Division, AF Flight Dynamics Laboratory, Wright-Patterson Air Force Base, Ohio under Air Force Contract No. AF 33(657)-10125. This research is part of a continuing effort to refine methods of structural vibration prediction and control. The investigation is part of the Research and Technology Division, Air Force Systems Command exploratory development program. This work was performed under Project 1370 "Dynamic Problems in Flight Vehicles", Task 137005 "Prediction and Control of Structural Vibration".

The work under the above contract was monitored by the Air Force Flight Dynamics Laboratory, Research and Technology Division, with Mr. Ralph N. Bingman acting as project engineer. The reported work was performed during the period of December 1962 to April 1964 under the technical direction of Dr. Eric E. Ungar.

The author gratefully acknowledges the assistance rendered by Messrs. J. R. Carbonell, C. W. Dietrich, C. M. Gogos, and D. C. Miller, and other members of the staff of Bolt Beranek and Newman Inc., as well as the valuable comments provided by Mr. R. N. Bingman of RTD.

Contractor's report number is 1137.

ABSTRACT

A largely experimental study is described, which indicates that dissipation of vibratory energy at multi-point-fastened (bolted, riveted, spot-welded) joints connecting panels to stiffeners or to other panels, at frequencies considerably above the panel fundamental, is primarily due to the "pumping" of air produced as adjacent surfaces between fasteners move away from and toward each other.

Heckl's absorption coefficient concept (J. Acoust. Soc. Am. 34, 803-808, June 1962) is shown to apply to the aforementioned joint types, and it is demonstrated that the joint absorption coefficient is a function of the ratio of fastener spacing to plate flexural wavelength. Based on these findings and on empirical data, an approach is developed for estimating the damping of panels with joints.

A study of the energy dissipation characteristics of plate-strips whose ends are bolted to rigid supporting structures is discussed. From comparison of data obtained by direct measurement of energy dissipation with analysis for a number of possible mechanisms it is concluded that interface slip plays a minor role in such bolted joints. Damping here appears to be primarily associated with relative motions normal to the mating surfaces.

This technical documentary report has been reviewed and is approved.

Howard A. Magrath

HOWARD A. MAGRATH
Chief, Vehicle Dynamics Division

TABLE OF CONTENTS

TABLE OF CONTENTS (continued)

TABLE OF CONTENTS (continued)

TABLE OF CONTENTS (continued)

ILLUSTRATIONS

ILLUSTRATIONS

ILLUSTRATIONS

INTRODUCTION

The capability of a structure to dissipate vibratory energy plays an important role in establishing the levels of the structure's responses to broad-band acoustic or mechanical excitation, such as that from rocket noise. The designer of aerospace structures must be able to estimate this energy dissipation capability or "damping" in order to predict the responses of his structures. In addition, he desires to understand the most important mechanisms responsible for damping in order to be able to design configurations incorporating favorable damping characteristics with the minimum weight or economic penalty.

Much useful information is available concerning the damping properties of materials and homogeneous structures (Refs. 1, 2)*, concerning the design of highly damped structures incorporating viscoelastic materials (Refs. 3, 4), and concerning energy dissipation associated with slip at some simple structural interfaces (Refs. 5, 6). On the other hand, the damping of built-up structures (such as aircraft fuselages, which consist of a multitude of panels and reinforcing members joined together by various fastening means) has not been studied extensively, particularly for frequencies above the fundamental resonances of the substructural panels.

Built-up structures have been found to exhibit considerably higher damping than similar one-piece structures. Since the former differ from the latter only in that they incorporate joints, it appears that the higher damping of built-up structures may be ascribed to the action of these joints, and that an improved understanding of this damping action is desirable. The presently reported study accordingly concerns itself with obtaining an increased understanding of the dominant mechanisms responsible for the damping of structural joints, with developing means for predicting the magnitudes of such damping, and with delineating approaches for obtaining joint designs with improved damping characteristics.

REVIEW OF PRIOR WORK

Joints of interest for aerospace structures may perhaps be most usefully classed according to the methods of joining and according to the types of structures being joined. The joining methods and structural configurations of greatest importance are tabulated below.

---

*Reference list appears at end of Appendix I.

This manuscript released by the author July 1964 for publication as a RTD Technical Documentary Report.

Joining Methods

1. Rivets
2. Bolts or screws
3. Spot welds
4. Continuous welds
5. Adhesives

Structures

1. Rigid structures joined to rigid structures*
2. Plates joined to rigid structures
3. Beams joined to rigid structures
4. Plates joined to plates
5. Beams joined to plates (e.g., ribbed panels)
6. Beams joined to beams (also, built-up beams)

The damping of joints in beams has received considerable prior attention. From the work of Pian (Refs. 6, 7) one may calculate the damping of riveted or bolted built-up or joined beams with sufficient accuracy for most practical purposes. Goodman's studies (Refs. 5, 8, 9) provide one with similar capabilities concerning the damping of beams made up of pressed-together leaves. These analyses assume Coulomb friction to be the dominant damping mechanism, pertain to flexural motion of the beams for frequencies up to the fundamental resonance, and agree reasonably with experimental measurements. Understanding of the damping of gross flexural motions of riveted beams, such as may be used as primary load-carrying members, thus appears to be reasonably well in hand.

The damping of built-up or jointed beams with adhesive joints may be calculated relatively directly from Refs. 4 and 10; joints in which an adhesive is used in conjunction with rivets are discussed in Ref. 11. Again, the damping of such joints seems to be fairly adequately understood.

A number of studies by Mentel and his associates (Refs. 12-15) have dealt with the damping of beams and plates whose ends or edges are joined to rigid structures. Mentel has studied both Coulomb (dry) and viscoelastically damped (bonded) joints, primarily under the condition where the beam and plate

---

*By rigid structures are meant structures whose deformations are everywhere negligibly small compared to the motions of their centers of gravity and to the relative motions at the joints.

edges only translate within slots in the supporting structures, and has obtained reasonable agreement between theory and experiment. He has also obtained some indications that rotation of beam or plate edges in bonded joints may be able to dissipate energy more effectively than translation, but seems not to have carried this work to completion.

Welded joints appear generally to have escaped study, except that some configurations have been devised (Ref. 16) that seemingly promote energy dissipation by friction in regions near the welds.

The damping action of beam-plate systems, such as beam-reinforced plates approximating aircraft fuselage construction, has only been touched upon (Refs. 17, 18) prior to the present study. The mechanisms at work there have not been identified, but some evidence has been obtained that indicates the dominance of mechanisms other than classical Coulomb friction.

A more detailed review of the prior literature dealing with damping of structural joints appears in Appendix I.

PRESENT STUDY

The prior state of the art, as summarized in the previous paragraphs and in Appendix I, and the estimated greater relative importances of some of the various structural configuration types listed previously permits one to select some areas in which further investigation may be most useful. The present study accordingly concerns itself with the damping of joints between plates and stiffeners (such as reinforcing beams or bulkheads) and between plates and other plates (i.e. plate seams) at frequencies considerably above the plate fundamental; and of joints between plates and relatively rigid supporting structures at and near the plate fundamental frequency.

The fastening methods considered here include "point-connections", such as rivets, bolts or screws, spot welds, and distributed connections, such as continuous welds, with emphasis on the former type.

Because of the desire for practical utility of the results, the present study emphasizes joint configurations that are structurally acceptable (that do not aggravate the usual joint strength problems, nor create new ones) and small amplitude motions (since these are usually associated with less damping than larger amplitudes, and since one usually attempts to avoid large response amplitudes by proper design).

PART I

PLATE-STIFFENER AND PLATE-PLATE JOINTS AT FREQUENCIES ABOVE PLATE FUNDAMENTAL

RELATIVE MOTIONS AT PLATE-STIFFENER JOINTS

An understanding of the relative motions occurring at joint interfaces is essential to the study and delineation of the dominant damping mechanisms that occur in joints. Accordingly, some brief experiments were undertaken in order to obtain an indication of these relative motions.

Stroboscopic Observation

An initial stroboscopic study was made of the relative motions occurring at the interface between a plate and a beam bolted to it. This study was carried out using a 3 ft long 1 in x 1 in x 1/8-in aluminum angle beam, attached along one edge of a 4 ft x 4 ft aluminum plate of 1/32-in thickness by means of screws spaced 3 in apart. The plate was suspended from long strings attached at two of its corners, so that the edge with the attached beam was vertical. A small shaker, attached at the lower corner opposite the edge at which the beam was mounted, was used to drive the plate sinusoidally. Observations were made with the aid of a hand-held stroboscopic light source, adjusted to frequencies near the driving frequencies.

A considerable amount of motion of the plate portions between the bolts could be observed relative to the beam, over a fairly wide range of frequencies. This motion appeared to consist essentially of flexing of the plate portions between rivets away from the beam and of a subsequent slapping of these portions against the beam. The deflected portions of the plate generally were simply curved, but also assumed more complicated multiply curved shapes at higher frequencies.

The previously described observations were limited to low frequencies, and thus to long plate flexural wavelengths, since limited shaker capacity permits one to generate the large amplitudes required for the motions to be visible only at low frequencies. In order to extend the stroboscopic study to shorter plate wavelengths a beam-plate system was constructed similar to the previously described one, but made of a rubber (Nichols NE 7585) in which the longitudinal wave velocity is roughly 3% of that in aluminum. With this arrangement one could observe the relative

motions for plate flexural wavelengths smaller than the bolt spacing. The system behavior here was found to parallel closely that previously noted for the aluminum beam-plate system, except that more complicated curvatures of the plate portions between rivets were observed for the shorter plate wavelengths.

In the aluminum as well as the rubber structures the observed relative motions were perpendicular to the joint interface (or plate surface). No tangential or interface shearing motions were observed.

Accelerometer Survey

In order to supplement the previously described information, particularly in relation to effects of higher frequencies (where stroboscopic observation is not feasible) and of variations in amplitude, the previously described aluminum beam-plate arrangement was provided with small piezoelectric accelerometers. One accelerometer was cemented to the beam at a point midway between two adjacent bolts, one to the plate midway between two other bolts, and one approximately in the center of the plate. All accelerometers were mounted with their sensitive axes perpendicular to the plate surface.

When the plate was driven sinusoidally and the waveforms of the accelerometer signals were displayed on oscilloscopes, it was found that all accelerometer signals appeared like pure sinusoids for low enough excitation amplitudes, at all test frequencies. However, at each frequency there appeared to exist a threshold amplitude above which the accelerometers mounted on the beam and on the plate directly behind the beam produced grossly non-sinusoidal signals. The accelerometer mounted at the center of the plate produced essentially undistorted sinusoids when the amplitudes did not exceed the aforementioned threshold by much, but also registered distortions at higher amplitudes.

For driving amplitudes slightly above the threshold all accelerometer signals appeared like sinusoids with distorted (multiply indented) tops, but undistorted bottom portions. Thus, distortion occurred only at one extreme of the oscillatory displacement, as one would expect for a motion in which impacts occur when the beam and plate surfaces move toward each other, but where no such impacts are produced in the portion of the cycle where these surfaces move apart. At higher levels both the top and bottom portions of the sinusoids were distorted, or the entire waveform had superposed on it high frequency ripples of considerable magnitude.

An attempt was made to detect tangential motions by means of accelerometers mounted at a number of points along the beam and plate with their sensitive axes parallel to the beam axis. This attempt was unsuccessful; any small signal that may have been generated by actual tangential motions was obscured due to the cross-sensitivity of the accelerometers and the much greater relative magnitude of normal motions.

Surface Markings

An effort was made to obtain a direct visual indication of where in a beam-plate joint relative normal or tangential motions occur. To this purpose the interface surface of the previously described aluminum angle beam was finely polished before attachment to the plate, the assembled beam-plate system was vibrated at a large amplitude for several hours, and then the beam was removed from the plate. Examination of the polished surface by means of a high power stereo-microscope revealed a number of scattered markings; however, a repetition of the experiment without subjecting the assembly to vibration revealed that the markings were caused by the assembly and dissembly process, and not by the vibration.

Thus, the aforementioned attempt at obtaining an indication of the relative motions from surface markings on a polished beam surface proved unsuccessful. Similar lack of success also was obtained with fine sand, grit, or "dycum" (a lacquer used by machinists to make scribe marks readily visible) interposed between mating surfaces.

EXPERIMENTAL STUDY OF EFFECTS OF VARIOUS PARAMETERS

An experimental program was undertaken to determine which parameters affect the damping of beam-plate joints most significantly. From a knowledge of such parametric effects one may hope to gain an insight into the damping mechanisms operative in such joints.

Experimental Arrangement

All of the experiments reported in this section, unless otherwise noted, were performed on essentially the same set-up and used the same instrumentation system and procedures. The test structure in each case consisted of a plate, with beams attached near one edge and/or at other positions. The plate was suspended vertically, from two 10 ft long strings attached at two plate corners and to a beam near the test room ceiling.

The plate was excited via a voice coil cemented to it, and its response was sensed by means of a small bolted-on piezoelectric accelerometer. The plate size and shape, as well as the beam and instrumentation attachment positions on it are shown in Fig. 1.

Damping measurements were performed using a variation of the well-known decay-rate technique (Refs. 25, 26). This technique consists of exciting the test system with white noise, filtered in a 1/3-octave band, until steady state is reached, then suddenly turning off the excitation and observing the rate of decay of the accelerometer signal, filtered in the same band as the excitation.

Several instrumentation systems were tried; the one found most convenient and used throughout these experiments is indicated in Fig. 1. In using the decay-rate meter shown there one matches the oscilloscope trace of the logarithm of a known decaying signal to that of the logarithm of the envelope of the decaying accelerometer output to be measured, and then reads the signal "reverberation time" T_{60} (i.e., the time for the signal level to be reduced by 60 db, or by a factor of 10^6) directly. The damping of the system may then be simply computed from

$$\eta \approx 2c/c_c \approx 2.2/f\ T_{60} \qquad (1)$$

where η denotes the (dimensionless) loss factor of the system, c/c_c the ratio of the damping coefficient to the critical damping coefficient (assuming viscous damping), T_{60} the decay time in seconds, and f the center frequency in cps of the band under consideration.

Equation (1) is strictly valid only if the system being tested behaves linearly, so that the decay rate (the rate of change of the logarithm of the envelope of a decaying sinusoidal signal) or η is independent of amplitude. For linear systems the envelope of the oscilloscope trace of the logarithm of the acceleration signal (vs. time) is a straight line whose negative slope is proportional to the decay rate. For nonlinear systems this envelope appears curved or as a segmented line. By comparing the logarithmic oscilloscope trace of a test signal with calibrated slanted straight lines provided by the decay-rate meter, one may thus readily judge the linearity of the systems under test.

All systems for which data are reported subsequently were observed to behave linearly for the relatively low excitation levels used in these experiments. Although their linearity may not be maintained at higher excitation levels, small amplitudes were of primary interest in the present study, as previously discussed.

Third-octave band filtered noise was chosen for the measurements described here rather than pure tone (single frequency) signals, because of the much simpler experimental procedure and the more easily interpreted data obtained in this manner. Use of noise in bands avoids the tedium of adjusting the test frequencies to system resonances and yields data devoid of the confusing details one would otherwise observe due to the presence of many resonances in the frequency band of interest.

All bolted connections in all of the experimental specimens discussed here were made by means of number 6-32 stainless steel nuts and bolts, with standard steel washers under the bolt heads and nuts. The torque-tension characteristics of these nut-bolt-washer combinations were studied in a series of preliminary experiments discussed in Appendix II. The nuts in the test assemblies were in all cases tightened to the desired torque by means of a torque-wrench or torque-driver. Each nut-bolt-washer combination was tightened and loosened several times before final assembly in order to decrease the spread in the torque-tension characteristics, in accordance with the test results described in Appendix II.

Experimental Data

Effect of Bolt Torque - Figures 2 and 3 show the results of a series of loss factor measurements on the previously described beam-and-plate system, for several different values of bolt torque. Figure 2 pertains to a 1/16" thick aluminum plate, Fig. 3 to a similar 1/32" plate. The data in these figures are presented in terms of curves pertaining to the loss factors η_o of the plates in absence of any attached beams, plus curves for the loss factor contribution $\eta-\eta_o$ made by the attached beams, where η represents the loss factor of the plate with the beams attached.

From Figs. 2 and 3 one cannot discern a general dependence of loss factor on bolt-torque. The spread of the indicated loss-factor values corresponding to a given frequency (but to different torque) is generally of the order of the precision of the experiment.

Effect of Beam Length - The top portion of Fig. 4 shows the variation in loss factor contribution $\eta-\eta_o$ one obtains by removing one or more of the beams from the test plate of Fig. 1. No data are indicated below 500 cps, because of questionable experimental precision in this range.

The lower portion of Fig. 4 shows the same data as the upper portion, but in the form of loss factor contribution $\eta-\eta_o$ per unit total effective length L of the attached beams. If one visualizes

waves travelling on the test plate in all directions, then the effective length of an attached beam may be defined as the total beam length on which these waves can impinge. Thus, the effective length of a beam attached at a plate edge is equal to its actual length, whereas the effective length of a beam portion near the plate center is twice its actual length. The total effective length L is the sum of the effective lengths of the various beam portions. This definition of effective length was chosen with an eye toward the absorption coefficient idea introduced by Heckl (Refs. 17, 18) and discussed further later in this report; the quantity $(\eta-\eta_o)/L$ is in fact proportional to the absorption coefficient of the beam.

From the superposition of the data pertaining to different beam lengths, as evident in the lower portion of Fig. 4, one may conclude that the damping contribution per unit effective beam length is independent of the total beam length for all practical purposes.

Effect of Bolt Spacing - Figure 5 shows the results of loss factor measurements performed on the plate sketched in Fig. 1, with all bolts in place (1-1/2 inch bolt spacing), with every other bolt removed (3 inch bolt spacing), and again with every other one of the remaining bolts removed (6 inch bolt spacing). The three parts of Fig. 5 pertain to three different bolt torques and serve as a further illustration of the relative independence of damping behavior on torque (except perhaps for very low torques).

The results clearly show that the loss factor contributions of beams are by no means proportional to the number of bolts present. Instead, greater damping at a given frequency is found in general to correspond to the presence of fewer bolts. The damping mechanism thus appears not to be associated with the bolts themselves.

The fact that the peaks of Fig. 5 occur at lower frequencies for greater bolt spacing leads one to suspect that the ratio of the wavelength λ of the flexural plate motion to the bolt spacing d may play a significant role. For a plate $\lambda \propto \sqrt{hc_L/f}$, where f denotes frequency, h plate thickness, and c_L the velocity of longitudinal waves in the plate material. For a given plate one thus may write $f(d/d_o)^2 \propto d^2/\lambda^2$, where d_o is some convenient constant reference length. One may then expect that dependences on d/λ of the data of Fig. 5 would be more clearly evident if the data were replotted on the basis of a "reduced frequency" defined as $f(d/d_o)^2$. Figure 6 is such a re-plot, with d_o taken as 3 in; it shows that maxima of the damping contributions made by the beams in general do occur where the bolt spacing d is equal to an integral multiple of half wavelengths.

Effect of Plate Thickness - The results of loss factor measurements carried out on two beam-plate systems that differ only in the thicknesses of the plates are indicated in the upper portion of Fig. 7. Here it appears that the loss factor contribution of a beam at a given frequency is greater if this beam is attached to a thinner plate.

In view of the dependence of flexural wavelength λ on plate thickness h discussed in the previous section one may write $f(h_o/h) \propto d^2/\lambda^2$, where h_o denotes a convenient constant reference thickness. Dependences on wavelength may then be expected to be revealed more readily if one re-plots the aforementioned data against a new reduced frequency defined as $f(h_o/h)$. The lower portion of Fig. 7 is such a re-plot, from which one may observe that the data for the two plate thicknesses superpose reasonably well when plotted on this basis.

Effect of Beam Width - Figure 8 shows the results of a series of damping measurements carried out with a number of beams of different widths, including three channel sections designed to have approximately the same bending stiffness. It appears from this figure that beams of greater width w provide greater damping contributions.

The curves of Fig. 8 have peaks approximately at frequencies where the bolt spacing matches a half or a whole plate flexural wavelength, in agreement with previous observations. No clear relation between wavelength and contact width is evident.

Effect of Beam Section - Figure 9 summarizes the results of two series of loss factor measurements carried out on plates of two different thicknesses, with beams of several different cross-sections.

The lower set of curves (obtained with a 1/32" thick aluminum plate) shows no discernible effect of stiffness on the damping contributions provided by the beam. The upper set of curves (pertaining to a 1/16" thick plate) on the other hand, shows generally greater damping corresponding to stiffer beams. The latter set includes data for beams that are relatively "soft", however; one may conclude from all of the data of Fig. 9 that the loss factor contributions of attached beams (having the same contact width) are insensitive to beam cross-section changes as long as the beams are considerably stiffer than the plates to which they are attached.

Effect of Spacers Between Beam and Plate - Figure 10a shows how the damping contribution made by a bolted-on beam is affected by the addition of washers between it and the plate to which it is attached. With washers placed on the bolts the only connection between the beam and plate occurs in the vicinity of the bolts; the resulting damping is found to be essentially equal to that measured with the beam totally absent. The effect of washers clamped between the beam and plate, midway between the bolts (and with no washers placed on the bolts), is discussed below.

Effect of Restraints on Relative Motion - The effect of clamping washers between the beam and test plate at locations midway between the bolts may be seen from Fig. 10a. One may observe that these added washers served to produce a marked reduction in the damping. The washers here appear to act like additional connectors, reducing the effective spacing between connectors from 1-1/2 to 3/4 inches.

Reduced damping due to increased constraint of the relative motion between beam and plate is also evident from Fig. 10b. This figure shows that the damping obtained with two beams mounted back-to-back on the two sides of a plate is considerably less than that obtained with a single beam, at frequencies where the bolt spacing exceeds the half wavelength of plate flexural waves (i.e., above about 1250 cps).

Effect of Interface Lubricants and Additives - The damping changes obtained by introducing lubricants of various viscosities between the beam and plate are evident from Fig. 11a. Very viscous oils are seen to reduce the observed damping, with higher viscosities resulting in lower damping. On the other hand, with low viscosity oils one finds that one obtains somewhat greater damping at the low frequencies than in the absence of lubricants. Viscous oils apparently act somewhat like adhesives, providing a more continuous connection between the beam and plate and thus reducing the relative motion and the attendant damping. Oils with low viscosity restrict the relative motion to a lesser extent and may contribute some energy losses due to their being "pumped" back and forth by the relative motion.

It is likely that the higher damping obtained with low viscosity oils for plate flexural half-wavelengths that are greater than the bolt-spacing (i.e., at frequencies below about 1250 cps) is associated with interface shearing motion resulting from the beam and plate bending in unison, somewhat like a laminated beam. This type of bending is not likely to occur at the higher frequencies, where the plate half-wavelengths are less than the distance d between connectors.

Figure 11b illustrates the effect of introducing small beads (approximately 1/16" diameter spheres) of a very soft and tacky viscoelastic substance (Daubert Chemical Company's "Quietape" material) between the plate and beam before assembly. These beads were placed midway between the bolt locations and were squashed into about 1/4" diameter disks by the assembly process. The effect of these beads is found to be very much like that of the 12,500 centistoke oil; they evidently restrict the relative beam-plate motion to a much greater degree than they contribute to energy dissipation by virtue of their internal losses. The viscoelastic beads provide slightly more damping than steel washers at the same location (See Fig. 10a), undoubtedly because the beads are softer, more adhesive, and of a more dissipative material.

Effect of Surface Finish - Figure 11c shows that changes in surface finish affect the damping contributions of beams only slightly, and that smoother finishes tend to result in increased damping. This result is somewhat analogous to that obtained for lubricants; less viscous lubricants and smoother surfaces both facilitate relative motion and produce greater damping.

Effect of Beam and Plate Materials - The results of damping measurements carried out on similar steel and aluminum plates, each with attached steel and aluminum beams are shown in Fig. 12. The damping contributions made by the steel and aluminum beams, when attached to the steel plates, are seen to be very nearly the same. On the other hand the two beams attached to the aluminum test plate are seen to act somewhat differently. (Data for an aluminum channel are shown here, since it matches the stiffness of a solid steel beam more closely than would data for a similar aluminum beam of solid rectangular cross-section.)

Effect of Ambient Atmospheric Pressure - The data summarized in Fig. 13 pertain to a plate and beam configuration that was chosen to fit a small available vacuum chamber. This configuration consists of a 1/64 inch thick aluminum plate (a thin plate was chosen to provide good resolution of the damping data) of roughly rectangular shape with 20" x 14" overall dimensions, with a 17-inch long aluminum beam of 1/4" x 1" rectangular cross-section attached approximately diagonally by means of six 6-32 bolts spaced 3 in. apart and tightened with 4 in-lb of torque. The test plate was suspended in the vacuum chamber from strings attached at two of its corners and to support columns mounted on the floor of the chamber. Excitation and accelerometer arrangements similar to those employed previously were used, but within the vacuum chamber.

The upper portion of Fig. 13 indicates a dramatic dependence of the damping contribution of the beam on ambient atmospheric pressure. At one atmosphere (760 mm Hg) the average loss factor

contribution of the beam is about 0.008, whereas at 1 mm Hg it is practically zero. Curiously enough, somewhat higher damping than at 760 mm was found for a pressure of 400 mm. (This is also true for pressures of 200 and 100 mm, but these data points have been omitted from Fig. 13 for the sake of clarity.) One may also note, incidentally, that damping peaks again occur essentially at frequencies at which the bolt spacing is an integral multiple of the plate flexural half-wavelength.

The data shown in the lower portion of Fig. 13 indicate that the damping behavior of the plate in the absence of any attached beam is unaffected by changes in ambient pressure; the changes apparent in the upper portion of the figure must thus be attributable to changes in the action of the joint.

Results; The Dominant Mechanism

From the data presented in the previous section one may conclude that the damping of point-connected structures in the frequency (or plate-wavelength) range studied here is

1) markedly dependent on:
   a) the ratio of connector spacing to plate flexural wavelength
   b) the presence and viscosity of interface lubricants
   c) the presence of restraints on normal relative motions of mating surfaces
   d) the ambient atmospheric pressure

2) relatively slightly dependent on:
   a) the smoothness of the mating surfaces
   b) the beam and plate materials

3) essentially independent of
   a) interface pressure (bolt torque) and connector details
   b) plate thickness (except insofar as thickness is related to wavelength at a given frequency)
   c) beam mass and stiffness, as long as the beam is considerably stiffer than a plate strip of the same width.

4) essentially proportional to
   a) total effective beam length
   b) beam contact width.

These observations indicate rather clearly that the dominant damping mechanism here is not associated with interface slip or friction. Rather, damping appears to be primarily due to a "pumping" of air, produced by relative motions akin to slapping of the plate surfaces against adjacent beam surfaces. The fact that these motions are greatest midway between adjacent connectors and very small near the connectors is consistent with the present and earlier (Ref. 17) observations that the damping is practically independent of the connector configuration (e.g., that bolts, rivets, and spot welds all produce the same damping).

The previously cited linearity of the experimentally observed damping also points toward the plausibility of an air pumping mechanism. Damping due to interface slip is inherently amplitude-dependent, and would manifest itself in terms of nonlinearities. The analysis of normal relative beam-plate motions presented in Appendix III leads to dependences on the ratio of fastener spacing to plate wavelength which are in agreement with that observed for damping, thus further corroborating the primary importance of normal relative motions.

PREDICTION OF BEAM-PLATE DAMPING

The previously described information concerning the important parameters, some theoretical considerations, and the considerable amount of empirical data that have been amassed, make it possible to develop a method for estimating the damping of any beam-plate system. The following pages deal with the basis for this method and with the development and presentation of pertinent charts.

Absorption Coefficients

The absorption coefficient of a beam attached to a plate is an extremely useful concept, which was first introduced by Heckl (Refs. 17, 18) in direct analogy to the corresponding quantity in room acoustics. The absorption coefficient of a beam is defined as the fraction of the bending wave energy impinging on the beam which is dissipated, and thus is intimately related to energy dissipation due to the attached beam.* Heckl has shown that the absorption coefficient γ of a beam of effective length L attached to a plate of surface area S is given by

---

*One may alternately define an absorption coefficient which accounts both for the energy transmitted past the beam and the energy dissipated by it. The definition used throughout this report involves dissipated energy only.

$$\gamma = \pi^2 \frac{S}{L\lambda} (\eta - \eta_o) \qquad (2)$$

where η_o denotes the loss factor of the plate in absence of the beam, η the loss factor of the plate with the beam attached, and λ the average wavelength of bending waves on the plate. All of the quantities γ, η, η_o, and λ refer to the frequency band being considered. The wavelength λ is related to plate thickness h, frequency f, and longitudinal wave velocity c_L in the plate material as

$$\lambda \approx \sqrt{1.8\ h\ c_L/f} \quad . \qquad (3)$$

The validity of the absorption coefficient concept and of Eq. (2) has been demonstrated previously (Ref. 17). Additional verifications of the linearity of the damping and of the independence of γ on total beam length L have also been obtained in the course of the work described in the previous section (See Fig. 4).

It is important to recall (Ref. 17) that the absorption coefficient concept as previously discussed must be modified for beam segments that are shorter than a wavelength (such segments produce significantly greater absorption coefficients) and for beam segments placed at or near nodal or anti-nodal positions. Significant nodal and anti-nodal behavior occurs only with narrow-band excitation; beam segments near nodes may then be expected to result in lesser, beams near anti-nodes in higher absorption coefficients than those measured in broader frequency bands.

As mentioned previously, the absorption coefficients considered here account only for the dissipation of energy by the attached beams. They do not account for energy conduction past the beams, such as from one panel (e.g., the panel whose damping is of interest) to others attached to it. The resonant or gross decaying response of an entire array of panels with attached beams depends essentially only on the energy dissipation in the beam-plate joints, whereas the response of an individual panel of the array depends on energy conduction as well as on the aforementioned dissipation.

Reduced Variables; Loss Factor Estimation

The previously discussed dimensionless absorption coefficient permits one to describe the damping contributions of attached beams of all lengths in simple form, subject only to the limitations of the absorption coefficient concept. The empirical observation that

the damping contribution of a beam is roughly proportional to the contact width w of the beam may serve as the basis for defining a reduced absorption coefficient, which is practically independent of beam width and which should again result in more compact presentation of data. Such a reduced absorption coefficient may be defined as

$$\gamma_r = \gamma(w_o/w) \quad , \tag{4}$$

where w_o denotes an arbitrarily chosen constant reference width.

It has been observed experimentally (and suggested theoretically) that the damping action of beams attached to plates depends on the fastener spacing to wavelength ratio d/λ, rather than on frequency itself. Thus, by plotting the absorption coefficient data against d/λ or against a function of d/λ one may hope to be able to present all of this data in compact form. Since the user of damping information may generally be expected to be more interested in dependences on frequency than on wavelength, it appears useful to define a reduced frequency f_r as

$$f_r = f(h_o/h)\left(c_{L_o}/c_L\right)(d/d_o)^2$$

$$\approx f_o\left(\frac{\lambda_o}{\lambda}\right)^2\left(\frac{d}{d_o}\right)^2 \approx \frac{1.8\ h_o\ c_{L_o}}{d_o^2}\left(\frac{d}{\lambda}\right)^2 \tag{5}$$

where the subscript o denotes arbitrary constant reference values.

Figures 14 and 15 present the previously discussed data pertaining to unlubricated and unbonded joints at one atmosphere ambient pressure in terms of reduced absorption coefficients plotted against reduced frequency. Figure 14 summarizes data obtained for a single beam width, but for three plate thicknesses and three bolt spacings. Figure 15 presents data for three beam widths, two plate thicknesses, but only one bolt spacing.

The larger shaded area in both of these figures represents the region into which fall all of the considerable body of data resulting from measurements made on 1/32-inch thick plates with 1-1/2 inch bolt spacing. The smaller shaded area similarly pertains to 1/16-inch plates, again with 1-1/2 inch bolt spacing. These shaded areas encompass data pertaining to several bolt torques, total beam lengths, beam cross-sections, surface finishes, and beam and plate material combinations; these variables are considered to have relatively little effect on damping.

The curves shown in Fig. 14 represent the extreme damping values obtained for three values of torque (including 1 in-lb, which results in a relatively loose joint), for bolt spacings of 3 and of 6 inches.

Figures 14 and 15 indicate a considerable scatter in the total body of data presented, but do indicate a trend from which one may hope to be able to estimate a likely absorption coefficient value for a given beam-plate configuration at a given frequency. The data for constant plate thickness are seen to cluster more closely together than does the entire body of data. This clustering might indicate a plate-thickness effect which is not taken into account by the reduced variables considered here. In using these figures for damping prediction purposes one would obviously do best to concentrate on those portions of the available data which correspond most closely to the case with which one is concerned.

In order to estimate the loss factor η of a plate of area S and thickness h, to which are attached a number of beams (or other stiff structures) one may use the relation

$$\eta = \eta_o + \frac{\lambda}{\pi^2 S} \Sigma \gamma_i L_i \quad , \tag{6}$$

which follows from Eq. (2). Here γ_i represents the absorption coefficient of the i^{th} beam element, and L_i represents the effective length of that element. The summation extends over all of the attached beam elements.

Values of γ_i for given plates, frequencies, fastener spacings, and contact widths may be estimated from Figs. 14 and 15. The plate wavelength λ may be calculated from Eq. (3) or, for steel or aluminum plates from

$$\lambda(\text{in}) \approx 610\sqrt{h(\text{in})/f(\text{cps})} \quad . \tag{7}$$

The loss factor η_o of a plate in absence of beams may generally be taken as the loss factor of the plate material. Loss factors of many materials are available in the literature (Refs. 1, 2, 27 and 28). Some measured values for 2024 T3 aluminum plates appear also in Figs. 2 and 3, but these may include some minor damping contributions from the supports. In general one may expect that with several attached beams the contribution of η_o to the total damping η will be far overshadowed by that of the beams, so that η_o may often be neglected in practice.

It may be useful to state once more that Figs. 14 and 15 pertain only to beam-plates systems surrounded by air at atmospheric pressure with conventional (unlubricated and unbonded) point-connected joints. At present insufficient information is available to permit one to extrapolate these estimates reliably to higher or lower pressures or to other ambient gases. It is also important to keep in mind that the suggested estimation approach does not account for energy transmitted to structures other than the plate considered or to fluids in contact with the plate (i.e., acoustic radiation). For plates in contact with air the damping due to acoustic radiation is generally considerably smaller than that due to attached beams; for other ambient media, notably liquids, this may not be true.

PLATE-PLATE JOINTS

The damping produced by plate-seam joints was studied in order to obtain information concerning the mechanisms responsible for this damping and to obtain data from which one may estimate the damping contributions made by plate seams in practical structures.

Exploratory Studies of Bolted Seams

Relative motions occurring at a single-row bolted plate seam in a 1/32-inch thick aluminum plate having the shape sketched in Fig. 16 were briefly examined with the aid of a stroboscope while the plate was being driven sinusoidally at relatively low frequencies. Similar observations were made on a somewhat smaller 1/8-inch thick rubber plate. The relative motions observed were found to be essentially of a slapping nature, (i.e. perpendicular to the interface surfaces), as was found for beam-plate joints. Again, no interface shearing motions could be observed.

The high-frequency behavior of plate seams was studied by means of light-weight accelerometers attached to the plate portions at several locations halfway between two adjacent bolts, with the accelerometers' sensitive axes perpendicular to the plate surface. The plate was driven sinusoidally, at various frequencies and amplitudes, and the waveforms of the accelerometer signals were displayed on oscilloscopes. The behavior of the plate seams was again found to be much like that of beam-plate joints. All accelerometer signals appeared like pure sinusoids at the driving frequency for small excitation amplitudes, exhibited distortion near the maxima above a certain driving amplitude, and became more generally distorted for even greater amplitudes.

Parameter Studies of Bolted Seams

A number of measurements were made using aluminum test plate configurations having either one or two seams, as sketched in Fig. 16, and the experimental arrangement described in Fig. 1.

Bolt Torque - A brief series of measurements were carried out on a 1/32-inch thick aluminum plate with single-row bolted joints, using 1-inch overlap, 1-1/2 inch bolt spacing, and bolt torques of 4, 12, and 20 in-lb. The damping contributions of the joints were found to be virtually the same for the three torque values that were used. The damping produced by bolted plate seams thus appears to be independent of bolt torque for all practical purposes. This result implies that the damping of multi-point-fastened seams, like that of beam-plate joints, is essentially independent of fastener details.

Seam Length - From Figs. 16-18 one may discern that the absorption coefficients of the three joint types studied are independent of total seam length. The absorption coefficients shown here were again calculated according to Eq. (2), from measured values of the loss factor η_0 of the continuous plate and of the loss factor η of the plate incorporating the seam under study. The effective seam length L is here taken as twice the actual total seam length, in accordance with the previous discussion of effective length, and since a plate seam can by definition not occur at the edge of a plate.

Bolt Spacing and Plate Thickness - Figure 16 summarized absorption coefficient data for single-row bolted lap joints in plates of two different thicknesses, and using two different bolt spacings. Figures 17 and 18 present data for two types of double-row joints; each of these figures pertains to a single bolt spacing, but to two plate thicknesses. All three figures are plots of absorption coefficients *vs.* reduced frequency, as defined by Eq. (5). The good superposition of the various data portions of Fig. 16-18 thus indicates that damping produced by point-fastened plate seams, like that produced by beam-plate joints, depends on the wavelength of bending waves in the plate rather than on frequency *per se*.

Parameters Not Studied - In the present study no experiments were undertaken to ascertain the effects of 1) reduced or increased ambient atmospheric pressure, 2) overlap width, 3) joining plates of different thicknesses. The effects of these parameters need to be investigated further if one desires a complete picture of the damping contributions made by bolted plate seams.

Several parameters that were studied for beam-plate systems were not studied for plate-seams, because these beam-plate studies were primarily aimed at discovering the dominant mechanism and it is felt that the dominant mechanism here is the same. These parameters include 1) spacers between joint surfaces, 2) restraints on relative motions, 3) interface lubrication, 4) surface-finish, and 5) materials.

Welded Seams

A number of measurements of the damping contributions of continuously welded joints in aluminum plates were undertaken. Butt joints and 1-inch and 3-inch wide (doubly welded) lap joints were tested, using the same plate geometry, seam arrangement, and instrumentation as for bolted joints. No measurable damping contribution was observed for any of the welded joints studied.

Dominant Mechanism; Damping Estimation

The similarity of the damping behavior of bolted plate seams to that of bolted beam-plate joints leads one to suspect that the dominant damping mechanism is the same in the two cases. Thus, although it was not proven conclusively (in absence of data obtained in vacuum), it appears likely that the damping produced by point-connected plate seams is produced primarily by the pumping of air that results as the mating joint surfaces between fasteners move apart and toward each other.

The absorption coefficient concept and the reduced frequency idea (i.e., plate flexural wavelength dependence) have been shown to apply to plate-seams, as well as to beam-plate joints. The damping of plates incorporating multi-point-fastened seams may thus be estimated with the aid of Eq. (6) and the absorption coefficient data of Figs. 16-18.

The absorption coefficient of welded plate seams was found to be zero for all practical purposes. The loss factor of a plate incorporating welded joints thus is the same as that of a similar continuous plate.

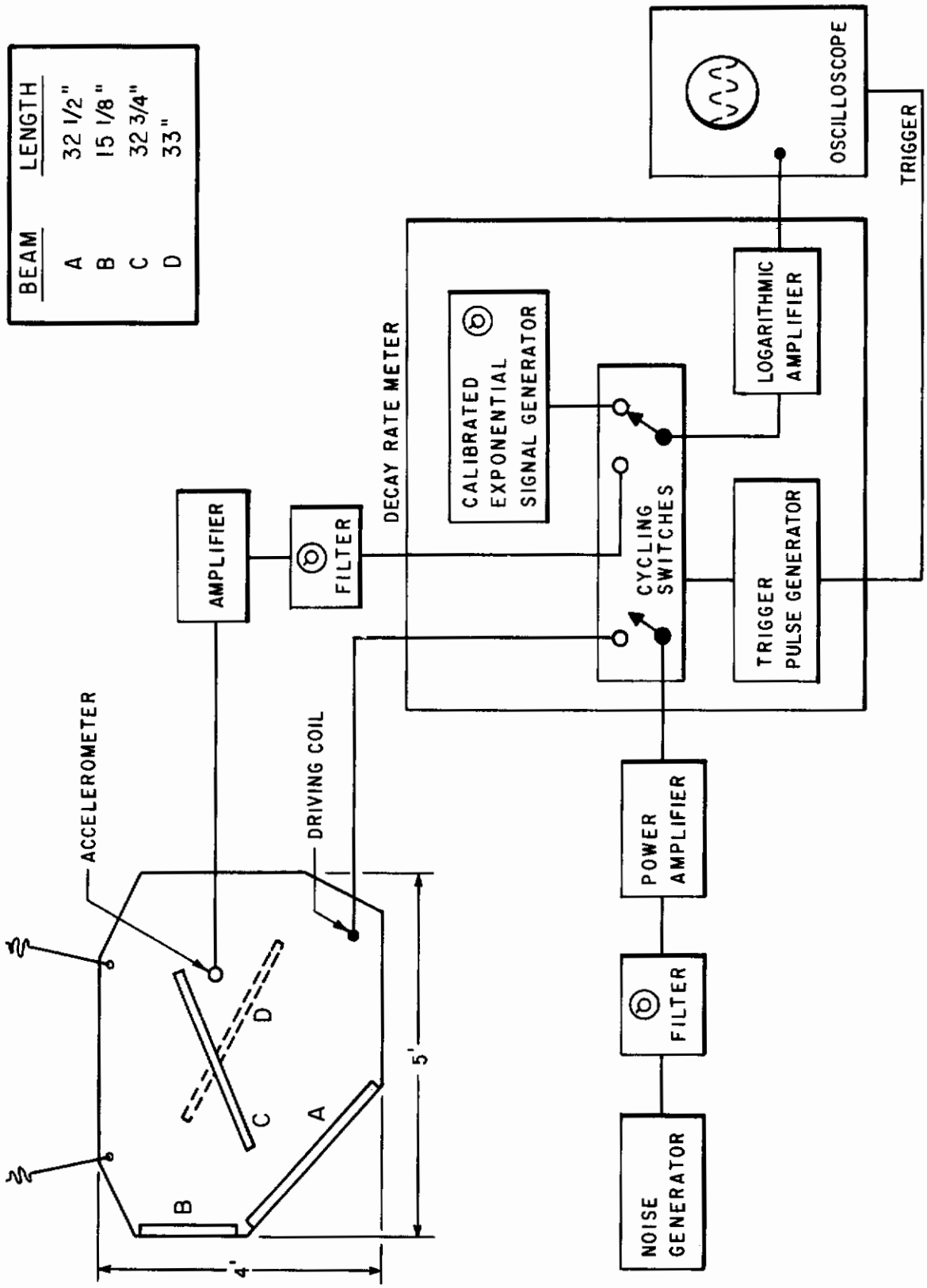

FIG. 1 TEST PLATE WITH ATTACHED BEAMS AND INSTRUMENTATION

TABLE I

Instrumentation List for Fig. 1

Component	Manufacturer	Model No.
Decay Rate Meter	Spencer-Kennedy Laboratories	507
Filter, 1/3 Octave Band	Bruel and Kjaer	1612
Amplifier	General Radio	1551-C
Power Amplifier	McIntosh	MC-40
Noise Generator	Grayson Stadler	901A
Accelerometer	Gulton	A314
Oscilloscope	Hewlett Packard	130B

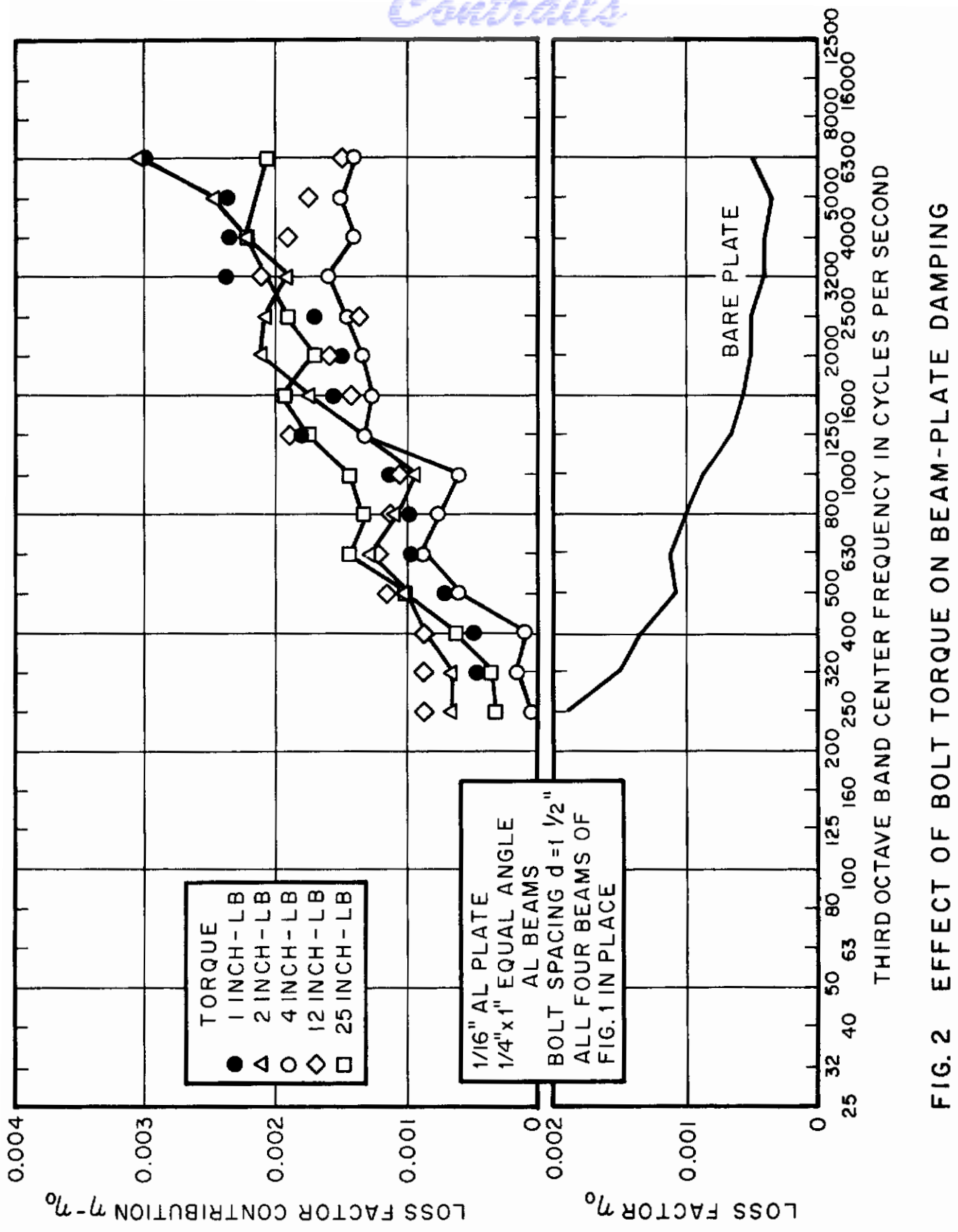

FIG. 2 EFFECT OF BOLT TORQUE ON BEAM-PLATE DAMPING

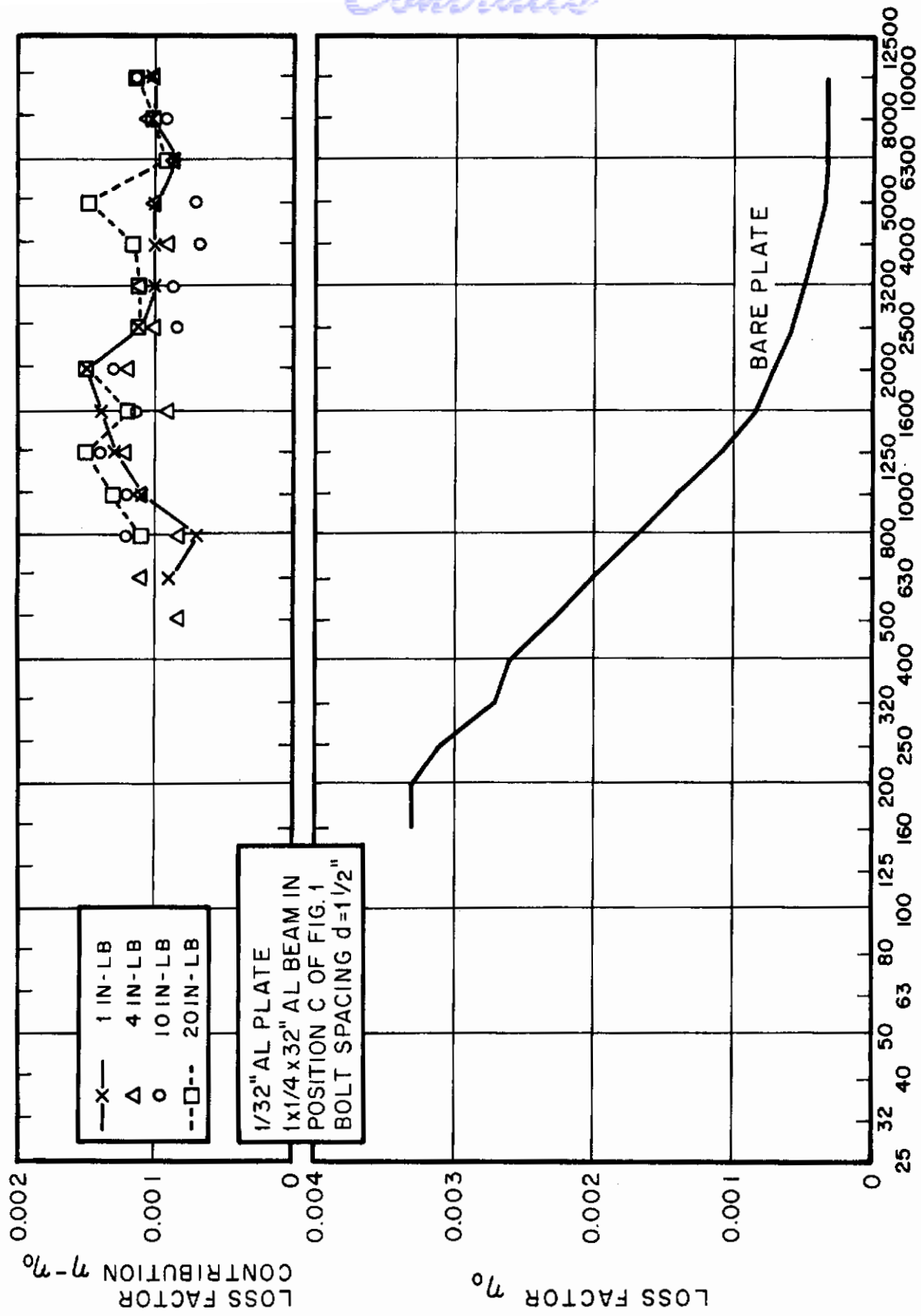

FIG. 3 EFFECT OF BOLT TORQUE ON BEAM-PLATE DAMPING – CONTINUED

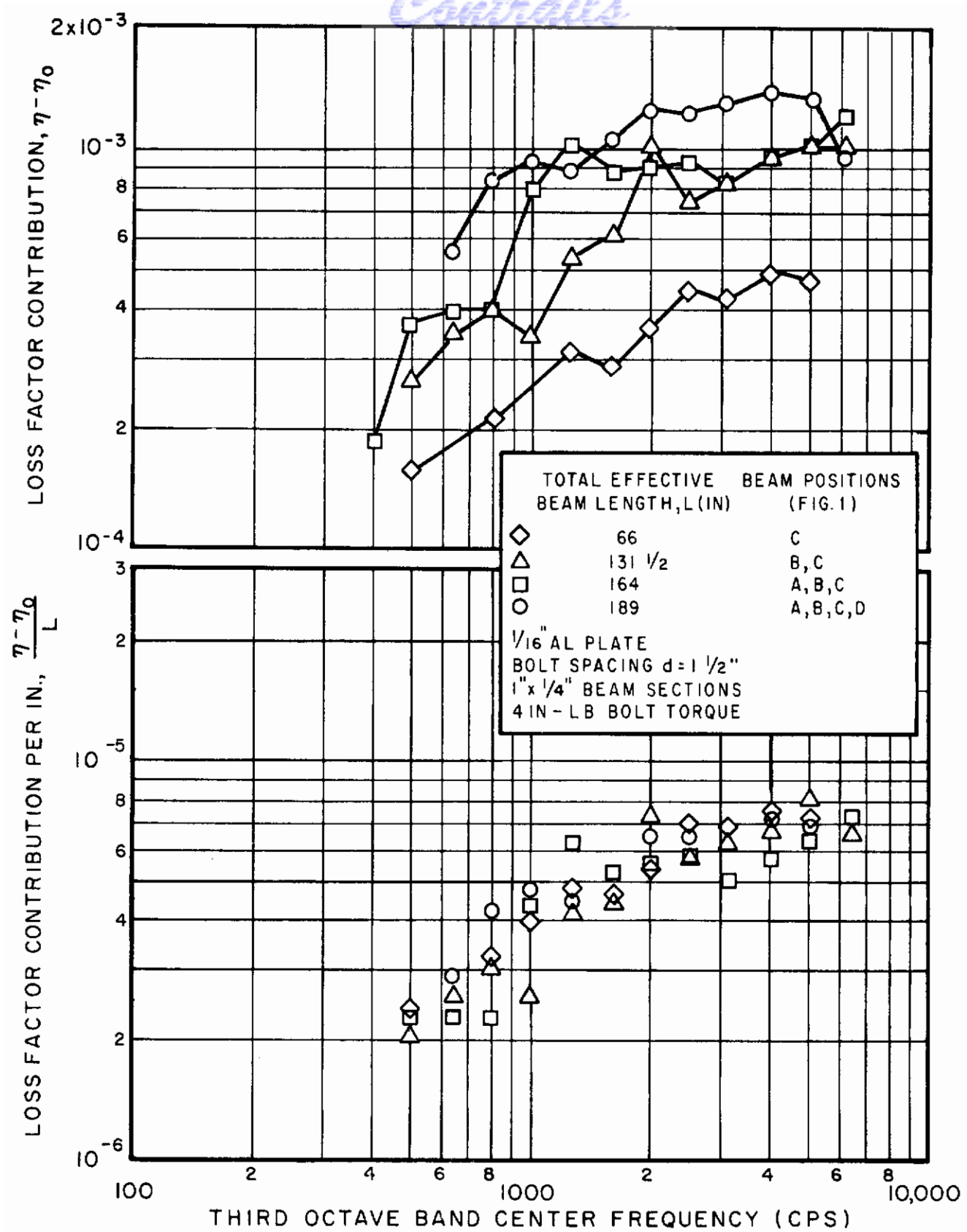

FIG. 4 EFFECT OF TOTAL BEAM LENGTH ON BEAM-PLATE DAMPING

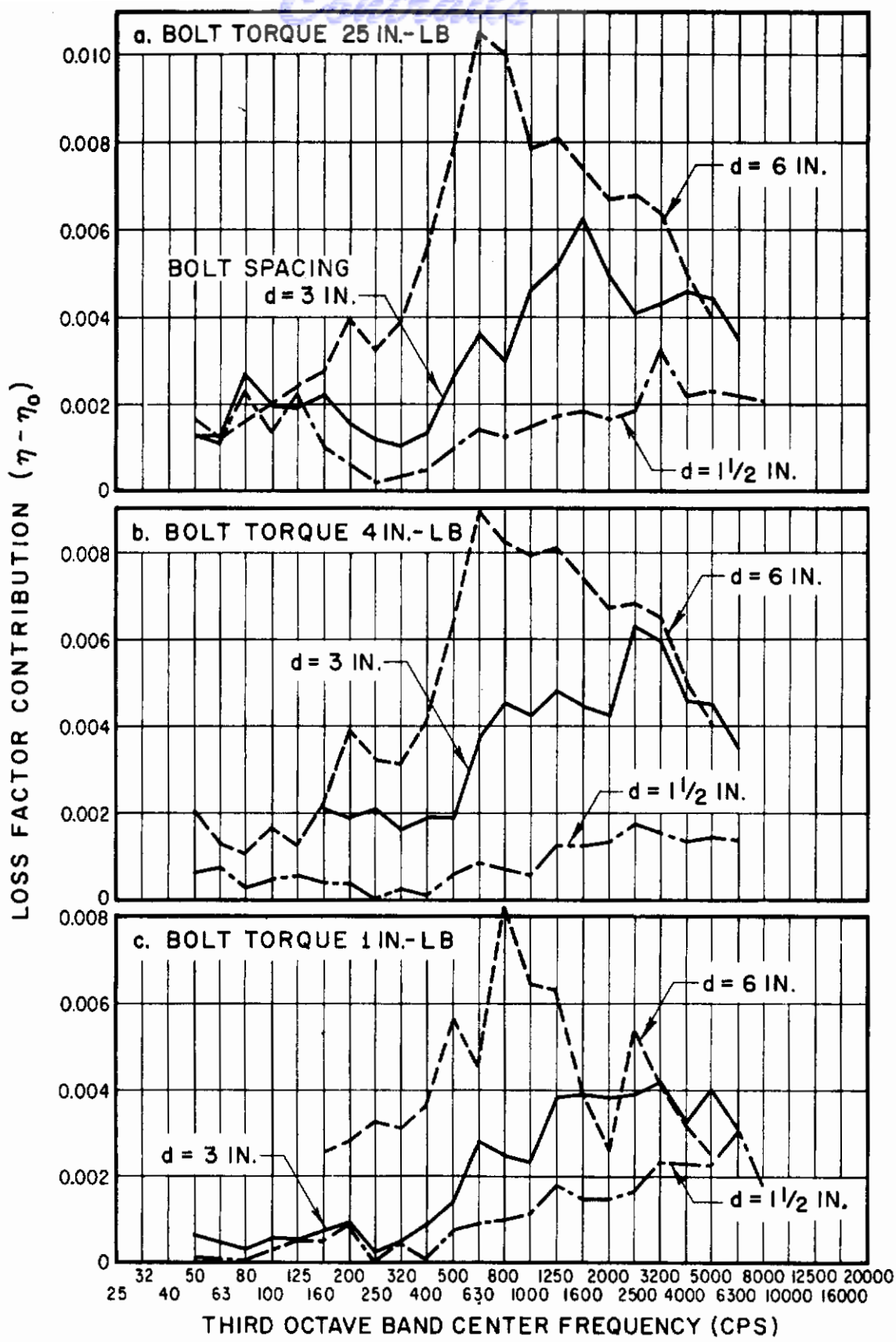

FIG. 5 EFFECT OF BOLT SPACING ON LOSS FACTOR CONTRIBUTION BY BEAMS. (1/16 ALUMINUM PLATE AS IN FIG. 1, ALL BEAMS ATTACHED)

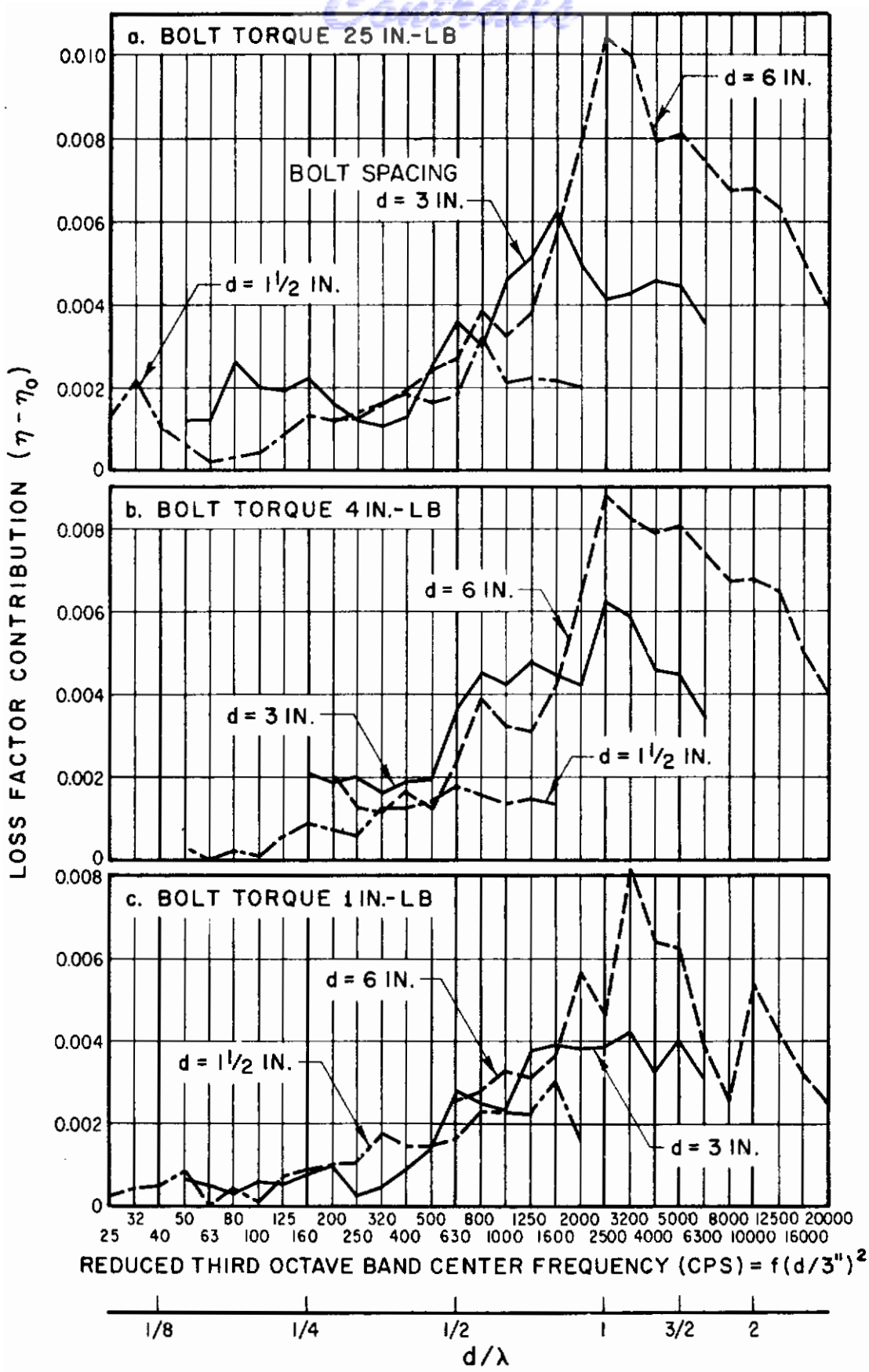

FIG. 6 EFFECT OF (BOLT SPACING/PLATE WAVELENGTH) RATIO ON LOSS FACTOR CONTRIBUTION BY BEAMS

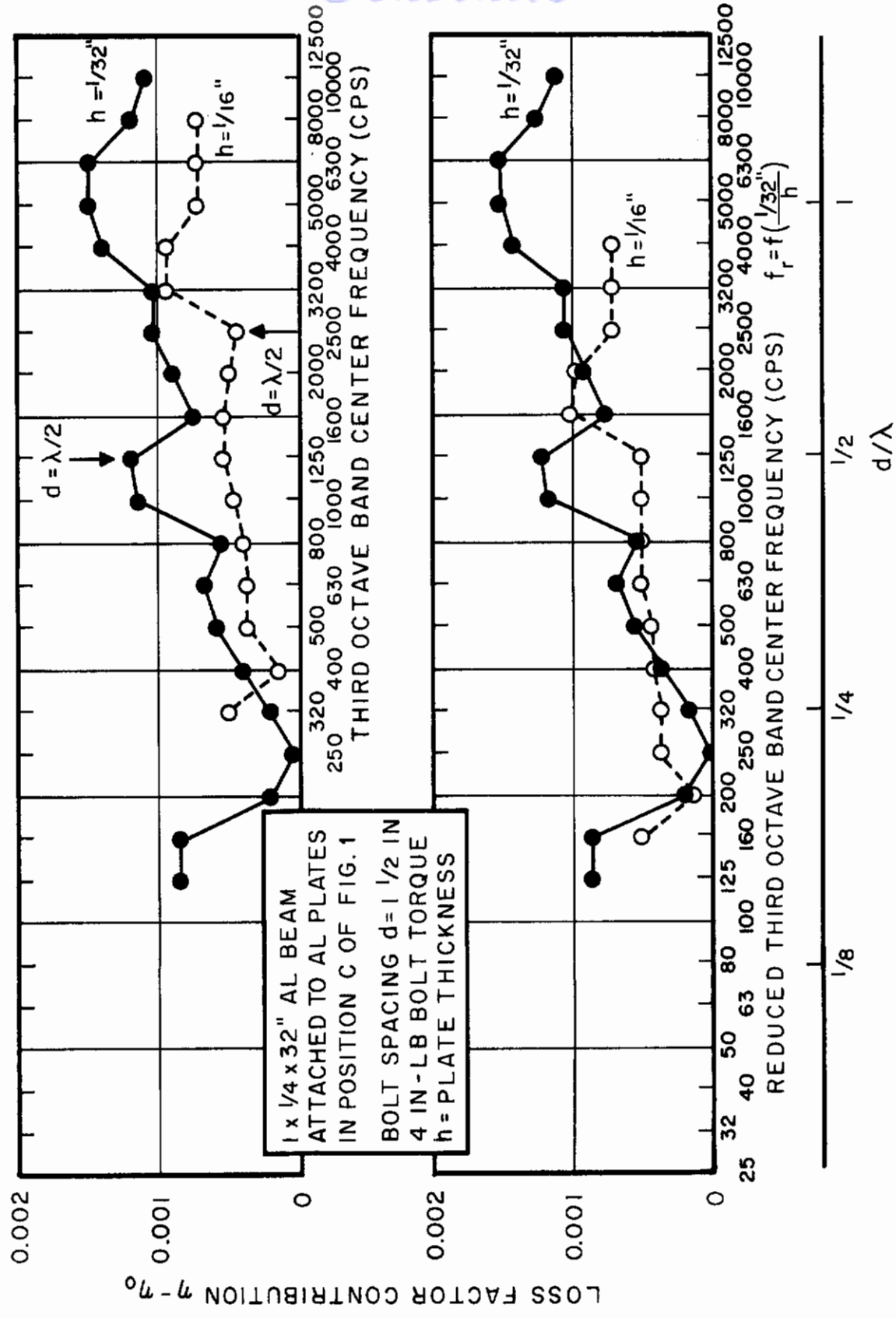

FIG. 7 EFFECT OF PLATE THICKNESS ON BEAM-PLATE DAMPING

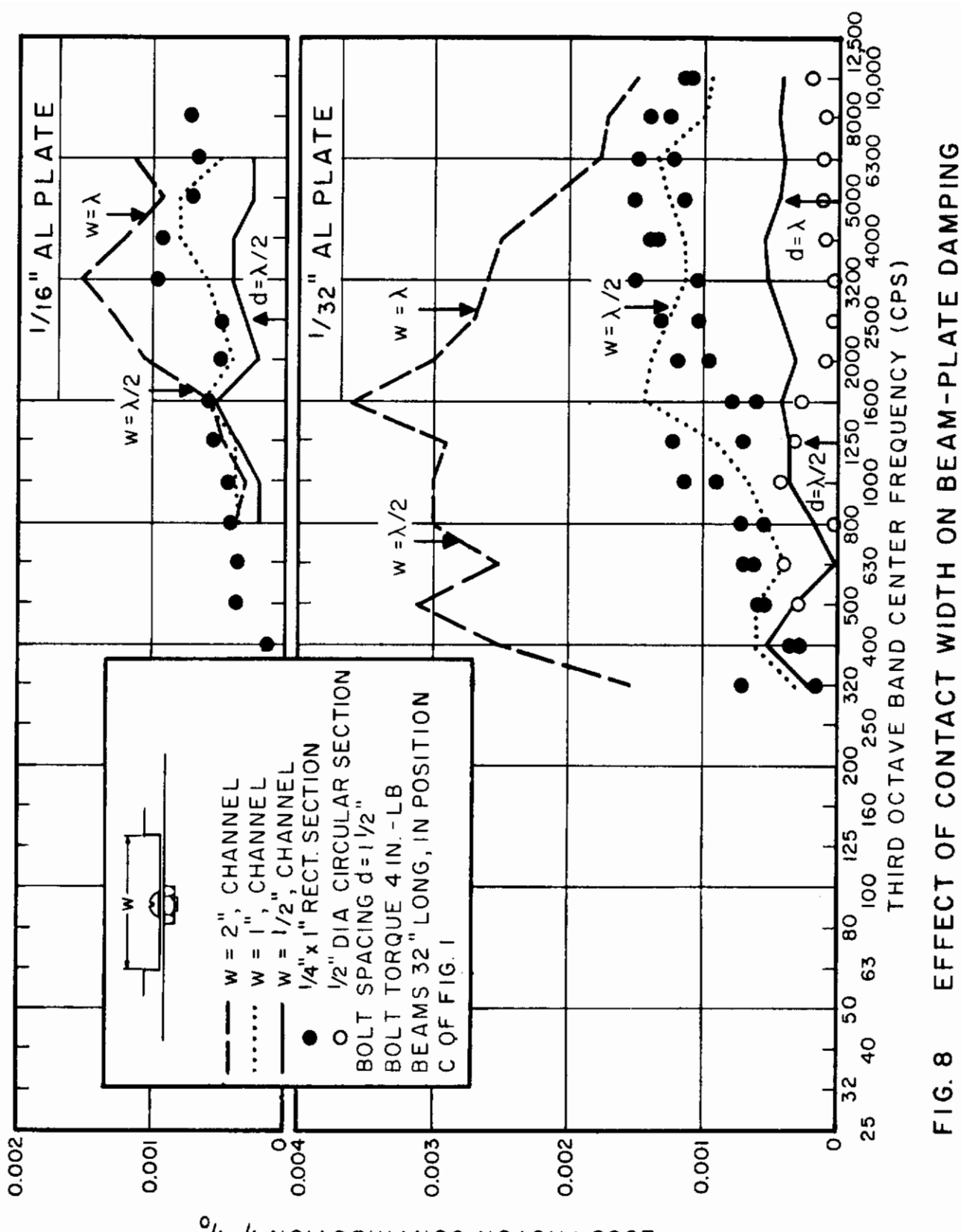

FIG. 8 EFFECT OF CONTACT WIDTH ON BEAM-PLATE DAMPING

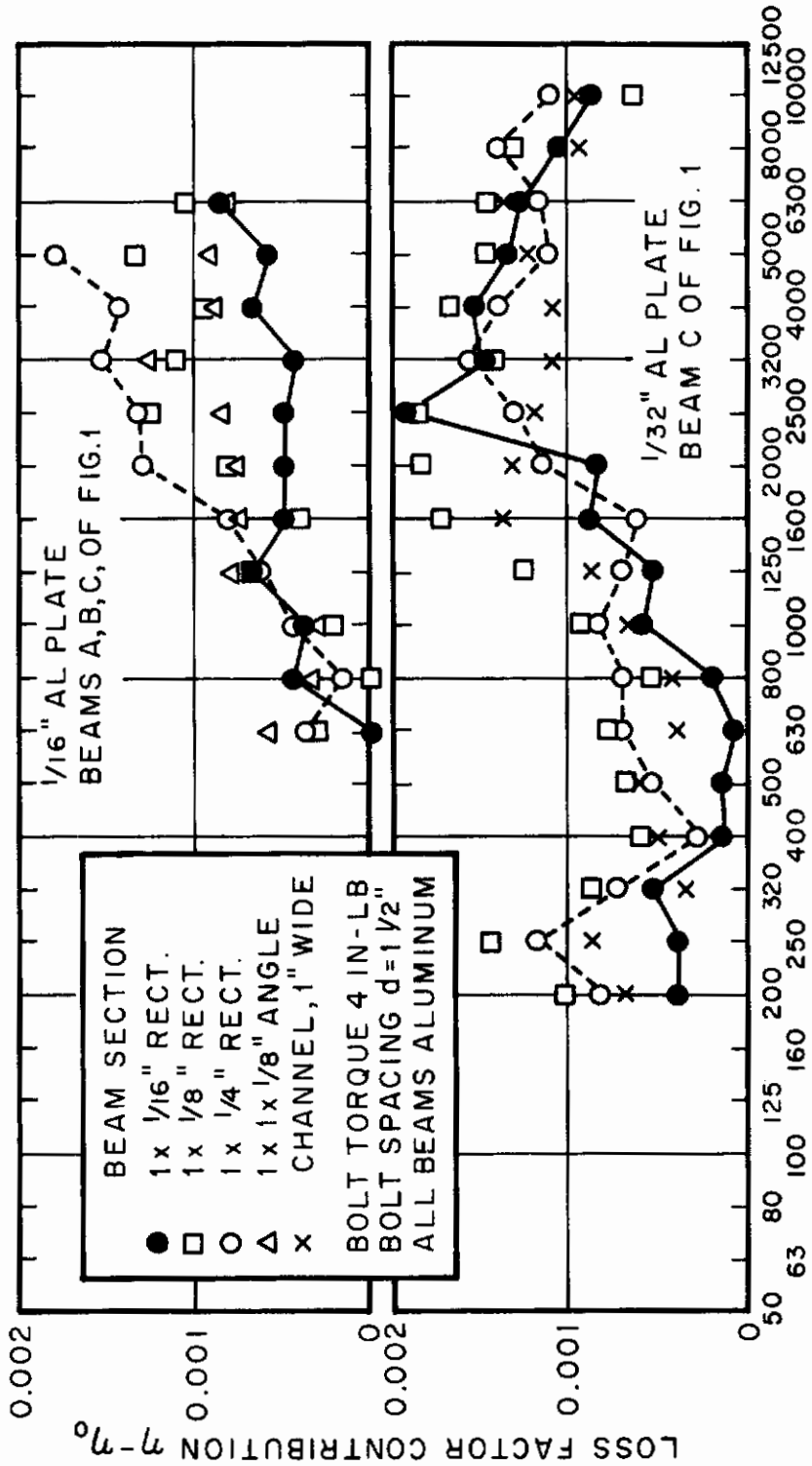

FIG. 9 EFFECT OF BEAM SECTION ON BEAM-PLATE DAMPING

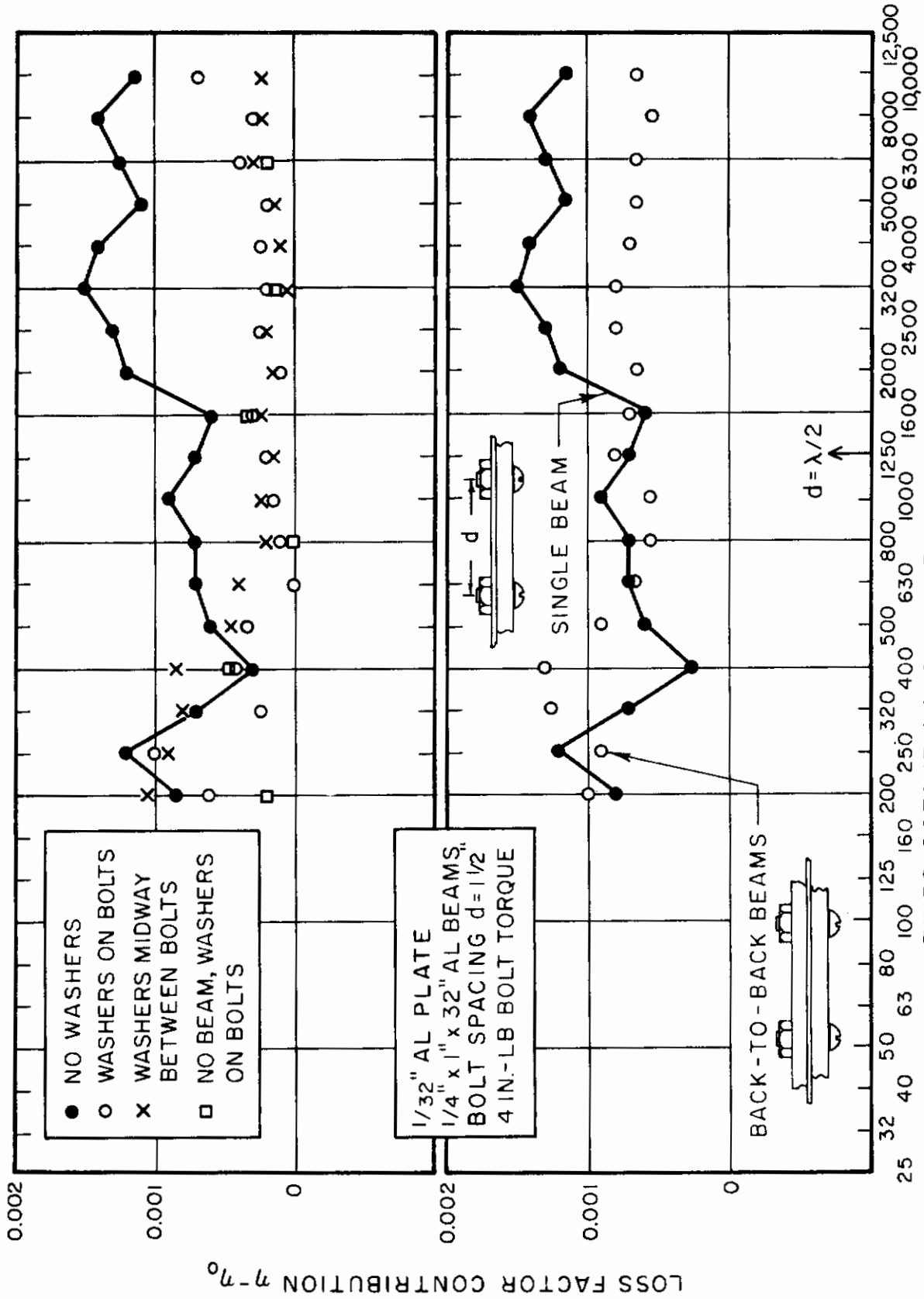

FIG. 10 a. EFFECT OF WASHERS BETWEEN BEAM AND PLATE
b. EFFECT OF TWO BEAMS BACK-TO-BACK

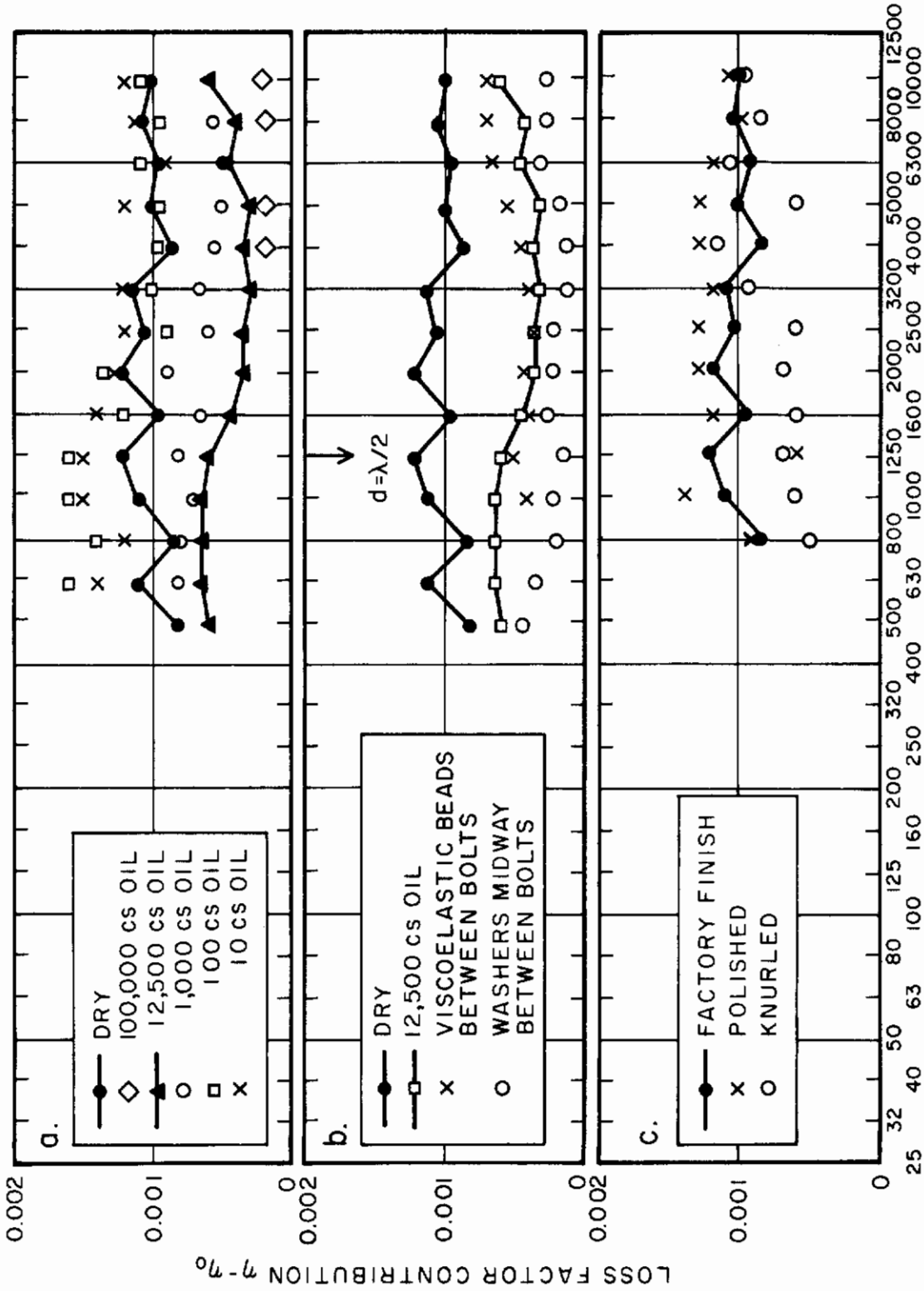

FIG. 11 EFFECTS OF: a. LUBRICATION, b. INTERFACE ADDITIONS, c. SURFACE FINISH

1/32" AL PLATE, 1" x 1/4" x 32" AL BEAMS IN POSITION C OF FIGURE 1, 4"-LB BOLT TORQUE, BOLT SPACING d = 1 1/2"

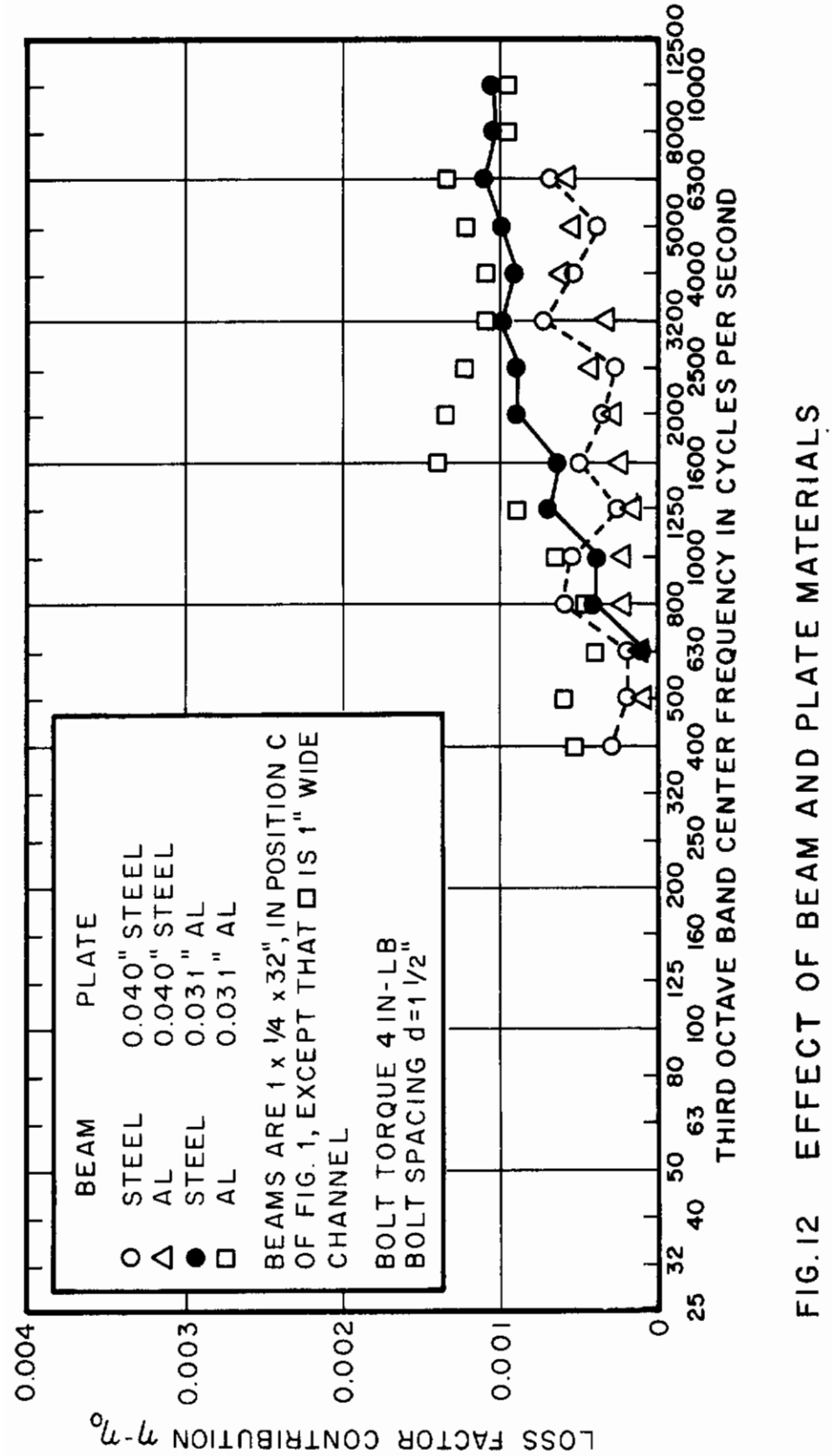

FIG. 12 EFFECT OF BEAM AND PLATE MATERIALS

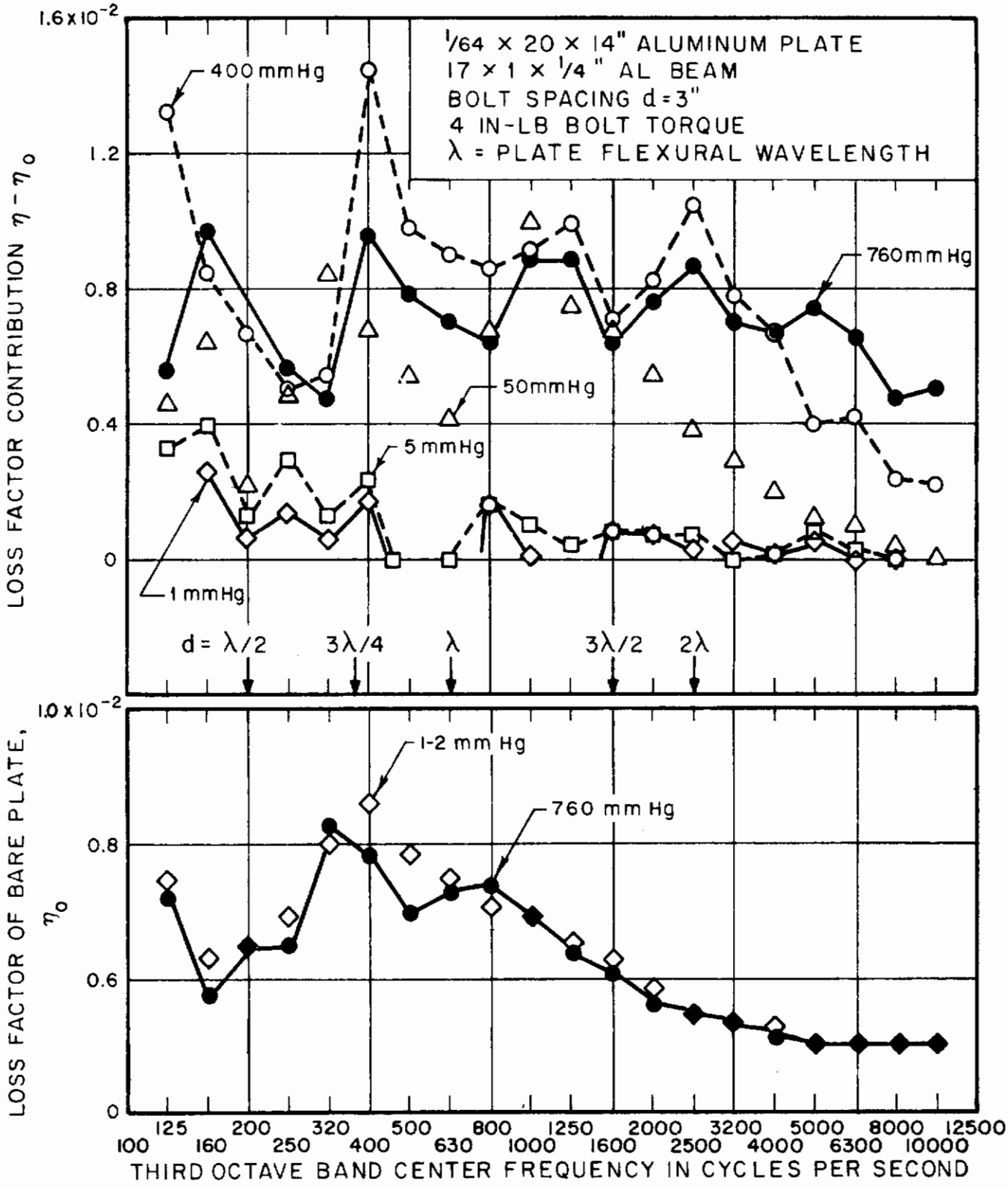

FIG. 13 EFFECT OF VACUUM ON BEAM-PLATE DAMPING

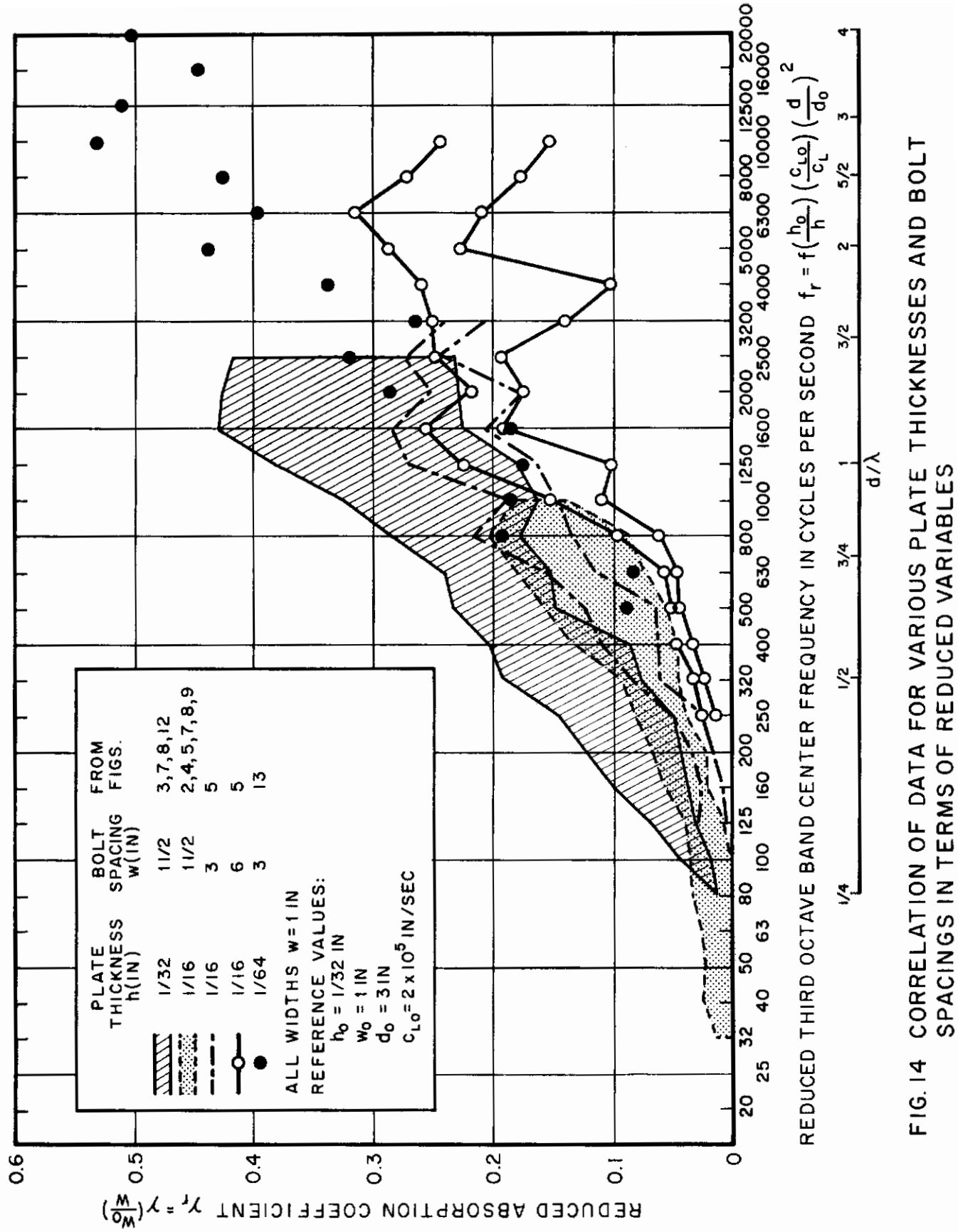

FIG. 14 CORRELATION OF DATA FOR VARIOUS PLATE THICKNESSES AND BOLT SPACINGS IN TERMS OF REDUCED VARIABLES

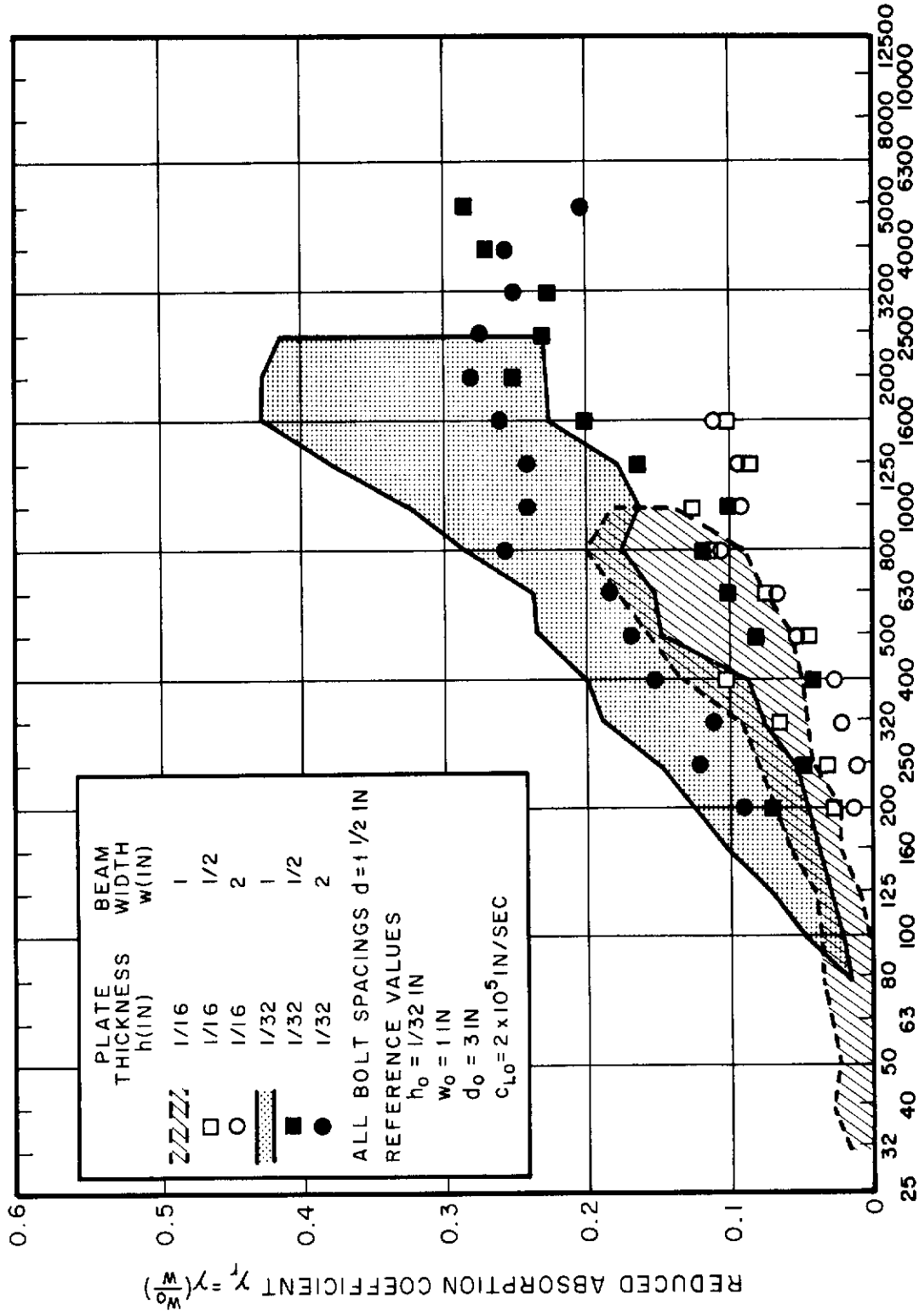

FIG.15 CORRELATION OF DATA FOR VARIOUS BEAM WIDTHS IN TERMS OF REDUCED VARIABLES

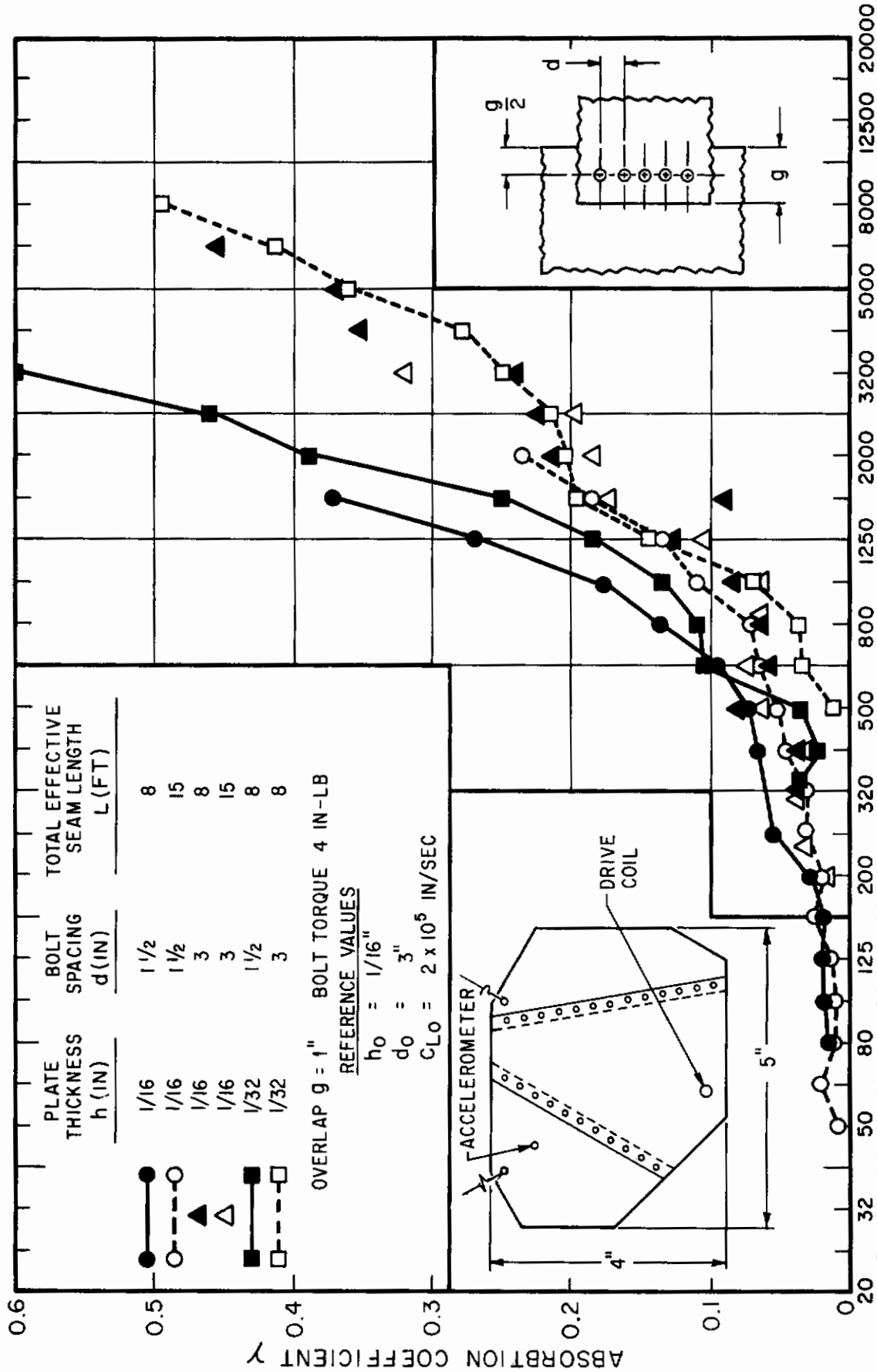

FIG. 16 ABSORPTION COEFFICIENT OF SINGLE-ROW BOLTED PLATE SEAM

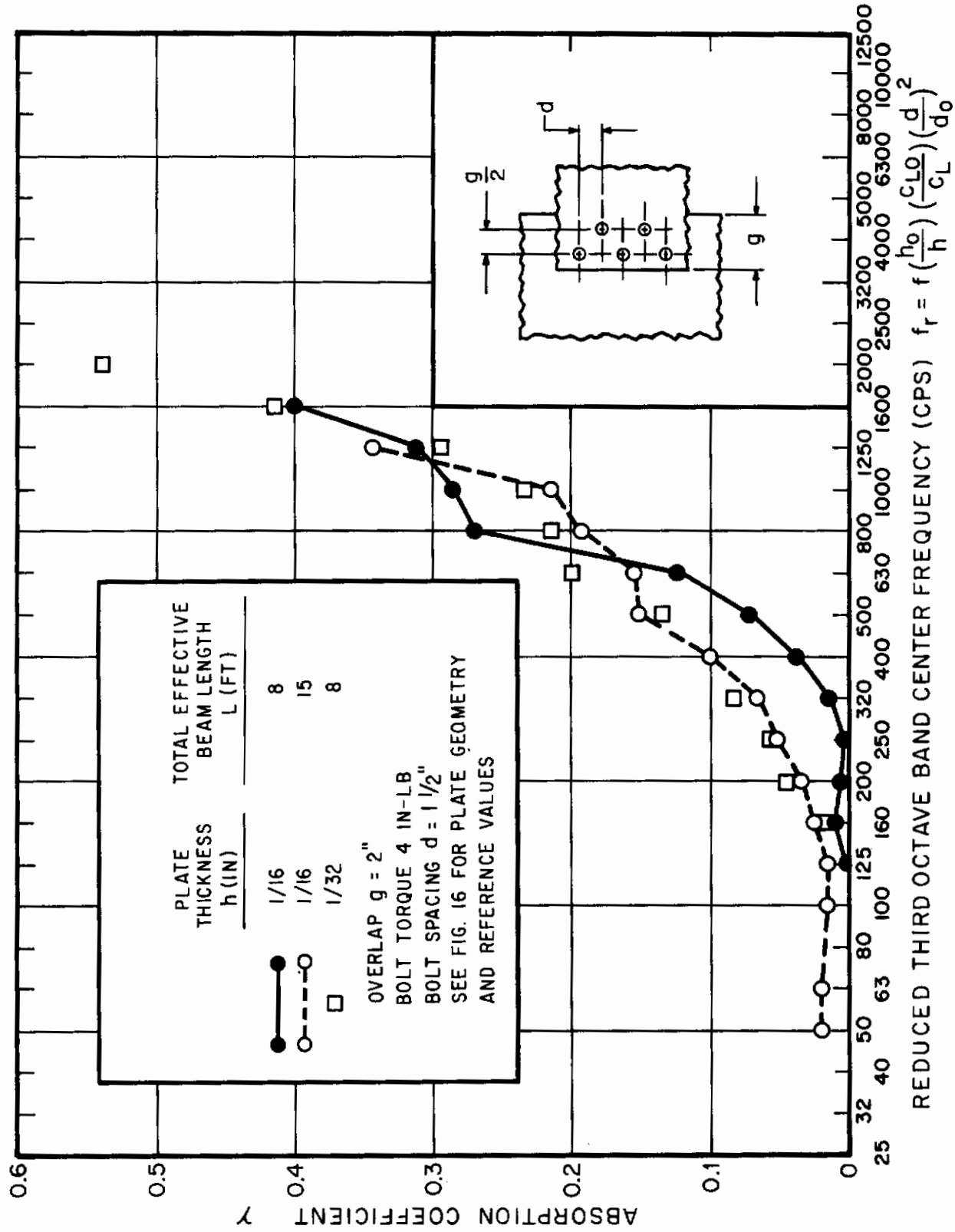

FIG. 17 ABSORPTION COEFFICIENT OF STAGGERED DOUBLE-ROW BOLTED PLATE SEAM

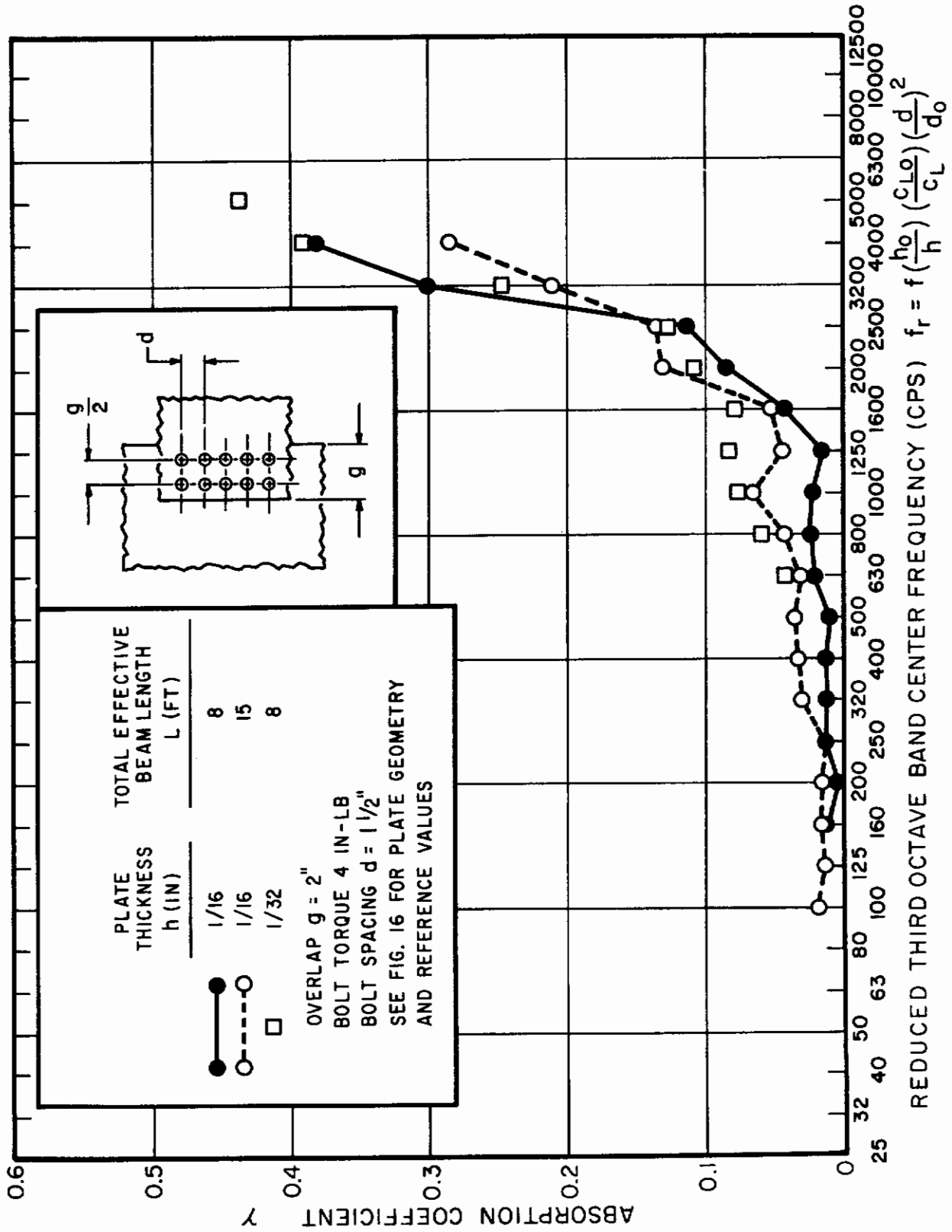

FIG. 18 ABSORPTION COEFFICIENT OF IN-LINE DOUBLE-ROW BOLTED PLATE SEAMS

PART II

EDGE-RIVETED STRUCTURES AT LOW FREQUENCIES

PURPOSE AND APPROACH OF INVESTIGATION

Purpose

As has been pointed out previously, Mentel's studies (Refs. 12, 14) of the damping of panels due to their edge supports were primarily concerned with highly idealized configurations and with supports incorporating viscoelastic inserts; they did not address themselves to determining the mechanisms that dominate the damping of panels whose edges are fastened realistically by bolts or rivets to supporting structures. Study of this mechanism was the prime purpose of the investigations discussed below.

Approach

The study reported here consists of 1) a series of experiments aimed at discovering the dependence of the damping under investigation on frequency, amplitude, and interface pressure; 2) of predicting these dependences theoretically for postulated mechanisms that might logically be present; and 3) of comparing the theoretical predictions with experimental results.

This approach permits one to determine which mechanisms cannot be responsible for the observed damping, and might help one to decide on "critical" experiments to distinguish which of the several mechanisms for which theoretical predictions are compatible with experimental results actually dominate the damping of practical joints.

EXPERIMENTAL ARRANGEMENT

Test Models

For the sake of experimental and theoretical simplicity, it was decided to work with narrow plate strips fastened only at the two shorter edges, rather than with, say, more nearly square panels riveted at all edges. It was felt that use of narrow strips would preserve all the salient features of edge-riveted panels, while reducing possible effects of acoustic radiation, assuring that flexural waves on the panel impinge perpendicularly on the supports, and resulting in modal properties more amenable to calculation.

The measurements reported subsequently were carried out on aluminum panel-strips with the following dimensions:

Panel "A": 1/16 x 2 x 8 in
Panel "C": 1/8 x 2 x 16 in.

These panels were attached to test jigs, as shown in Fig. 19. Two jigs were constructed (one for each panel size); Fig. 19 shows the larger jig to approximately half scale, the smaller is merely a shortened version of the one shown.

The test jigs were designed to be as rigid as possible, in the hope of eliminating the support elasticity variable from the studies. The "supporting jaws" were made separately from the main blocks, so that they could be changed, e.g. for determinations of the effects of support width or sharpness of edges. The slots in these jaws permit one to insert torque wrenches, so that one may have some control over interface pressures. Throughout the work reported here #6-32 stainless steel nut-bolt-washer assemblies were used, whose torque-tension characteristics have been investigated as described in Appendix II.

Measurement Methods and Instrumentation

Two types of damping measurement techniques were used: the relatively conventional one of measuring the rate of decay of free vibrations, and the rather new one of measuring the power dissipated under steady state forced vibration conditions.

For the rate-of-decay measurements the panel-and-jig assembly was suspended from a suitable support by means of long strings. A light piezoelectric accelerometer was attached to the panel near its center, and care was exercised to prevent the accelerometer cable from affecting the panel motion. The panel was excited by tapping it lightly with a finger or small wood block, and the resulting decay rate was measured by means of the instrumentation arrangement indicated in Fig. 1.

Steady-state power dissipation measurements were performed with the relatively newly developed instrumentation system shown in Fig. 20. An important advantage of this type of measurement is that it permits amplitude and frequency to be adjusted independently, so that effects of these parameters may be studied most readily.

Actually, the mechanical power supplied to the test system was measured, and not the power dissipated. However, at steady state the power supplied (averaged over a cycle or over many cycles) is equal to the power dissipated. The power supplied

to the system was determined by means of an impedance head bolted to the test structure (Fig. 20). This impedance head is a compact device which generates two voltages, one proportional to acceleration, one to force. The instrumentation indicated in the figure integrates the acceleration signal to produce a velocity signal, multiplies this by the force signal to obtain a voltage proportional to instantaneous mechanical power. Time-average values of this voltage may then readily be obtained by use of an rms voltmeter.

The concept of this power measurement arrangement is simple, but it involves many practical instrumentation difficulties. These include the usual loading effects of one piece of equipment on the other and the presence of hum and other extraneous signals. Elimination of these effects and the matching of the phase characteristics of all portions of the two signal channels are of particular importance in measuring small amounts of damping, since one then must essentially measure small phase angles.

Figure 20 and the instrumentation list accompanying it show the best instrumentation system devised in the course of the work being reported here. It is the result of a considerable amount of effort and is believed to be the optimum presently possible without using markedly more precise (and expensive or specially built) components.

The summing amplifier shown in Fig. 20 permits one to subtract from the force signal a voltage proportional to the inertia force associated with a constant mass; e.g. with the mass of the part of the impedance head between the force gage and the test structure. Although a pure mass cannot contribute to energy dissipation, this subtraction was introduced here in order to provide a signal proportional to the actual force acting on the test structure for the sake of being able to display on an oscilloscope this actual force vs. any of the other variables of interest, as well as for the sake of increased precision.

EXPERIMENTAL RESULTS

Amplitude Effects in Tight Joint

In order to study how power dissipation in a tightly bolted joint varies with amplitude at constant frequency the test jig with panel "A" attached was clamped tightly to a column of the laboratory building, with the plane of the panel vertical. This arrangement permitted driving the test panel at significant amplitudes relative to the jig and avoided "biasing" of the panels by gravity. The impedance head was carefully aligned normal to the surface of the panel.

Figure 21 shows how the driving-point velocity and power dissipation of a tightly bolted panel "A", driven at its third mode, varies with driving force amplitude. The resonant frequency of this mode was found to be independent of amplitude, so that Fig. 21 pertains to a constant frequency. The third mode was selected for these studies because it was found to be the lowest one for which the response quantities could be measured with the available instrumentation. The mode number was ascertained by stroboscopic observation of the mode shape and by comparison of the observed with calculated resonance frequencies.

From Fig. 21 one may observe that the driving point velocity remains proportional to driving force up to a certain level, the "nonlinearity threshold". At a level of excitation somewhat above this threshold there occurs a response discontinuity, which was found to be associated with the occurrence of gross slip at the joint. When the drive was turned off after an experiment at such high excitation levels, one found that the plate did not return to its flat equilibrium position, but remained bowed. No such bowing was found for excitation below the "discontinuity" level indicated in the figure.

It is also interesting to note that the curve of power dissipation vs. driving force is essentially parabolic for low amplitudes, deviates from the parabolic nature at high amplitudes, and also exhibits a discontinuity where the velocity curve is discontinuous. The dependence of power dissipation on amplitude is shown more clearly in Fig. 22, which is essentially a cross-plot of the information in Fig. 21. The fact that the slope of the power-velocity curve is 2 indicates that the power dissipated varies as the square of amplitude, as in classical viscously damped systems or other systems with amplitude-independent loss factor.

Amplitude Effect in Loose Joint

In order to determine what effects, if any, interface pressure at the support may have on the character of the power dissipation characteristics, further measurements were made on a test panel that was more loosely bolted to its supporting jig. These measurements were carried out in the same manner as the previously reported ones, except that panel "C" was used here. Use of panel "C" instead of "A" results in a shift of the resonances to lower frequencies where the instrumentation has greater precision.

Figure 23 shows how the driving point velocity and the power dissipated at the third mode of panel "C" vary with driving force. This figure is analogous to Fig. 21, but pertains to a different test panel and a lesser bolt tightening torque. The character of

the curves of Figs. 21 and 23 is roughly the same. However, unlike for the tight joint of Fig. 21, the resonant frequency of the loose joint exhibited an amplitude dependence, as indicated at the top of Fig. 23. The resonant frequency was found to decrease with amplitude until about the onset of nonlinearity, to remain constant in the region of nonlinearity, and to increase again for amplitudes beyond the response discontinuity.

Figure 24, which is a cross plot of Fig. 23 and is analogous to Fig. 22, shows that here the slope of the power vs. velocity curve is 2.5; i.e., that the power dissipated here varies as $(\text{velocity})^{2.5}$. Thus, although the energy dissipating action of the previously discussed tight joint could be likened to ideal viscous and amplitude-independent damping, this is not the case for the present looser joint.

Effect of Frequency (Mode Number)

The effect of frequency or mode number on damping was investigated by use of both the decay rate and power dissipation measurement techniques. Results from both types of experiments on panel "C" are summarized in terms of loss factor in Fig. 25. Decay data at frequencies below the fundamental (105 cps) were obtained with lead masses bolted to the plate center. Figure 26 shows the power dissipation data* on which the corresponding loss factors indicated in Fig. 25 are based. Conversion of these data to loss factor form was accomplished by use of Eq. (14). More is said later about the discrepancy between the results obtained from decay and those from power measurements.

---

*For the measurements reported in Fig. 26 the test jig was suspended from strings instead of clamped to a column (to reduce possible energy losses via the attachment). All of the data of Fig. 26 are seen to fall reasonably well on lines having slopes of 2, indicating that power dissipated here increases as the square of amplitude. The data for the third mode at bolt torques of 4 and 20 in-lb are shown as falling along two linear segments; the offset between these is ascribed to phase shifts introduced by changes in amplifier gain settings and indicate a shortcoming of the instrumentation rather than information about the mechanical system under study.

Measurements like those summarized above for panel "C" were also carried out on panel "A"; results in terms of loss factor are shown in Fig. 27. Again, some discrepancy between the results from the two types of measurements may be noted. Power dissipation data appear in Fig. 28. These are confined to the first mode, because no measurable power dissipation levels could be attained for the higher modes with the (small) jig suspended from wires to reduce extraneous losses. The first mode data do lie along lines of slope 2, as previously observed for panel "A". No decay results for frequencies above the fundamental could be obtained from decay measurements either; the decay there occurred so rapidly and erratically that the available instrumentation was unable to cope with it.

Effect of Interface Pressure (Bolt Torque)

Figure 29 summarizes the dependences of loss factor on bolt torque implied by all of the previously presented and some additional data. It includes the results of decay, as well as of power dissipation measurements. Although the agreement between different measurements made for the same mode of the same panel is not too good, one may observe that all the various sets of measurements exhibit roughly the same trend. Increased bolt torque appears to result in decreased damping, with damping decreasing at a lesser rate for higher bolt torques.

Effect of Number of Edges Supported

Figure 30 summarizes the results of a series of experiments intended to resolve the question whether the dominant damping mechanism in the plate strips under discussion is associated with axial slip. These experiments consisted of two sets of decay-rate measurements on the same test panel. In one set the test panel was supported on the jig in the condition sketched in Fig. 19, i.e. attached at both its ends. In the other the test panel was attached as a cantilever to only one jaw, and the other jaw was removed from the test jig.

In these experiments the test jig was suspended at one of its ends from a long string. A small hand-held shaker supplied the excitation and was moved away from the test structure when decay was to be observed. A very light accelerometer was used, and great care was taken to ascertain that it did not influence the measured values. Measurements were taken at the first and second modes of the plate as a cantilever, and at the first mode of the panel on two supports. Measurements at frequencies lower than the cantilever fundamental were obtained with lead weights attached at the beam center.

Figure 30 again indicates a difference between the character of the damping of a "loose" joint (1 in-lb torque) and that of a "tight" joint. The loose joint exhibits a loss factor that is practically independent of support configuration. With higher tightening torques, on the other hand, higher loss factors are observed for the panel on two supports than for it supported as a cantilever. No amplitude dependence of loss factor was observed during the various cantilever tests, whereas for the panel on two supports amplitude-dependent damping was observed for amplitudes greater than some threshold value. The values shown in Fig. 30 pertain to amplitudes below this threshold, i.e. to amplitude-independent conditions.

In order to ascertain that the previously reported damping values are not associated with acoustic radiation or with inherent damping of the panel material, a panel identical to panel "A" was supported in a vise by a small stud welded to the panel center. The panel was excited by impact, and its loss factor was determined from decay measurements, using a microphone as a sensing device. A value somewhat less than 0.0002 was obtained.

Since one might expect two structural joints to produce twice as much damping as one, all other things being equal, it is instructive to look at the data of Fig. 30 in terms of the loss factor per joint. A corresponding plot is shown in Fig. 31. It appears that the single joint of the cantilever configuration provides more damping per joint than do the two joints supporting the plate in its regular configuration on the test jig. In the latter configuration longitudinal slip at the supports is promoted by the shortening of the projection of the panel onto the plane of the joints, whereas with the panel mounted as a cantilever this mechanism for the production of axial slip is absent. One may therefore conclude that longitudinal slip is not the dominant energy dissipation mechanism, at least for small amplitudes.

Critique of Experimental Results

The discrepancy between loss factor values obtained from vibration decay rate measurements and those computed from power dissipation data is troublesome. The decay rate technique is undoubtedly the more reliable one of the two. It is relatively simple, has been used extensively, and has the additional advantage that each loss factor reading is based on several repetitions of the experiment.

It is possible that a considerable fraction of the energy assumed to have been dissipated at the bolted joints was dissipated elsewhere. For example, the power dissipation measurements that were performed with the test jig bolted to a building column

may have been influenced by energy dissipated at the test jig connection or by energy transferred into the column and dissipated at some more remote location. It is also possible that some energy was dissipated at the connection between the test panel and the impedance head. (Power dissipation changes were observed for changes in the tightening torque applied to the bolt connecting the impedance head to the test panel.)

It is clear that resonances observed with the impedance head and shaker attached to the test panel are essentially resonances of the test panel with a lumped mass (impedance head plus shaker armature) attached at its center, and have associated with them different frequencies and mode shapes than one obtains for the panel in absence of mass loads. Since the mode shapes enter the calculations relating power dissipation to loss factor, as discussed below, errors in the mode shapes result in errors in the calculated loss factors. Although the mode shape properties for panels without mass loading were used in the calculations leading to the values plotted in Figs. 25, 27, and 29, it is believed that the associated errors are not so large as to be able to account for the magnitude of the discrepancies apparent in these figures.

Although the magnitudes derived from the power dissipation measurements reported here may be somewhat questionable, the trends indicated by them do appear to be valid and significant. The results of some additional experiments support this statement. One set of such experiments is summarized by Fig. 32. In this experiment the impedance head and shaker were mounted to move vertically. A 1/2-in thick plate was attached directly to the impedance head, and a test panel was attached to this plate at the ends. Thus, there were no supports present which might contribute energy leaks. The pertinent curve of Fig. 32 has the same character as that appearing in Fig. 22. (Also shown in Fig. 22 are results of a series of measurements aimed at establishing the "noise floor" of the system. These measurements were taken with only the thick or with only a single thin plate attached to the impedance head; i.e., without any joints that might contribute damping. It is clear that the damping data of Fig. 32 exceed this noise floor considerably.)

Data obtained with a stud inserted between impedance head and test panel "C" (instead of a direct bolted connection, as in all the previously reported results) are summarized in Figs. 33 and 34. These two figures correspond to Figs. 23 and 24, respectively, and pertain to the same nominal experiment, except for the aforementioned difference in the attachment. These two sets of figures are found to agree at least qualitatively.

ANALYTICAL RESULTS

One of the main reasons for undertaking the series of experiments described in the foregoing section was the hope that the experimental results would shed some light on the mechanisms involved in the energy dissipation processes. By comparing how the measured dependences of power dissipation on frequency and amplitude vary with the corresponding dependences obtained from analysis of several models one should be able to obtain some understanding of which energy dissipation mechanisms may and which may not be of primary importance.

Amplitude-Dependences of Power Dissipation for Several Mechanisms

In Appendix IV are derived relations between power dissipation and amplitude for center-driven and end-supported plate strips representative of the experimental configuration shown in Fig. 19, and for various energy dissipation mechanisms assumed to act (one at a time) at the supported ends.

The mechanisms considered (either explicitly in Appendix IV, or implicitly by simple extensions of results presented there) are listed in Table II, together with the amplitude-dependences they imply.

Frequency Dependences of Power Dissipation

The dependences of power dissipation on frequency implied by the end supported panel strip configuration and the various damping mechanisms are rather complicated. They are influenced by the frequency-response characteristics of the strip, as discussed in Appendix IV, as well as by the frequency-dependences inherent in the dissipative mechanisms themselves.

No further discussion of the frequency dependences implied by the analyses of Appendix IV is included here, because of the aforementioned complexity of the analytical results and since adequate power dissipation data are not available for a sufficiently wide frequency range to permit comparison of theory and experiment.

TABLE II

RELATION BETWEEN POWER DISSIPATION P_d AND PLATE-STRIP MIDPOINT DEFLECTION AMPLITUDE Y, FOR VARIOUS MECHANISMS ACTING AT SUPPORTS: $P_d \propto Y^n$

Energy Dissipation Mechanisms	Exponent n
I Mechanisms associated with relative motion tangential to interface	
A. Coulomb friction	
1. Rigid strip ends, slipping fully*	2[a]
2. Elastic strip ends, slipping over part of contact area	4 to 6[b]
B. Shear of thin layer of asperities	
1. Perfectly plastic layer	2[a]
2. Work-hardening plastic layer	>2[a]
3. Viscoelastic layer	4
C. Viscous friction over entire interface	4
II Mechanisms associated with rotation and relative motion normal to interface, rigid strip ends	
A. Coulomb friction associated with relative motion of asperities, motion normal to interface	1[a]
B. Compression of thin layer of asperities	
1. Viscoelastic layer	2
2. Perfectly plastic layer	1 to 2[a]
C. Viscous friction associated with relative motion of asperities motion normal to interface	2

*Corresponds to Mentel's Analysis (Ref. 12).

a Value shown applies above threshold amplitude for occurrence of mechanism.

b Depends on friction distribution.

Relation Between Loss Factor and Power Dissipation

The loss factor η_s of a structure may be defined as the ratio of the energy dissipated per radian (or per cycle/2π) during steady or slowly decaying vibration to the "energy of vibration" W (Ref. 10). From this definition one may establish that the loss factor is related to the dissipated power P_d as

$$\eta_s = P_d/\omega W \quad , \tag{8}$$

where ω denotes the radian frequency of the vibration.

For systems that are relatively lightly damped the "energy of vibration" W is the total (kinetic plus potential) energy contained in the system at any instant and is equal to the time-wise maximum kinetic energy. If the plate-strip's deflection amplitude distribution is given by y(x), where x is measured in the length-wise direction, then the maximum kinetic energy of the plate is

$$W_P = \frac{m}{2}\,\omega^2 \int y^2\, dx \quad , \tag{9}$$

where m denotes the strip's mass per unit length and the integration is taken over the entire plate strip. If a lumped mass M is attached to the plate strip at $x=x_M$, then it contributes the additional kinetic energy

$$W_M = \frac{M}{2}\,\omega^2 y^2(x_M) \quad . \tag{10}$$

Thus, by inserting the total kinetic energy for W in Eq. (8) one may write

$$\eta_s = \frac{2\,P_d}{\omega^3 [m\int y^2 dx + M\, y^2(x_M)]} \quad . \tag{11}$$

Evaluation of the deflection amplitude distribution y(x) is discussed in Appendix IV. There it is also shown that for the odd-numbered modes of beams or plate strips that are clamped on both ends (approximating the previously discussed experimental conditions) one finds

$$m\int y^2\, dx \approx \frac{1}{2}\, M_b\, Y_o^2 \quad , \tag{12}$$

where M_b denotes to total mass of the beam and Y_o the deflection amplitude of the mid-point. For an added concentrated mass attached at the mid-point (as was the mass of the impedance head and shaker armature in the previously discussed experiments), Eq. (11) may be written

$$\eta_s \approx \frac{4\ P_d}{\omega^3 Y_o^2 (M_b+2M)} = \frac{2\ P_d}{\omega\ V_{rms}^2 (M_b+2M)} \qquad (13)$$

where $V_{rms} = \omega\ Y_o/\sqrt{2}$ is the root-mean-square velocity of the mid-point.*

Although addition of a mass may be expected to alter the resonant deflection amplitude distribution to some extent, this alteration is expected to produce only relatively minor changes in values one would compute from Eqs. (12) and (13).

Comparison of Support Effects on Cantilever and Clamped-Clamped Beams

It is of some concern whether comparisons of measured loss factor data for cantilever and for doubly clamped plate strips (or beams) can be made legitimately, and whether any correction factors must be used in such comparisons.

An analysis presented in Appendix IV shows that the energy of vibration of a beam mounted as a cantilever is very nearly equal to that of the same beam in a clamped-clamped condition, provided the beam is vibrating at the same frequency (but in any mode**) in both cases and at amplitudes that produce the same

---

* Any consistent system of units may be applied to Eq. (13). For P_d in watts, V_{rms} in m/sec, M_b and M in pounds, and f in cycles/sec, (units in which experimental data have been presented here) Eq. (13) becomes

$$\eta_s \approx 0.35\ P_d/f\ V_{rms}^2 (M_b+2M) \quad . \qquad (14)$$

For the shaker and impedance head used in the reported experiments, M ≈ 0.315 lb.

**Except the cantilever fundamental. See Appendix IV.

bending moment at the supports in both cases. From Appendix IV one observes that equality of bending moments under the aforementioned conditions also implies equality of the shear forces at the supports. One may thus conclude that damping mechanisms that depend on the support moments and/or forces will produce the same energy dissipation for the two mounting conditions. One would then expect the loss factor per support to be the same for a clamped-clamped beam as for a cantilever, for the same support-moment. If experimental data show the loss factor to be essentially independent of amplitude (or support moment), then the loss factor of a clamped-clamped beam should be twice that of a cantilever.

POSSIBLE MECHANISMS

Implications of Observed Amplitude-Dependences

By comparing the amplitude-dependences of power dissipation predicted analytically for the various postulated damping mechanisms with the experimentally observed dependences one may determine which of the mechanisms studied analytically cannot dominate the damping of edge-supported plate strips. Experimentally, dissipated power was found to vary as the square of mid-point amplitude for tightly bolted edges and as approximately the 2.5 power for loosely bolted edges (Figs. 22, 24). By referring to Table II one may then conclude that some of the models listed there cannot represent the primary energy dissipation mechanisms in tightly bolted edges, because they lead to dependences of dissipated power on amplitude that are characterized by exponents that differ markedly from 2.0.

The following models of the mechanisms listed in Table II are characterized by exponents of about 2.0 and thus may dominate the energy dissipation in tight joints:

I. Mechanisms associated with relative motion tangential to interface

   A.1 Coulomb friction, with rigid strip ends slipping fully

   B.1.,2. Shear of perfectly plastic or slightly work-hardening layer of asperities.

II. Mechanisms associated with relative motion normal to interface

   B.1.,2. Compression of thin viscoelastic of perfectly plastic layer of asperities

   C. Viscous friction between inter-leaving asperities.

Some of the mechanisms listed in Table II result in exponents that are greater than 2.0. Although these mechanisms cannot dominate the damping behavior of tight joints, they may make some contributions to the damping of loose joints, and thus help to produce exponents that exceed 2.0. Mechanisms for which Table II lists exponents of the order of unity can play no significant role in either the tight or the loose joints studied experimentally.

Dominance of Normal Relative Motion

The experimental results summarized in Figs. 30 and 31 provide a comparison of the damping of a plate-strip with both ends bolted to a rigid structure to the damping of the same plate-strip fastened in cantilever fashion (i.e., at only one end). If axial relative motion played a significant role one would expect to obtain considerably higher damping when the plate is fastened at two ends than when it is fastened at only one, since in the two-support condition axial relative motion tends to be produced when the strip is deflected laterally. Since no such higher damping was observed it appears extremely likely that at the low amplitudes studied the dominant mechanism is not associated with tangential (axial) relative motion of the mating surfaces at the supports.

For damping mechanisms that depend only on the moment and/or normal force which a plate-strip exerts on its support(s) a plate strip supported on two edges exhibits twice the loss factor it has when supported as a cantilever (if material damping is small). In other words, the loss factor per supported edge for such mechanism is the same for both support conditions. Figure 31 indicates that this condition is approached for tightly bolted edges, but not for loosely fastened ones.

The dependence of damping on bolt torque evident from Fig. 29 shows that joint tightness has a definite effect on damping, with tighter joints resulting generally in lesser energy dissipation. Increased tightness is likely to result in lesser relative motion at the joint and thus to reduce the energy dissipation associated with virtually any mechanism. The available data do not permit one to judge whether joint tightness has any direct effect on the mechanism as such.

Conclusions

In view of the previously discussed results it appears reasonably likely that for tight joints the dominant mechanism here is due to relative motions of the mating surfaces in directions normal to the interface, and that the damping associated with these motions acts essentially like classical viscous damping. The primary effect of increased interface pressure probably is the reduction of the aforementioned relative motion, thus leading to reduced damping.

The damping behavior of "loosely" supported edges appears to be somewhat different from that of tightly supported edges. Mechanisms associated with tangential motions may contribute significantly to the energy dissipation in loose joints, even at very small amplitudes.

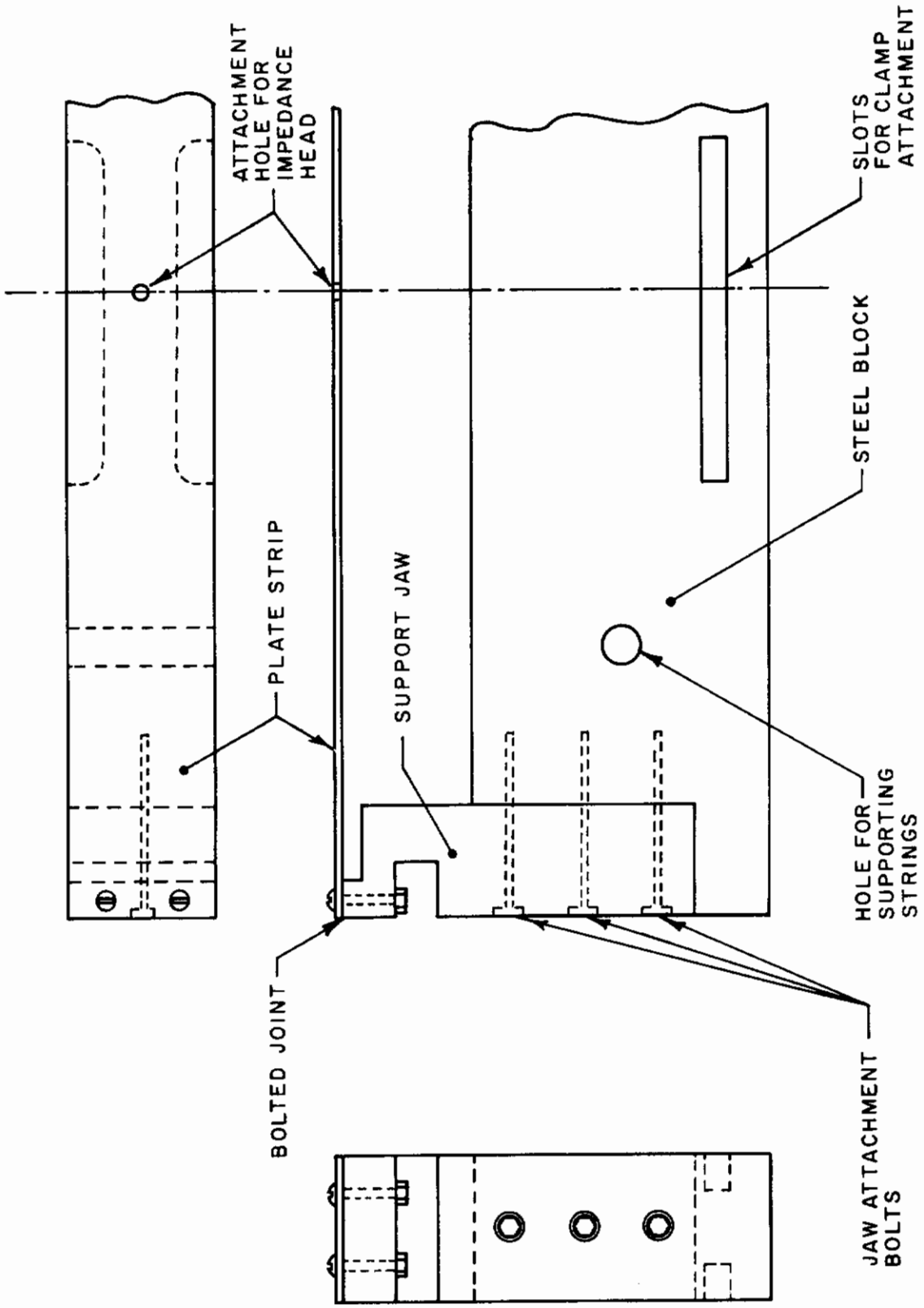

FIG. 19 TEST JIG FOR STUDY OF BEAM-PLATE JOINT DAMPING

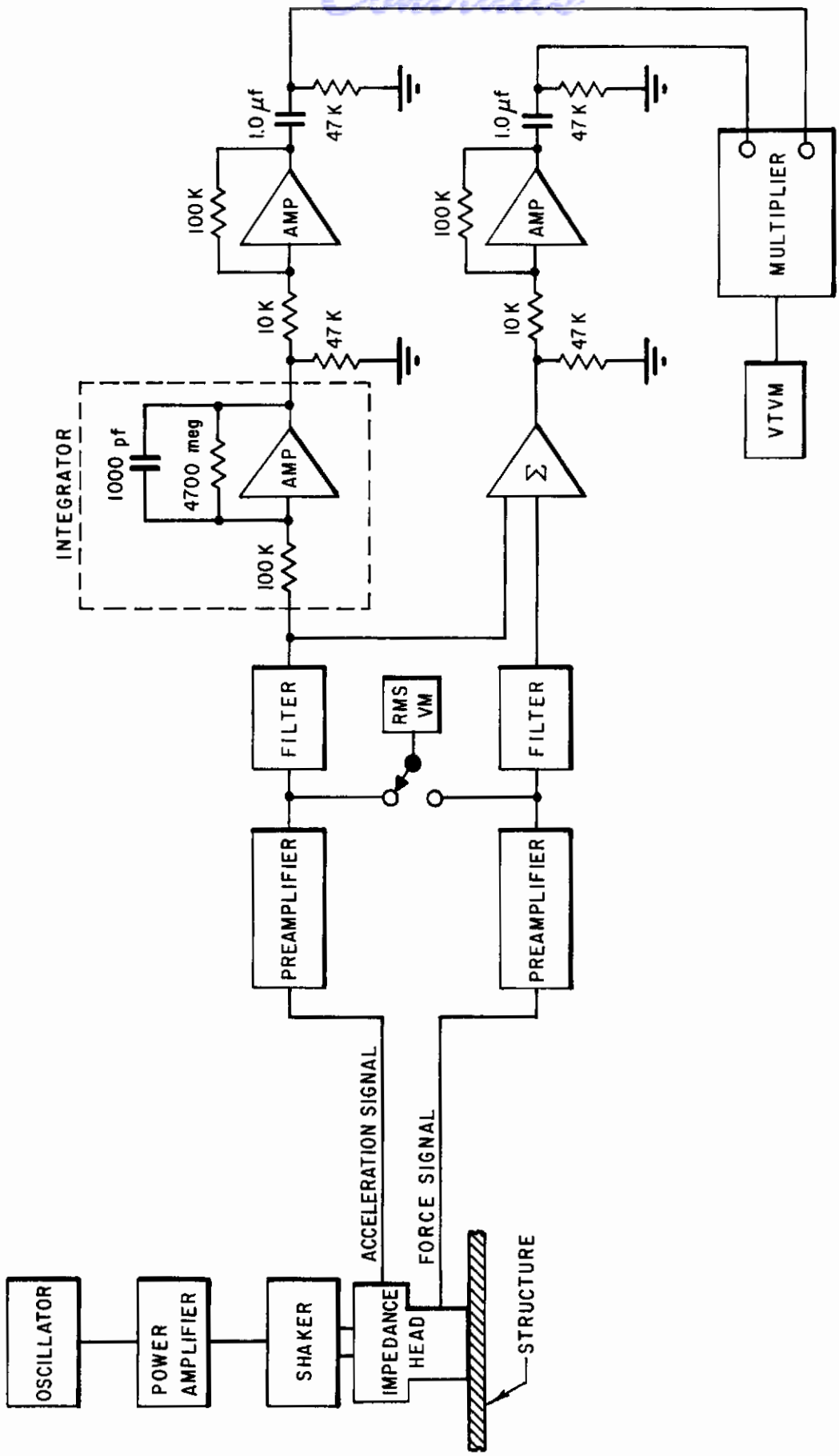

FIG.20 POWER INPUT MEASUREMENT INSTRUMENTATION
(SEE INSTRUMENTATION LIST ON NEXT PAGE)

TABLE III

Instrumentation List for Fig. 20

Component	Manufacturer	Designation and Model No.
Oscillator:	Hewlett-Packard	"Low Frequency Oscillator," Model 202C
Power Amplifier:	McIntosh	Model MC-30
Shaker:	Goodman	"Vibration Generator," Model 390A
Impedance Head:	Wilcoxon	"Impedance Head," Model Z602
Preamplifier(s):	General Radio	"Sound Level Meter," Type 1551-C
Filter(s):	Spencer-Kennedy Laboratories	"Variable Electronic Filter," Model 308A
RMS VM:	Ballantine Laboratories	"RMS Voltmeter," Model 420
Σ :	Bolt Beranek and Newman Inc.	"Sum or Difference Amplifier," Model 333A-1
Amplifier(s):	GAP/R	"Amplifier," Model UPA-2
Multiplier:	GAP/R	"Multiplier," Model MU
VTVM:	Hewlett-Packard	"Vacuum Tube Voltmeter," Model 412A

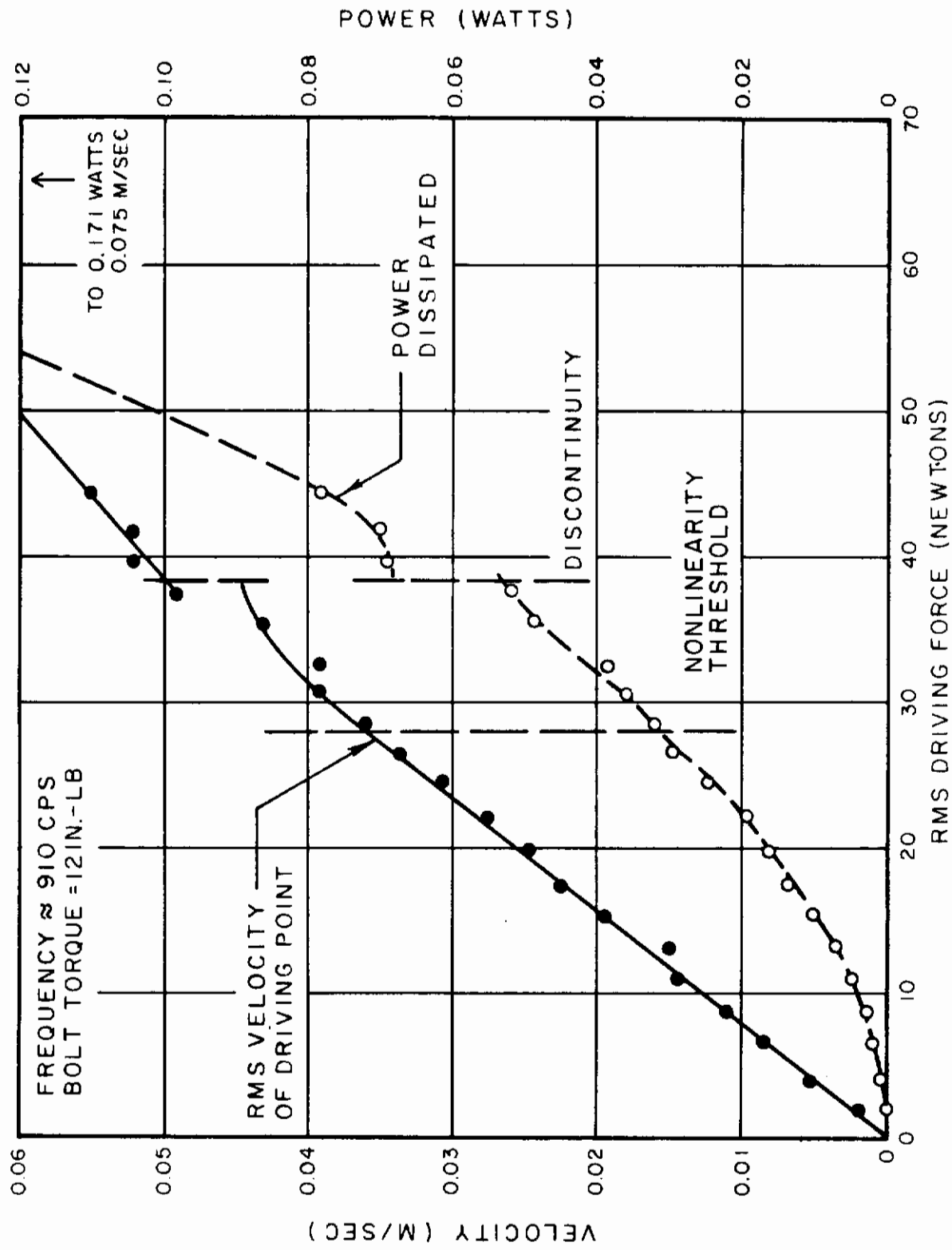

FIG.21 AMPLITUDE EFFECTS ON 3rd MODE RESPONSE OF TIGHTLY BOLTED PANEL "A"

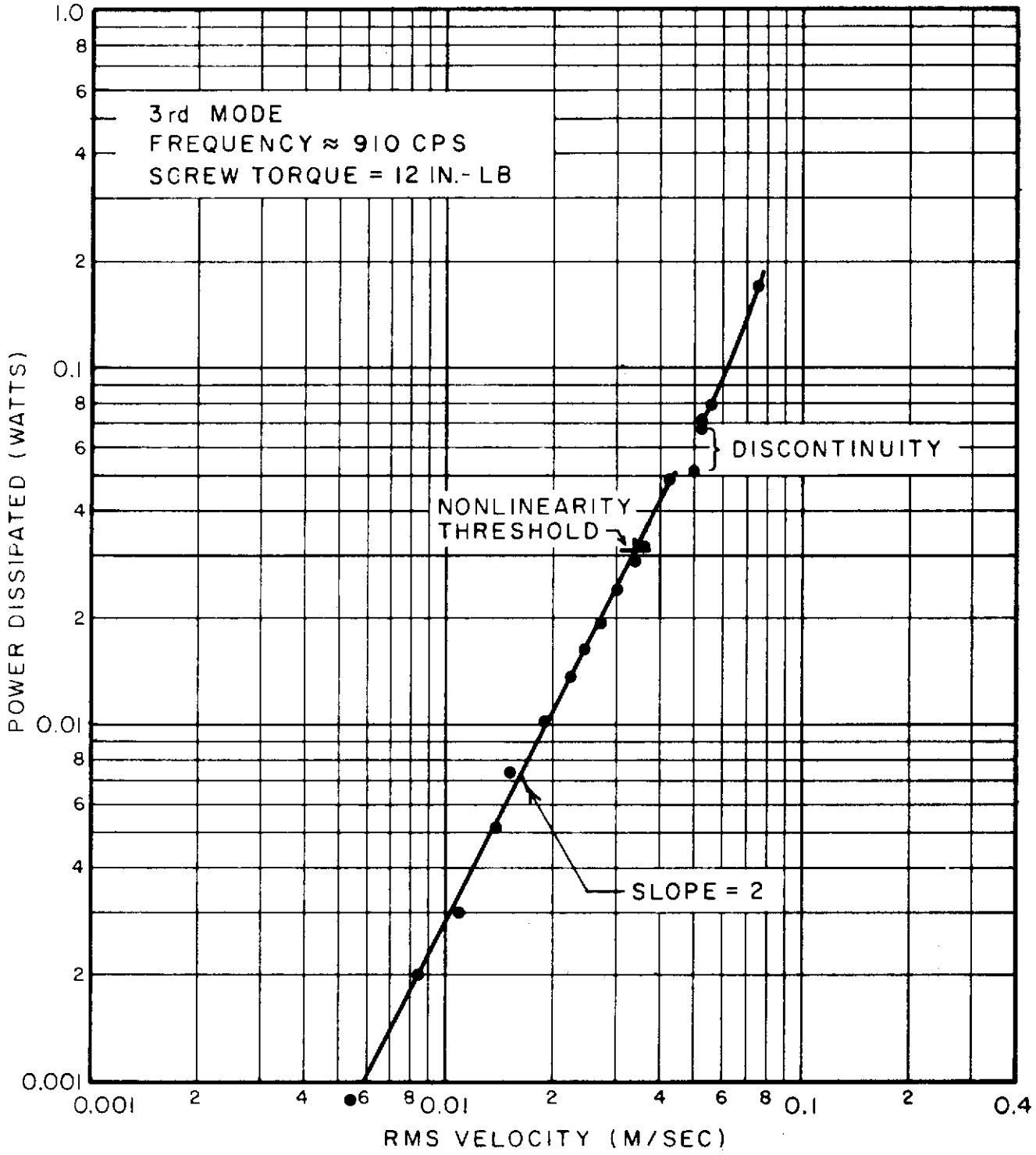

FIG. 22 POWER DISSIPATION AS A FUNCTION OF AMPLITUDE FOR 3rd MODE OF TIGHTLY BOLTED PANEL "A"

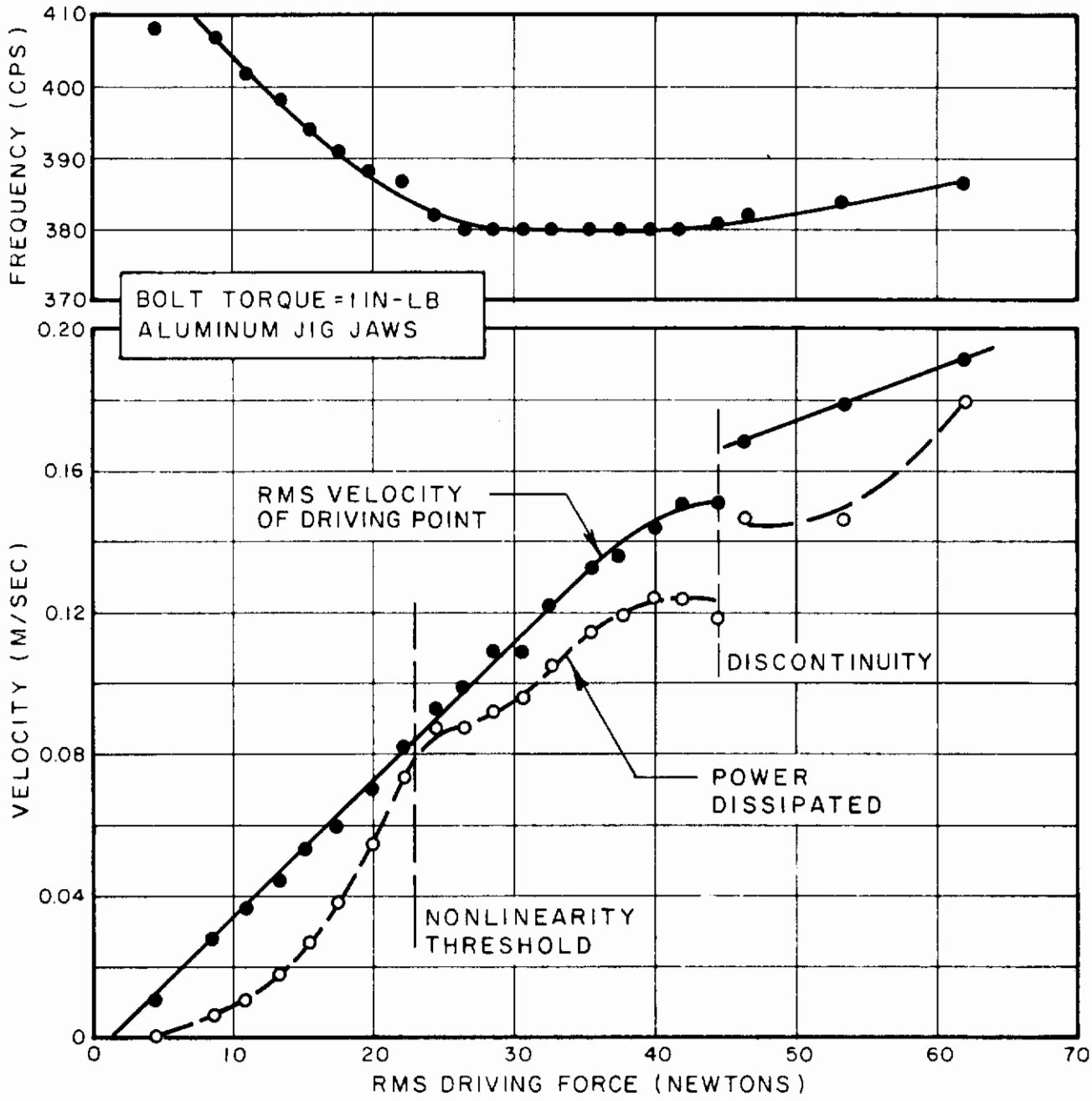

FIG. 23 AMPLITUDE EFFECTS ON 3rd MODE RESPONSE OF LOOSELY BOLTED PANEL "C"

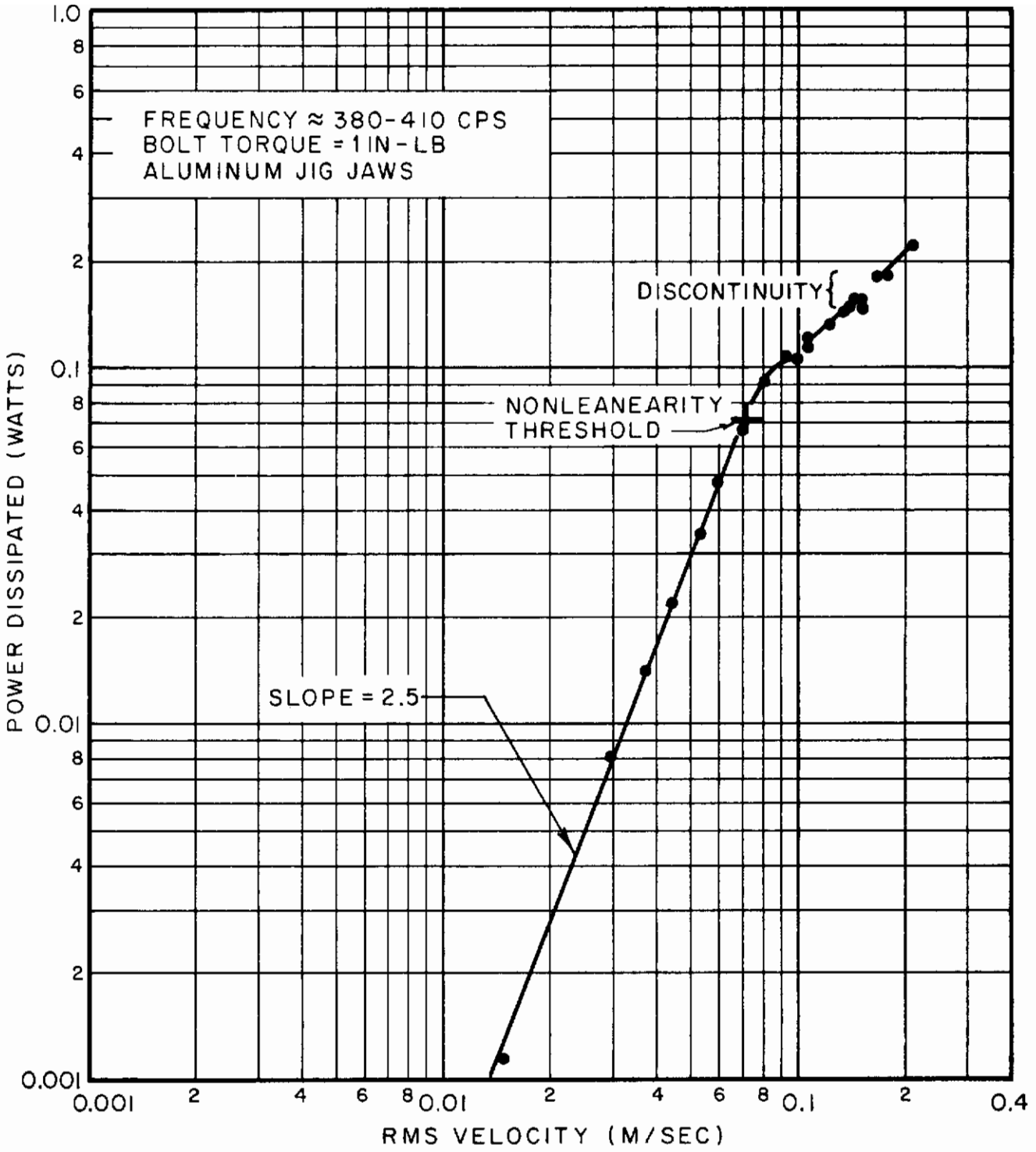

FIG. 24 POWER DISSIPATION AS A FUNCTION OF AMPLITUDE FOR 3rd MODE OF LOOSELY BOLTED PANEL "C"

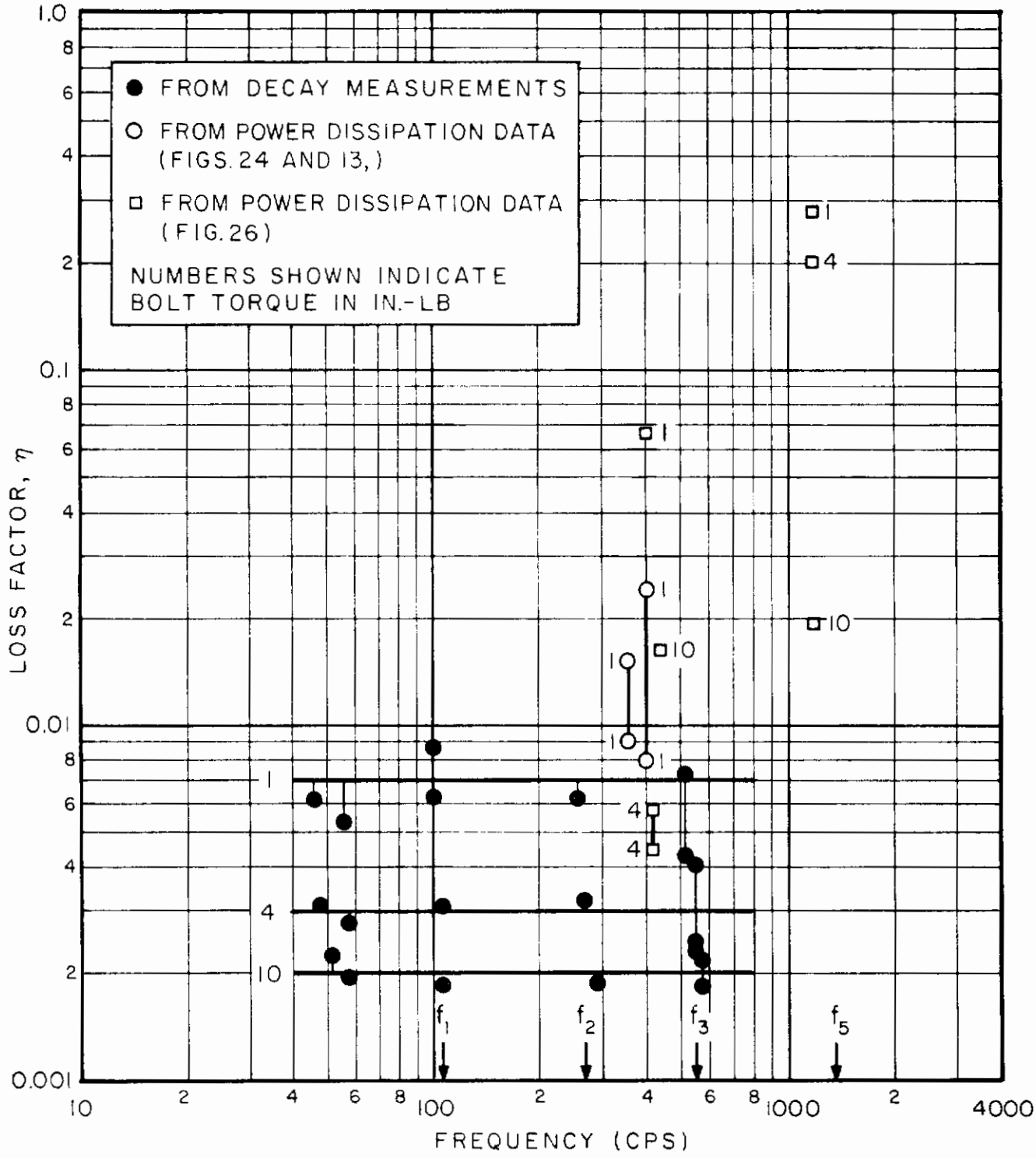

FIG. 25 MEASURED FREQUENCY-DEPENDENCE OF DAMPING, LOOSELY BOLTED PANEL "C"

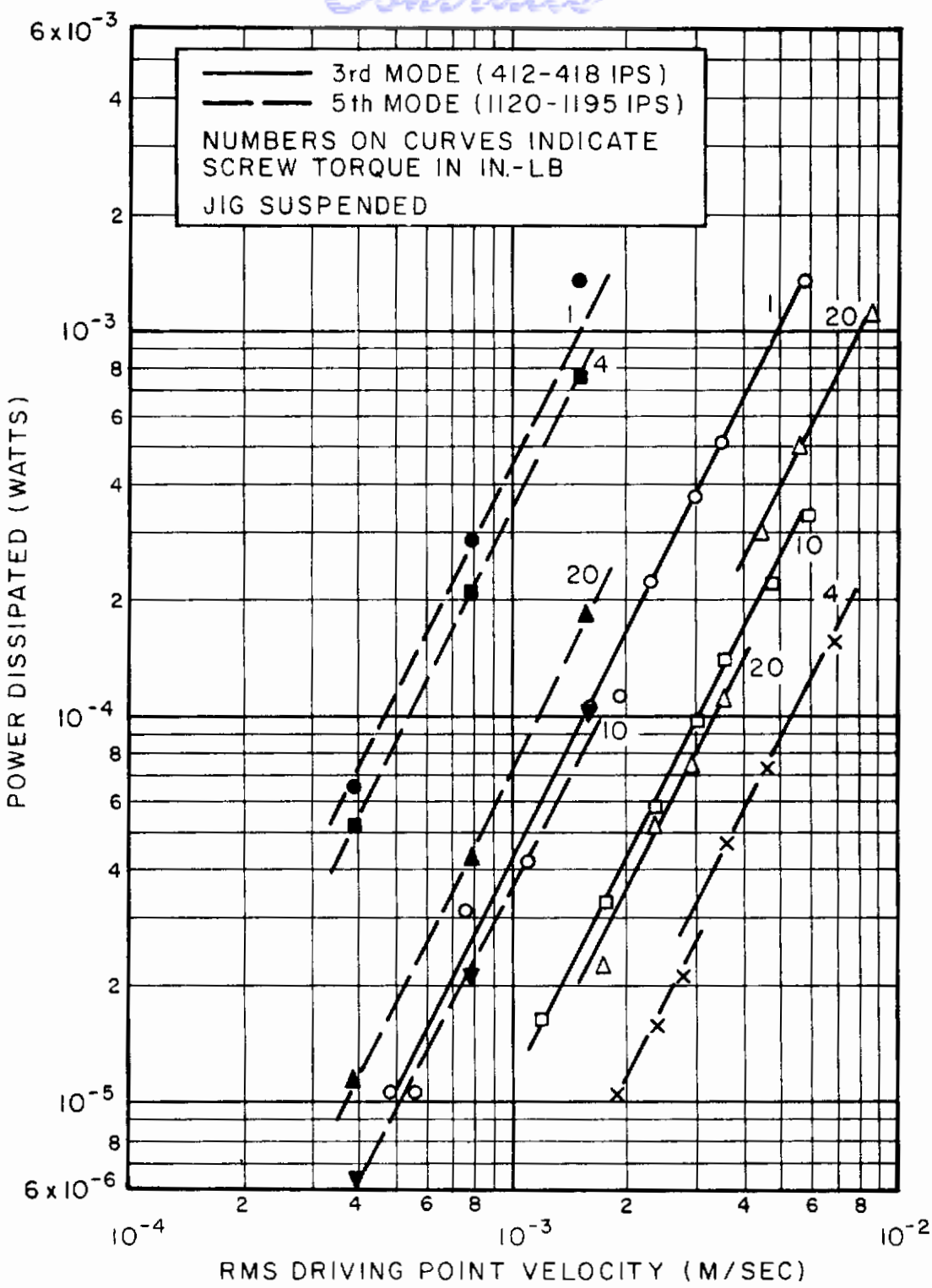

FIG. 26 MEASURED POWER DISSIPATION AS FUNCTION OF AMPLITUDE, 3rd AND 5th MODES OF PANEL "C"

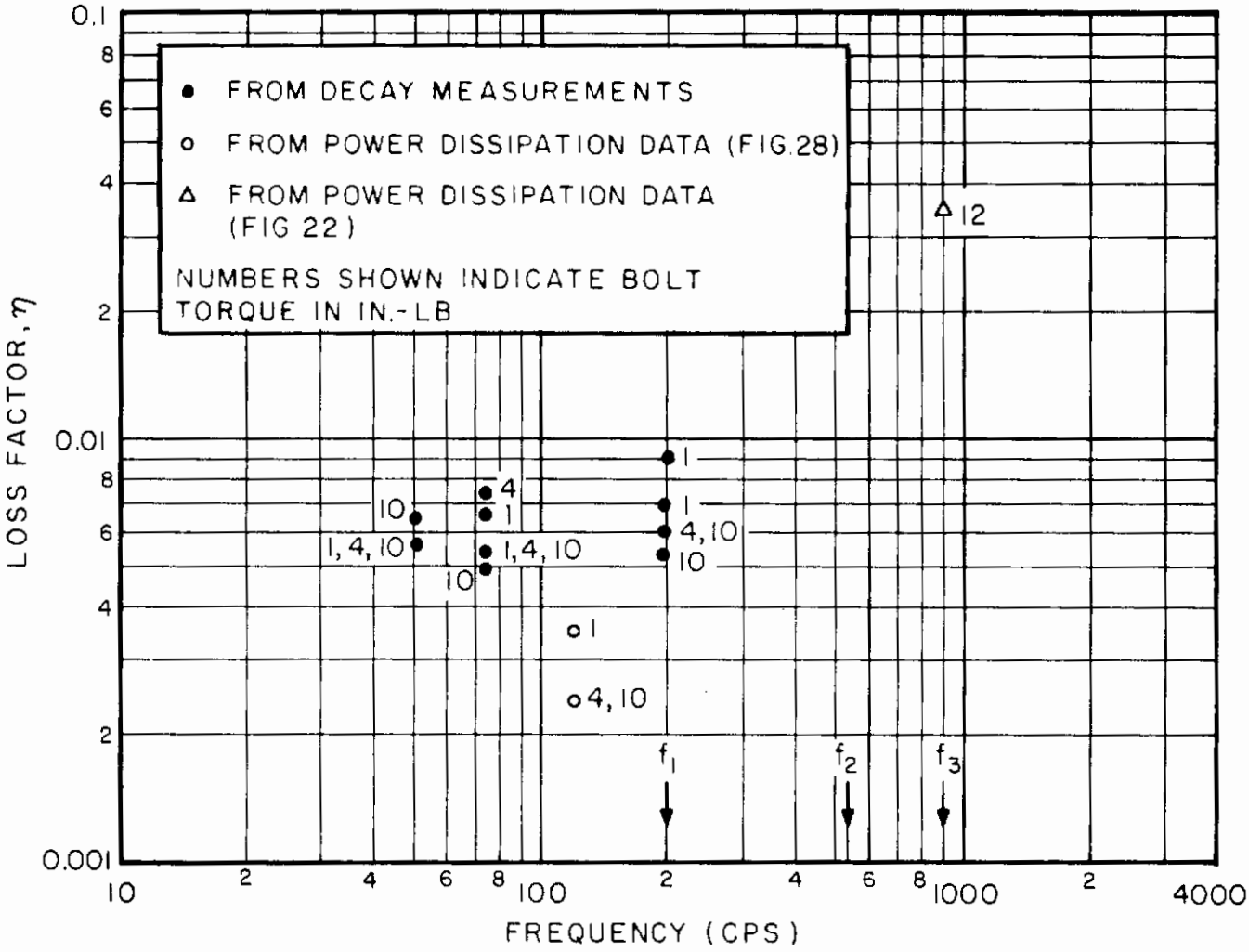

FIG. 27 MEASURED FREQUENCY-DEPENDENCE OF DAMPING, PANEL "A"

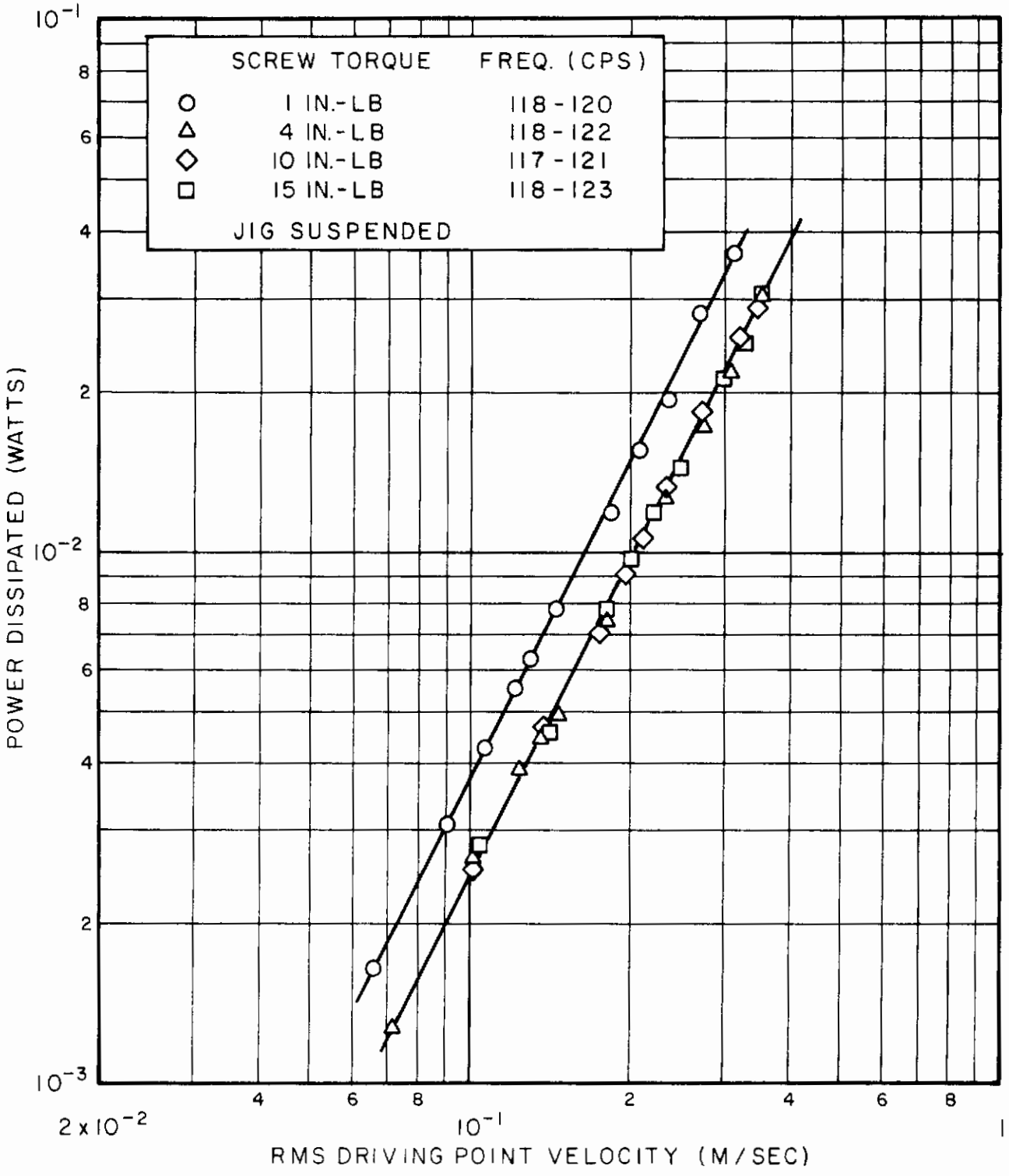

FIG.28 MEASURED POWER DISSIPATION AS A FUNCTION OF AMPLITUDE, FIRST MODE OF PANEL "A"

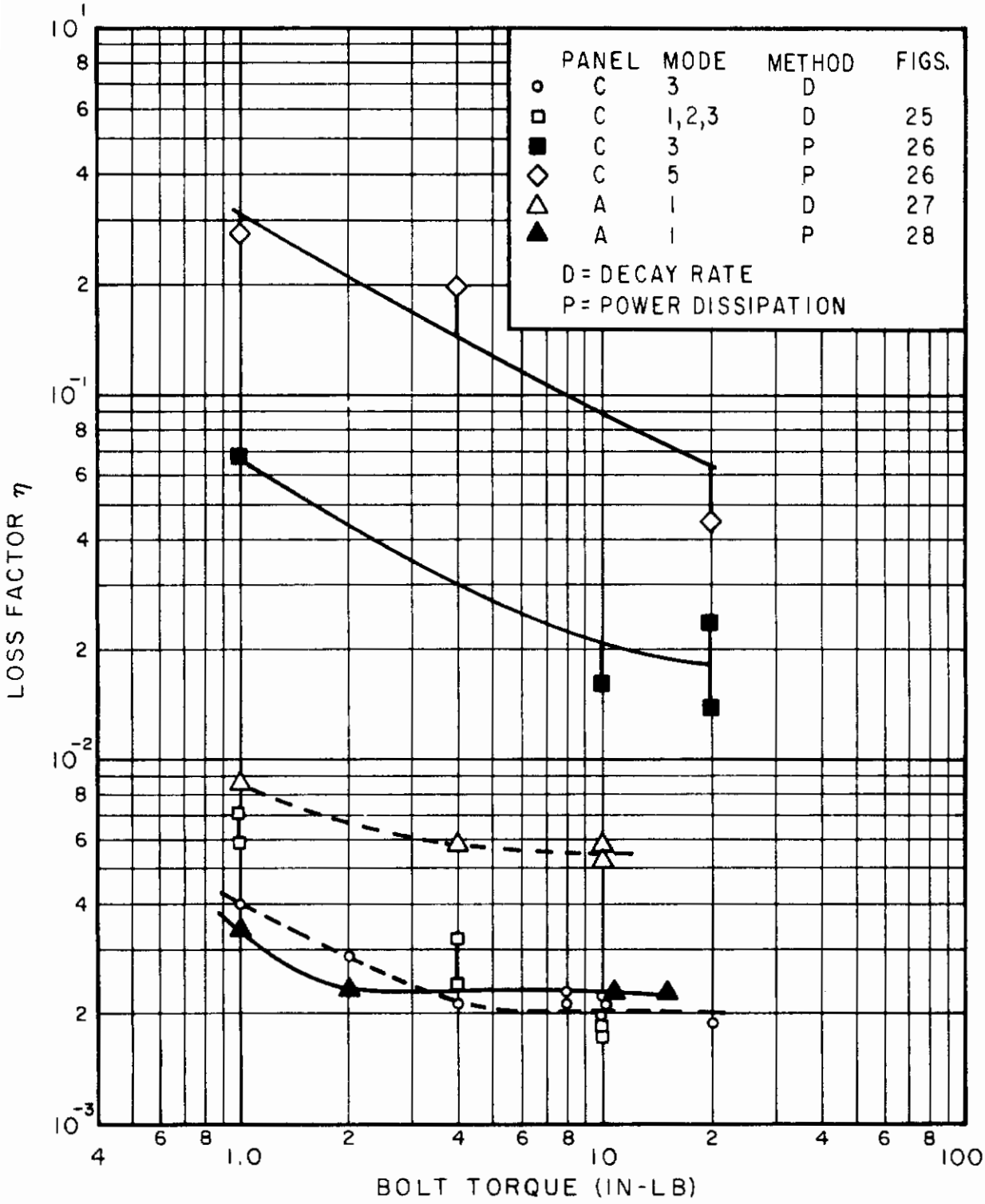

FIG. 29 EFFECT OF BOLT-TORQUE ON MEASURED LOSS FACTORS

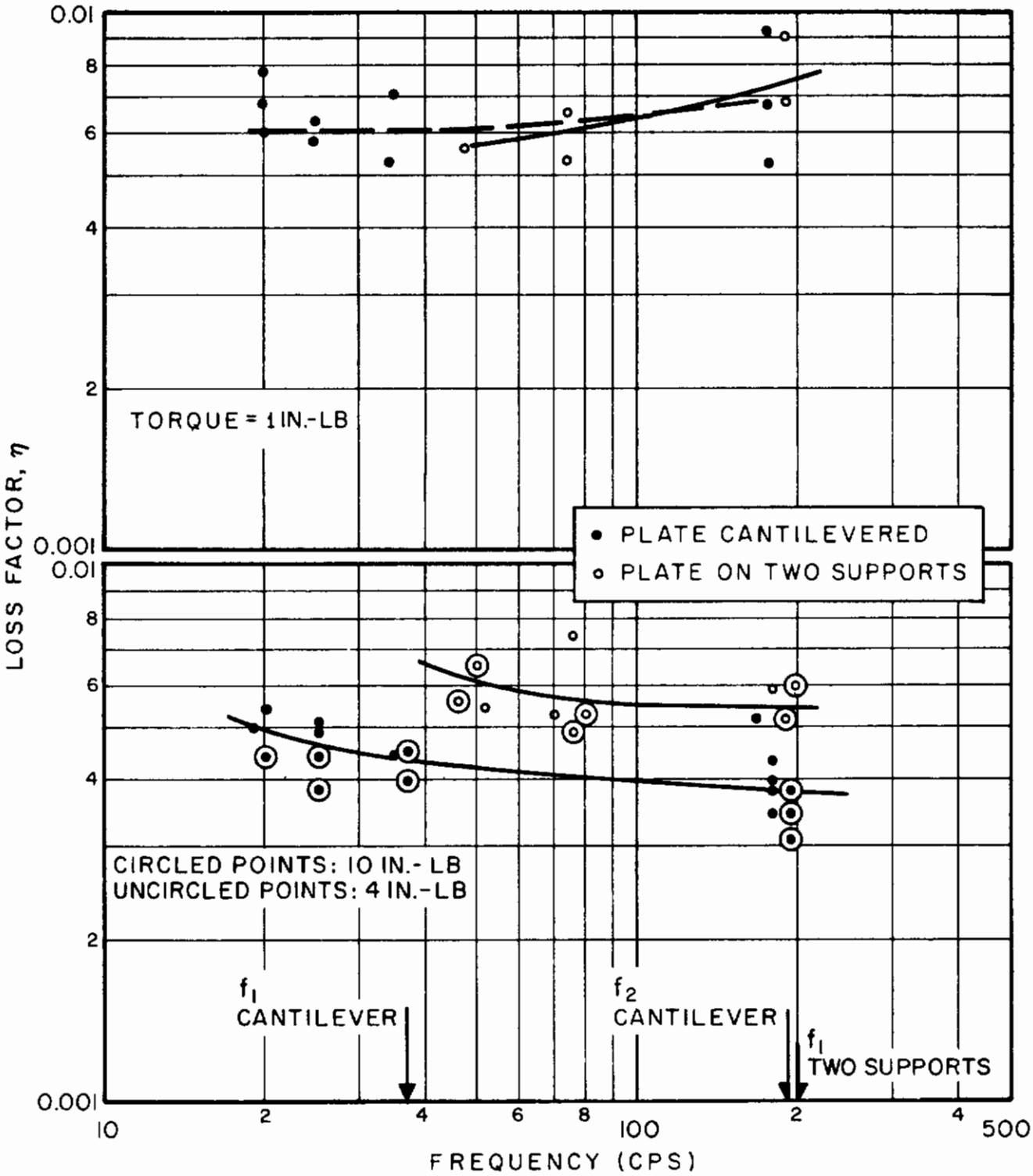

FIG.30 MEASURED DAMPING OF PANEL "A" CANTILEVERED AND ON TWO SUPPORTS

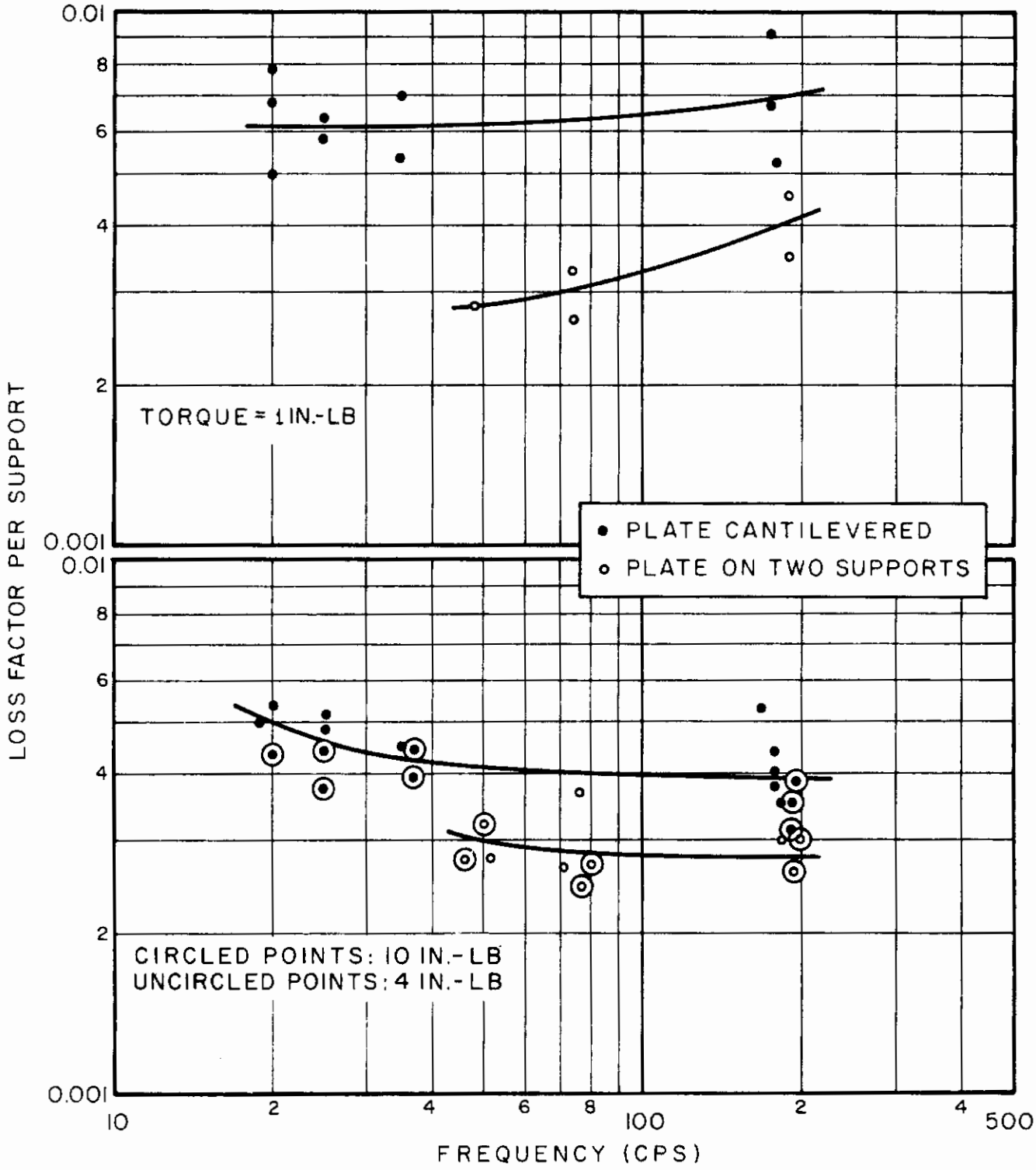

FIG. 31 DAMPING CONTRIBUTION PER SUPPORT, PANEL "A"

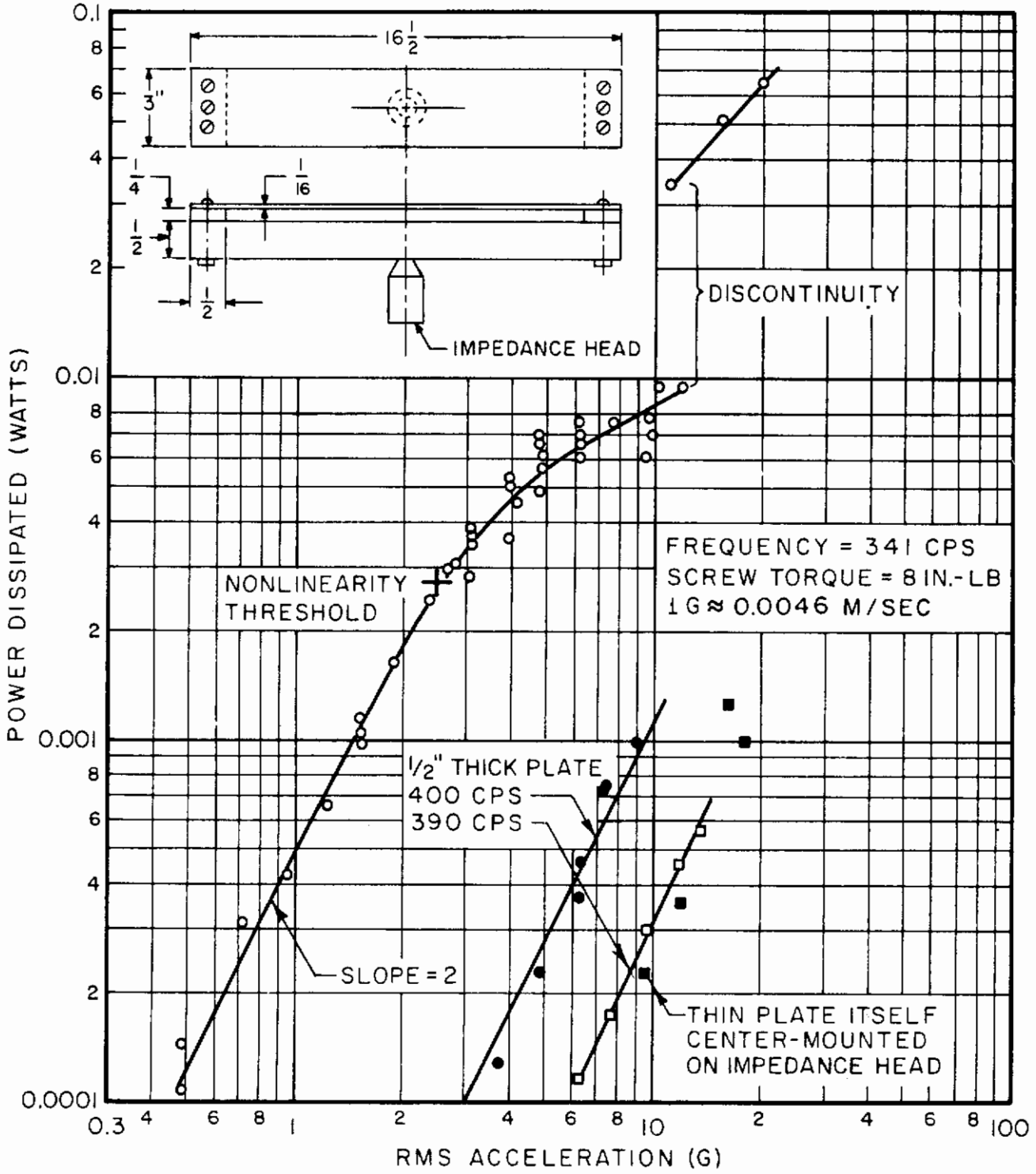

FIG. 32 POWER DISSIPATION AS A FUNCTION OF AMPLITUDE FOR 3rd MODE OF PANEL DRIVEN AT EDGES VIA THICK PLATE

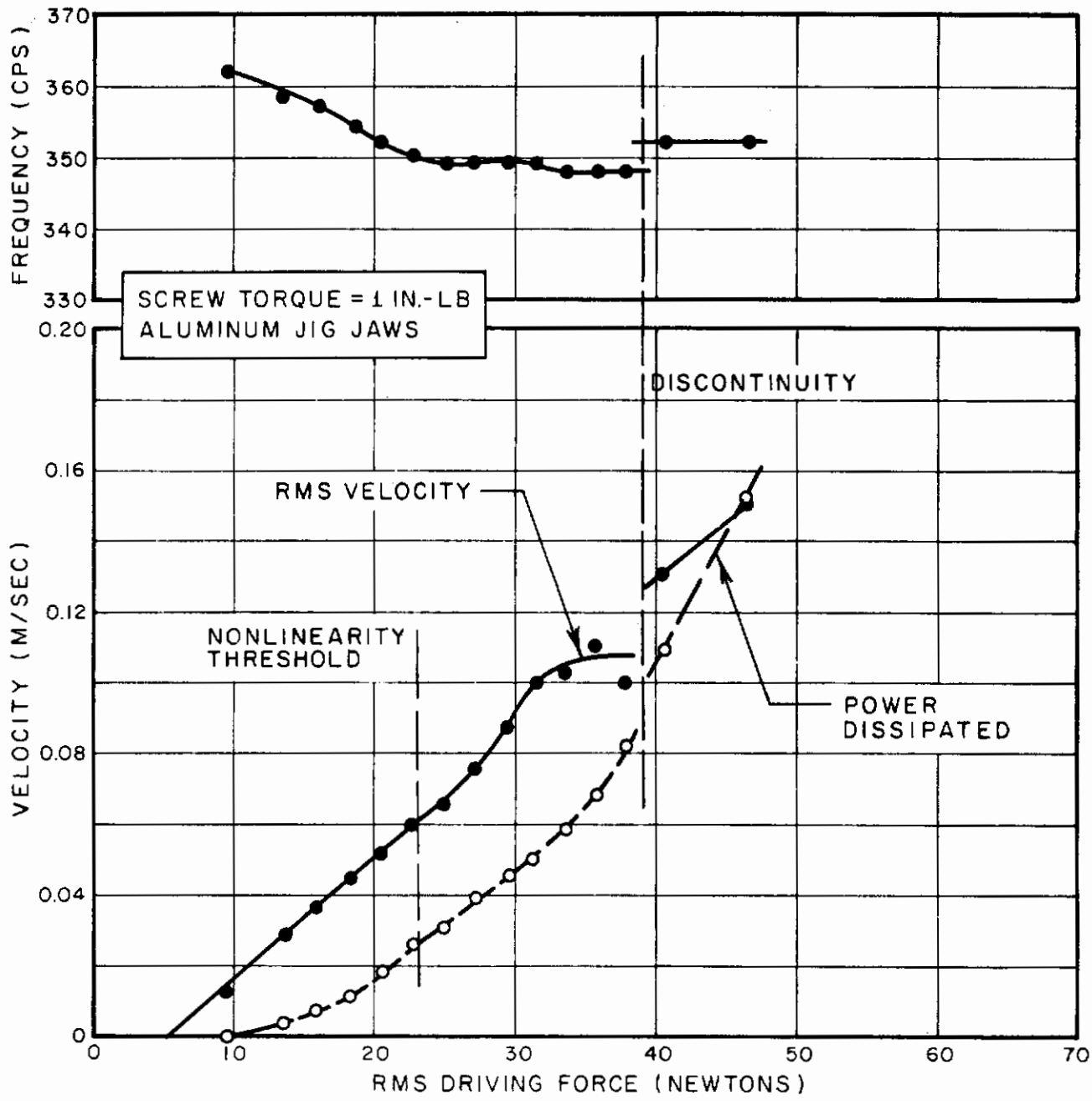

FIG. 33 EFFECT OF AMPLITUDE ON 3rd MODE RESPONSE OF PANEL "C", MEASURED WITH STUD CONNECTING IMPEDANCE HEAD TO PANEL

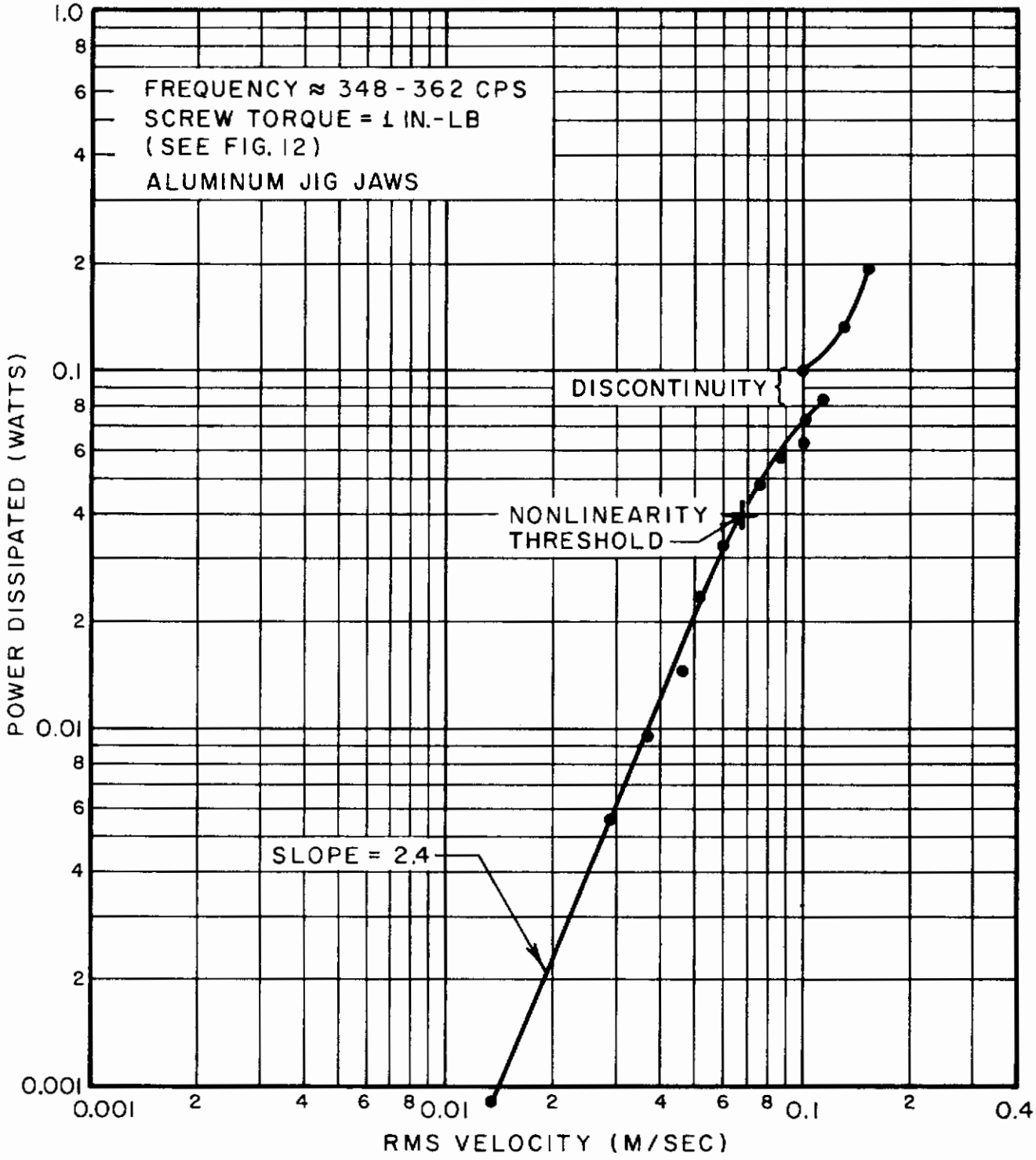

FIG. 34 POWER DISSIPATION AS A FUNCTION OF AMPLITUDE FOR 3rd MODE OF PANEL "C", MEASURED WITH STUD CONNECTING IMPEDANCE HEAD TO PANEL

CONCLUSIONS

SUMMARY

Plate-Stiffener and Plate-Plate Joints

The dominant mechanism responsible for energy dissipation at structurally acceptable multi-point-connected joints between plates and stiffening members or between two plate portions, at frequencies considerably above the plate fundamental, has been shown to be associated with "pumping" of air produced by motions of the mating surfaces between connectors away from and toward each other. These motions have been demonstrated to depend primarily on the ratio of plate flexural wavelength to connector spacing. The attendant damping has been found to be relatively insensitive to changes in connector tension (i.e., in local interface pressure) and details.

Proportionality of a joint's damping contribution to total joint length has been verified, and the applicability of Heckl's absorption coefficient concept has been demonstrated. The additional observation that the absorption coefficient of a beam-plate joint is approximately proportional to the joint (interface) width has been made the basis for definition of a width-independent reduced absorption coefficient. The theoretical relation between plate flexural wavelength and frequency has been used to define a reduced frequency parameter proportional to the square of the ratio of bolt spacing to wavelength. Since it has been found that most of the experimental data falls in a reasonably narrow region of a plot of reduced absorption coefficient vs. reduced frequency, it has been suggested that plots of this type be used to predict the damping of beam-plate and plate-plate systems.

Continuously welded joints have been found to produce very little damping. The loss factor of a plate with welded joints thus is essentially the same as that of a continuous joint-less one.

Edge-Riveted Structures

The mechanism dominating the low frequency energy dissipating action at panel edges bolted to rigid supporting structures has not been fully identified. Analyses and experiments making use of a relatively new mechanical-power-dissipation measurement system have indicated, however, that some mechanisms previously thought likely to act at such joints cannot account for the observed behavior.

The damping behavior of tight joints has been found to differ somewhat in character from that of relatively loose joints. It has been shown that the damping of tight joints is likely to be due to relative motions at the joint which are perpendicular to the mating surfaces, and that the damping action is essentially of a viscous nature. Slip at the interface has been shown to play no important role in tight joints, but may contribute to the damping at loose joints.

DISCUSSION

Some Implications of Results

The dominance of the air-pumping mechanism in conventional multi-point-connected plate-stiffener and plate-plate joints implies that one cannot rely on such joints to control the high frequency vibrations of skin structures of vehicles (or vehicle portions) operating in regions of reduced air pressure. It also appears that therefore tests of such structures at ground-level pressures may underestimate the vibratory responses at altitude, thus leading to non-conservative design or to an overestimate of the factor of safety of a given structure. Use of a low-viscosity lubricant in such joints may result in the maintenance of reasonable damping levels independent of ambient pressure.

The effects of the damping due to structural joints must also be taken into account in the construction of dynamic models and/or in the interpretation of model test results, unless damping mechanisms other than those associated with joints predominate. Continuously welded or bonded joints cannot reproduce the damping action of riveted, bolted, or spot-welded joints. Properly modeled joints must be of the multi-point-connected variety and must have the same fastener-spacing to panel-thickness ratio as the prototype structure if their damping is to have the proper scaled frequency-dependence. It may also be necessary to adjust the ambient atmospheric pressure in order to obtain representative damping magnitudes in models.

Although the precise way in which air pumping dissipates energy is not known, it appears possible that atmospheric pressure increases or the presence of ambient media other than air may produce significant damping increases. If such increases can be realized, appropriately designed joints incorporating them may provide light and efficient means for increasing the damping of sealed (or pressurized) components or instrument packages.

Further Studies Suggested

The work described in the present report provides one with information from which one may estimate the energy dissipation capability of a large class of structural joints of practical importance. However, in calculating the response of a substructure which is part of a larger structure and relatively intimately connected to other substructures, one generally needs to know how much energy is transferred away from the substructure of interest in addition to how much energy is dissipated. Simple and reliable means for predicting energy conduction in realistic structures still need to be developed.

The aforementioned air pumping mechanism is still insufficiently understood. One cannot state at this point whether frictional losses in the air, acceleration of air masses, or some other mechanism, is primarily responsible for the energy dissipation. The effects of changes in properties of the ambient fluid and of higher than atmospheric ambient air pressures still remain to be investigated.

Additional studies, perhaps using more sensitive instrumentation and test systems, are also required in order to identify more fully the prime mechanisms responsible for energy dissipation in edge-bolted panels. The effects of ambient pressure changes, surface finish, and overlap width and rigidity would appear to be of particular interest here. Estimation techniques for this type of joint also need to be developed after the mechanisms have been identified.

APPENDIX I

REVIEW OF JOINT DAMPING LITERATURE

RIVETED JOINTS IN BEAMS

Although one may visualize many different combinations of joint geometries and joining methods, many of the early investigations of joint damping were concerned with built-up beams involving riveted (or quasi-riveted) connections. This choice of structural system is a logical one; riveted beams play important roles as primary structures in many applications, and beam configurations of the types considered may generally be analyzed more readily than other structures. Even these highly idealized beam structures present analytical difficulties, primarily because of the nonlinearities associated with slippage and friction damping.

Coulomb Friction Analyses

The damping characteristics of simple built-up structures were first studied in some detail by Pian and Hallowell (Ref. 7).* They analyzed I-beams with narrow plates bolted to the flanges through oversized holes, so that the bolts would not make contact with the cylindrical surfaces of the holes. The bolts provided essentially only normal forces at the interface between the beam and cover-plate. These normal forces determine the limiting static friction force. The analysis was carried out by investigating where this limiting force is exceeded and slippage occurs, and by calculating from this information the energy dissipated per cycle. Experimental results were found to agree quite well with theoretical predictions; a relation between limiting friction force and screw tightness having been determined experimentally.

Pian (Ref. 6) later extended the previous built-up cantilever beam analysis to the case where sliding between the beam flanges and capping plates is prevented by the tight fit of the (closely spaced) screws. He performed the analysis by visualizing the effect of the screws as that of a continuous shear joint, and took the deflection of this joint into account in computing the slippage and the cyclic energy dissipation. He again obtained reasonable agreement between theory and experiment, using experimentally determined values of the shear joint stiffness and friction force.

---

*Reference list appears at end of Appendix I.

A structure whose damping action is closely related to that of a built-up beam was investigated by Goodman and Klumpp (Refs. 8, 9). They dealt with a cantilever composed of two identical leaves held together by a uniform pressure. This configuration may more readily be idealized than Pian's and Goodman and Klumpp were able to obtain some rather general insights into the damping action of their system and to verify their theoretical conclusions by some carefully performed experiments.

Goodman (Ref. 5) has pointed out that the previously discussed built-up or bi-leaf beam analyses involving Coulomb friction (and neglecting inertia effects) are special cases of a broader class of interfacial slip problems. This broader class includes other types as well as flexural primary deformations. Analyses of all of these problems show that effective joint stiffness is amplitude-dependent, that the cyclic energy dissipation varies as the cube of the exciting force amplitude, and that there exists an optimum interface pressure (for maximum damping). For very high interface pressure there occurs no slip, and therefore no energy dissipation; for very low pressure slip occurs readily but the friction forces are very low and thus dissipate little energy. Somewhere between these extremes, at some optimum clamping pressure, considerable slip is associated with considerable friction forces and maximum energy dissipation occurs.

Critique of Coulomb Damping Analyses; Comparison to Newer Results

All three of the aforementioned analyses were based on assumed ideal Coulomb damping. That is, it was assumed that slippage occurs only where the shear stress exceeds a certain critical value, and that the shear stress in slipped regions is equal to that critical value regardless of relative velocity or displacement. These assumptions appear justified for the small relative velocities and displacements one is likely to encounter in configurations of this sort at low frequencies, as evident from the reported agreement between theory and experiments carried out at or below the fundamental frequencies of test cantilevers. The applicability of Coulomb damping at higher frequencies remains to be verified, particularly since friction coefficients generally do depend on relative velocity (Ref. 19). Pian's work is subject to the additional limitation imposed on it by the assumption that the pressure field due to the fasteners is uniform. A recent analysis by Fernlund (Ref. 20) shows that such pressure fields may be obtained only with very closely spaced fasteners.

In linear (viscously or viscoelastically damped) configurations the stiffness, damping coefficient, and loss factor are independent of amplitude; and the energy dissipated per cycle varies as the square of amplitude. The previously discussed ideal joints involving Coulomb friction thus behave nonlinearly; such behavior has also been observed in full-scale aircraft structures (Ref. 21). On the other hand, in measuring the damping due to a cover plate riveted onto a partially cut-through beam Mead (Refs. 22 and 23) found the damping to behave linearly up to considerable amplitudes. Mead used riveting techniques more nearly representative of commercial practice than those used in the previously mentioned investigations. Essentially linear damping behavior over a wide range of amplitudes and frequencies was also observed by Heckl et al (Ref. 17) on joints cut from the fuselage of a production aircraft.

Mead (Ref. 22) has made a number of conjectures and experimental observations of considerable interest. He has observed that fretting occurs in an annular region around a rivet, but not directly at the rivet, and has indicated that the actual shape of the fretting area (where undoubtedly considerable frictional motion occurs) may be affected by the local plate roughness. This observation agrees with the general picture that slipping begins in a region of low interface pressure and progresses toward the rivet with increasing applied load. (Clamping pressures are highest nearest the rivet, as also demonstrated in Ref. 20.) Mead also has found different amounts of damping with different types of rivets and has ascribed these differences to the different shear stiffnesses of the rivet types. However, in comparing rivet types he seems to have been unable to control or measure interface pressure, which most likely is the single most important variable and unfortunately presents formidable measurement problems. Later measurements (Ref. 17) seem to indicate that rivet details are of perhaps lesser importance in some instances.

There seems to be little doubt that beams with riveted connections behave nonlinearly and exhibit amplitude-dependent damping, provided that Coulomb damping is the primary energy dissipation mechanism. The methods developed by Pian (Refs. 6, 7) and Goodman (Refs. 5, 8, 9) are able to predict the damping adequately under these circumstances - at least for frequencies up to the fundamental resonance. However, the aforementioned studies do not answer the questions (raised by some experimental results, Refs. 22, 17) as to if and under what circumstances Coulomb damping actually is the dominant mechanism.

Practical Joints Designed for Damping

Riveted joints made according to current industrial practice are by no means optimized with respect to damping; the design of such joints is generally dictated by considerations of static and/or fatigue strength. Increased damping may probably be obtained by the use of fewer and looser rivets, but it is doubtful whether such changes would be acceptable in practice, since the increased slippage then would produce increased fretting corrosion and an attendant increase in the structure's susceptibility to fatigue failure. Lubrication of the joints is capable of producing increased damping (Ref. 17), but the lubrication effects must then also enter the corresponding static joint strength calculations.

Perhaps the best understood and most reliable means for obtaining acceptable joints with improved damping characteristics consists of the use of viscoelastic inserts, as analyzed by Mead and Eaton (Ref. 11). In such joints relatively well understood material hysteresis takes the place of the somewhat nebulous and difficult-to-analyze Coulomb friction; thus even analytical and design problems are reduced. However, the damping of such joints may generally be optimized for only certain types of relative motion (e.g., tangential) of the adjacent surfaces, and use of added material and deviation from standard practice may be objectionable in some cases.

PLATE AND BEAM SUPPORT JUNCTIONS

The damping of beams attached at their ends to (rigid and massive) supporting structures has been studied by Mentel and his co-workers, who have also dealt with the analogous problem for some edge-supported plates (Refs. 12-15). They studied support junction damping with Coulomb friction and with dissipation in viscoelastic inserts, and considered contributions due to axial or in-plane translation of the structures' edges with respect to the supports, as well as those due to rotation (the latter only for viscoelastically bonded joints).

Reference 12 deals with translational motion only and demonstrates that properly designed Coulomb or viscoelastic joints under these circumstances may dissipate more energy than material hysteresis in the vibrating structure. It also indicates that the rotational motion at a bonded joint may contribute considerably more damping than the translational motion, but study of the rotational effects seems to have been neglected in comparison to the rather thorough investigation of the relatively insignificant translational effects.

Mentel's studies are concerned with perfectly rigid supporting structures, an idealization which simplifies the analysis and may sometimes be approached in practical situations. His results are probably upper bounds to the damping obtained in practice, since lack of stiffness of the supports would generally tend to reduce the relative motion at the interface and would thus reduce the damping.

OTHER JOINT DAMPING STUDIES

Welded Joints

Kronenberg, Maker, and Dix (Ref. 16) report that they have devised "damping joints" for welded assemblies. These joints utilize welding shrinkage forces to pull adjacent surfaces into close contact; rubbing of these surfaces then dissipates energy. Although the authors exhibit experimental results that indicate that these joints have some damping effect, they do not provide good quantitative data and do not indicate a clear knowledge of the damping mechanisms involved.

Beam-Plate Systems

Heckl (Refs. 17, 18) has reported some measurements of the "absorption coefficients" of beams attached to plates by various means. He made no concerted effort to identify the mechanisms responsible for the damping, however, but did advance some plausible qualitative explanation for some aspects of the behavior he observed. Heckl also studied the damping-interaction of beam-plate systems (Ref. 24), but was not concerned with identifying the damping due to the joints themselves.

REFERENCE LIST

1. B. J. Lazan, "Damping Properties of Materials and Material Composites," Applied Mechanics Reviews, 15, 81-88 (1962).

2. B. J. Lazan, and L. E. Goodman, "Material and Interface Damping," Chapter 36 of Shock and Vibration Handbook, Ed. by C. M. Harris and C. E. Crede, McGraw-Hill Book Company, Inc., New York, 1961.

3. J. E. Ruzicka, "Damping Structural Resonances Using Viscoelastic Shear-Damping Mechanisms," J. Eng. for Industry (Series B of Trans. ASME), 83, 403-424 (1961).

4. E. E. Ungar, "Loss Factors of Viscoelastically Damped Beam Structures," J. Acoust. Soc. Am., 34, 1082-1089 (1962).

5. L. E. Goodman, "A Review of Progress in Analysis of Interfacial Slip Damping," Sec. II of Structural Damping, Ed. by J. E. Ruzicka, Amer. Soc. Mech. Engrs., New York, 1959.

6. T. H. H. Pian, "Structural Damping of Simple Built-up Beam with Riveted Joints in Bending," J. Appl. Mech., 24, 35-38 (1957).

7. T. H. H. Pian and F. C. Hallowell, Jr., "Structural Damping in a Simple Built-up Beam," Proc. First U. S. National Congress of Appl. Mech., ASME, New York, 1952, pp 97-102.

8. L. E. Goodman, and J. H. Klumpp, "Analysis of Slip Damping with Reference to Turbine Blade Vibration," J. Appl. Mech., 23, 421-429 (1956).

9. J. H. Klumpp and L. E. Goodman, "Slip Damping of Press-fit Joints Under Linearly Varying Pressure" WADC TR 56-291 (September 1956).

10. E. E. Ungar and E. M. Kerwin, Jr., "Loss Factors of Viscoelastic Systems in Terms of Energy Concepts," J. Acoust. Soc. Am. 34, (July 1962), pp 954-957.

11. D. J. Mead and D. C. G. Eaton, "Interface Damping at Riveted Joints (Part I - Theoretical Analysis)" Univ. of Southampton, Dept. of Aeronautics and Astronautics, USAA Report No. 153; August 1960.

12. T. J. Mentel, "Vibrational Energy Dissipation at Structural Support Junctions," Sec. IV of Structural Damping, Ed. by J. E. Ruzicka; Amer. Soc. Mech. Engrs., New York, 1959.

REFERENCE LIST (continued)

13. T. J. Mentel, "Damping of Simplified Configurations with Additives of Interfaces," WADC-Univ. of Minnesota Conference on Acoustical Fatigue, Ed. by W. J. Trapp and D. M. Forney, Jr., WADC TR 59-676 (March 1961) pp 207-234.

14. T. J. Mentel, "Damping Energy Dissipated by Interfaces in Beam and Plate Supports and in Sandwich Cores," WADC TR 58-547 (December 1958).

15. C. C. Fu, "Response of Circular Plates Exhibiting Generalized Boundary Damping and Empirically Based Material Damping," ASD-TDR 61-647 (November 1961).

16. M. Kronenberg, P. Maker, E. Dix, "Practical Design Techniques for Controlling Vibrations in Welded Machines," Machine Design, July 12, 1956, pp 103-109.

17. M. A. Heckl, R. H. Lyon, G. Maidanik, E. E. Ungar, "New Approaches to Structural Vibration Analysis and Control," ASD-TDR 62-237 (April 1962), AD-290-798.

18. M. A. Heckl, "Measurements of Absorption Coefficients on Plates," J. Acoust. Soc. Am., 34, 803-808 (1962).

19. E. Rabinowicz, "Practical Approach to Friction Coefficients," Product Engineering, September 26, 1960, p 51-54.

20. I. Fernlund, "A Method to Calculate the Pressure Between Bolted or Riveted Plates," Institute of Machine Elements, Chalmers University of Technology, (Gothenburg, Sweden) Report No. 11, (1961).

21. D. O. Fearnow, "Investigation of the Structural Damping of a Full-Scale Airplane Wing," NACA TN 2594 (February 1962).

22. D. J. Mead, "The Damping, Stiffness and Fatigue Properties of Joints and Configurations Representative of Aircraft Structures," WADC-University of Minnesota Conference on Acoustic Fatigue, Ed. by W. J. Trapp and D. M. Forney, Jr.; WADC TR 59-676 (March 1961) pp 235-261.

23. D. J. Mead, "The Internal Damping Due to Structural Joints and Techniques for General Damping Measurements," Aeronautical Research Council, ARC 19,870, January 1958.

24. M. A. Heckl, "Wave Propagation on Beam-Plate Systems," J. Acoust. Soc. Am. 33, (May 1961), pp 640-651.

25. R. Plunkett, "Measurement of Damping," Section 5 of Structural Damping, Ed. by J. E. Ruzicka, Amer. Soc. Mech. Engrs. New York, 1959.

26. E. M. Kerwin, Jr., "Mechanisms and Measurement of Structural Damping," Proc. Conference on Structural Vibration Damping, Mare Island Naval Shipyard, Vallejo, California, 25 October 1962.

27. B. J. Lazan, "Energy Dissipation Mechanisms in Structures, with Particular Reference to Material Damping," Section I of Structural Damping, Ed. by J. E. Ruzicka; Amer. Soc. Mech. Engrs., New York, 1959.

28. J. Marin and M. G. Sharma "Material Design for Resonant Members," Section VI of Structural Damping, Ed. by J. E. Ruzicka; Amer. Soc. Mech. Engrs., New York, 1959.

APPENDIX II

TORQUE-TENSION CHARACTERISTICS OF NUT-AND-BOLT ASSEMBLIES

Since it appeared likely that interface pressure at structural joints may be an important parameter influencing the damping produced by these joints, it was thought desirable to obtain some idea of the variation in the bolt tension one obtains for a given type of bolt with a given value of tightening torque.

The simple test jig shown in Fig. 35 was designed to study the torque-tension behavior of small nut-and-bolt assemblies. The bolt to be tested is inserted in the block on the right and is prevented from turning by means of a lock-washer under its head. This washer is loaded by tightening of a nut against the block. The block is intended to make only light contact with the support and is designed to keep the narrow tension-measuring strip from twisting. Elongations of this strip are measured by means of the strain gages indicated in the figure; the strip is restrained by a second block attached at its left end. Shims between this block and the left support upright are used to establish the desired spacing between the right block and the right support upright.

For calibration of the tension measuring element it is removed from the test jig and suspended vertically (by a support placed under the block shown at the left in the sketch). Known weights are then hung from the second block, and the corresponding strains are measured by means of the usual strain gage bridge instrumentation. Calibration runs with weights up to 200 lbs (made before and after each series of measurements) showed that the strip behaved completely linearly and exhibited no residual deformation upon removal of the loads.

Figure 36 shows some torque-vs-tension curves measured with the apparatus of Fig. 35. The curves shown pertain to standard #6-32 stainless steel screws in conjunction with 1/4" stainless steel nuts and standard #6 steel washers between nut and test jig (at the right of Fig. 35). These screws were used in all of the reported experiments on bolted joints because their high strength permits one to study a relatively broad range of interface pressures. Torque measurements in all cases were made with a TQ5-1 torque-driver (Snap-on Tools Company), with which the nuts were tightened. This torque driver has a range of 12 in-lb and is accurate to about 1/4 in-lb.

Figure 36 pertains to the first tightening of a new nut on a new screw; each curve pertains to a different nut-and-screw assembly. Different behavior may be expected if the nuts are loosened and retightened a number of times. Figure 37 shows typical results obtained for the third tightening. It is evident that the curves of Fig. 37 have lesser slopes than those of Fig. 36, and that less tension is obtained for a given torque during the third tightening than during the first.

The effect on tension (obtained with a given torque) of the number of times a nut is tightened is summarized in Fig. 38, where each symbol refers to a different nut-screw-washer combination. The light curves of the figure indicate the spread of the data points for each torque level (disregarding data judged unreliable), the heavy curves represent estimated means.

From Fig. 38 it is evident that there is a considerable spread in the tension data for a given torque. It also appears that this spread decreases (in actual value and in terms of the percent of average tension it constitutes) with increasing number of tightenings. From the data and from visible scoring of the washers produced by the turning of the nut one may surmise that a considerable fraction of the applied torque is used to seat the nut during retightening, leaving less torque to produce tension in the bolt.

In view of the data summarized in Fig. 38 it is evident that one must use care when one is concerned with measuring the effects of interface pressure. For the interface pressure effect studies discussed in the main body of this report measurements were taken only after tightening each nut several times in order to reduce the spread of the resulting values of bolt tension.

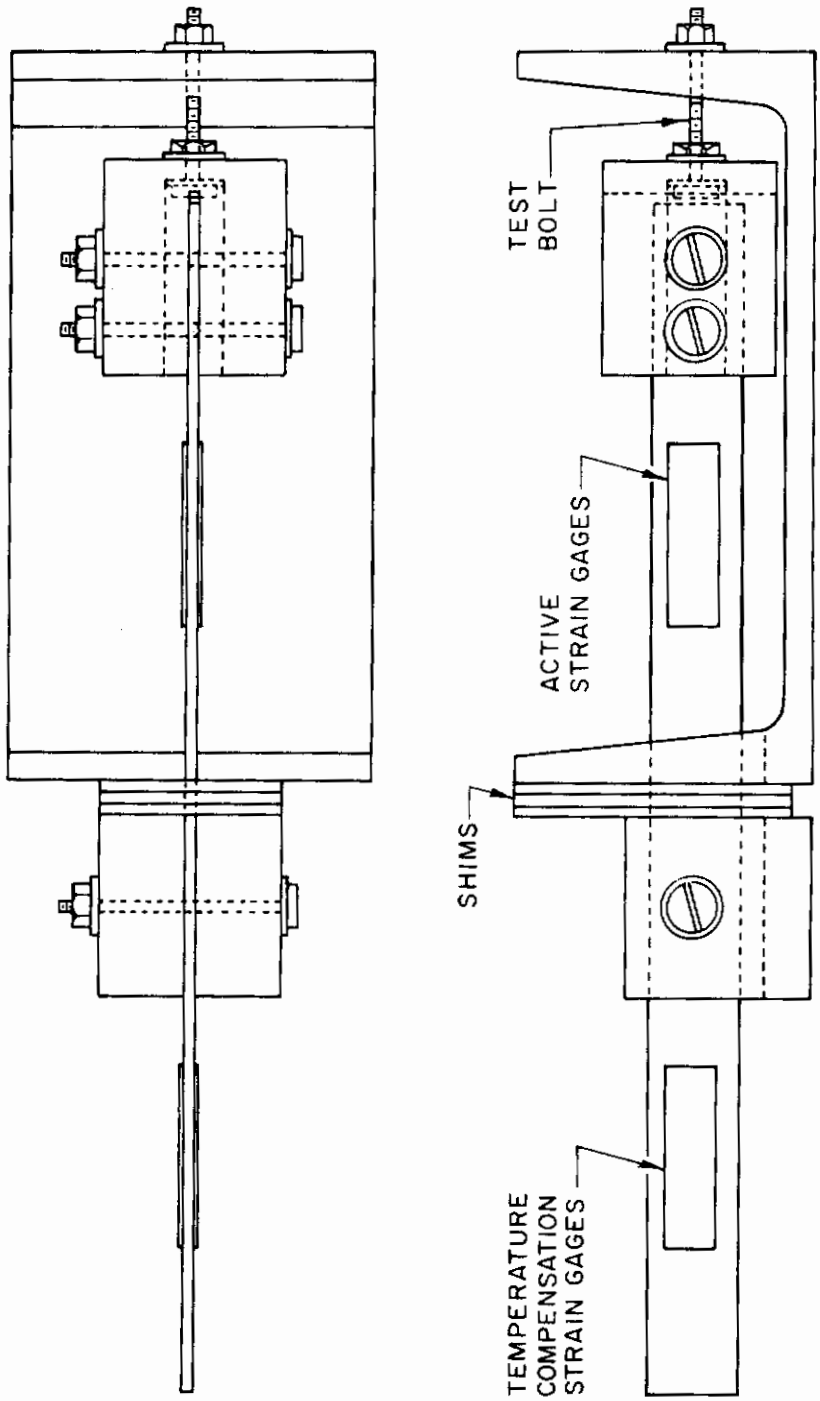

FIG. 35 BOLT TORQUE - TENSION TEST JIG

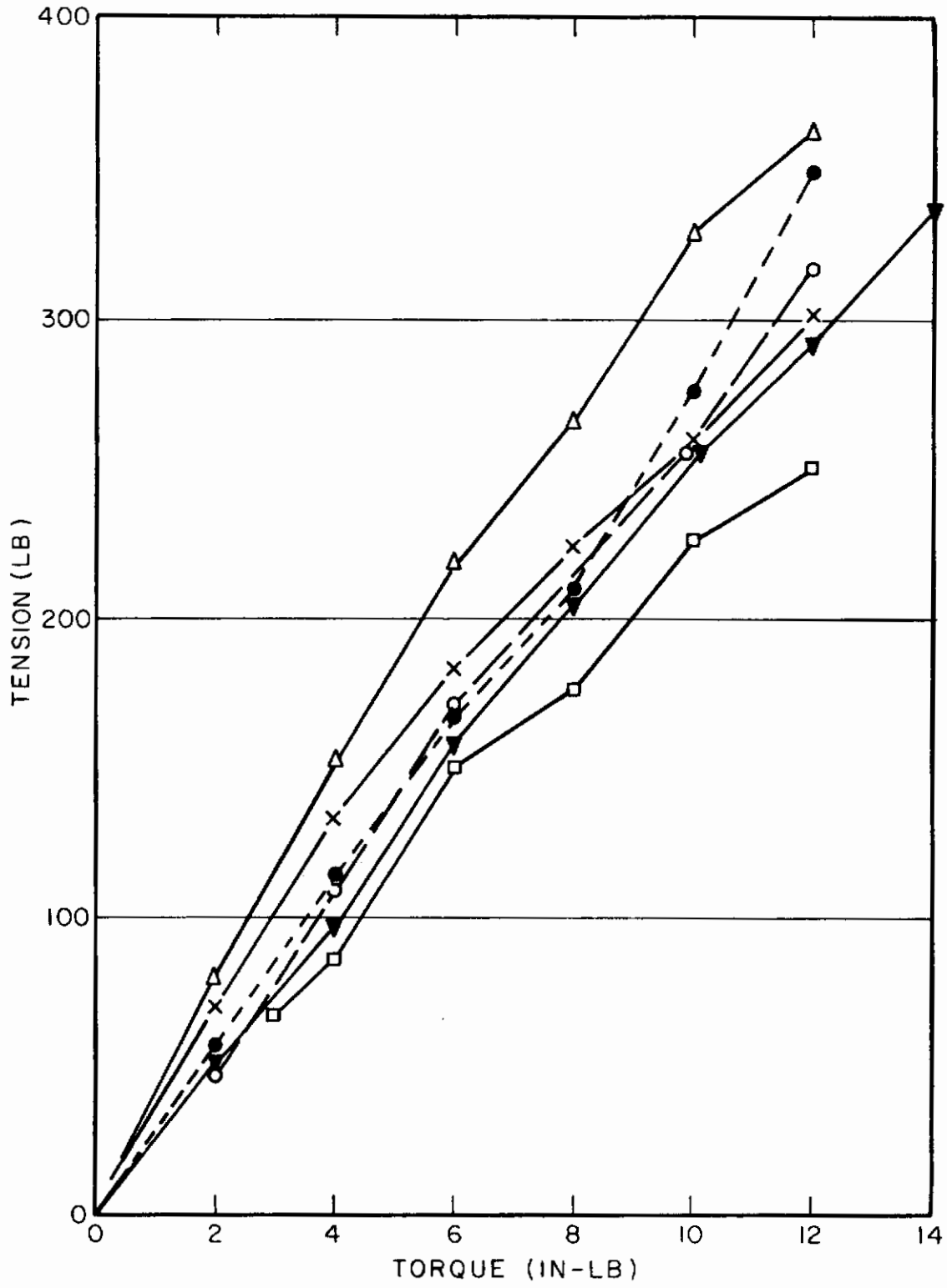

FIG. 36 TORQUE-TENSION CURVES FOR INITIAL TIGHTENING OF SEVERAL #6-32 SS BOLTS

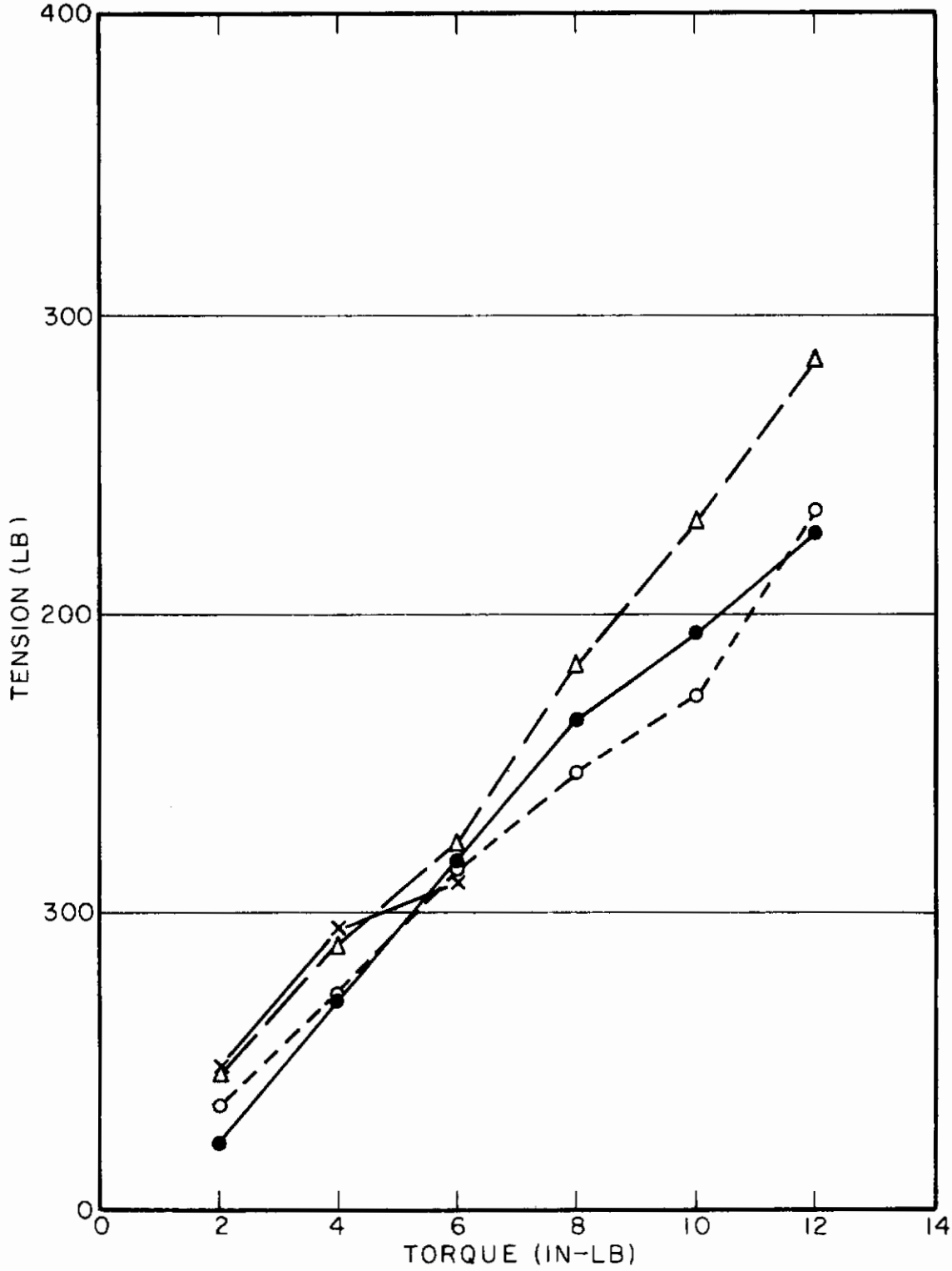

FIG. 37 TORQUE-TENSION CURVES FOR THIRD TIGHTENING OF FOUR #6-32 SS BOLTS

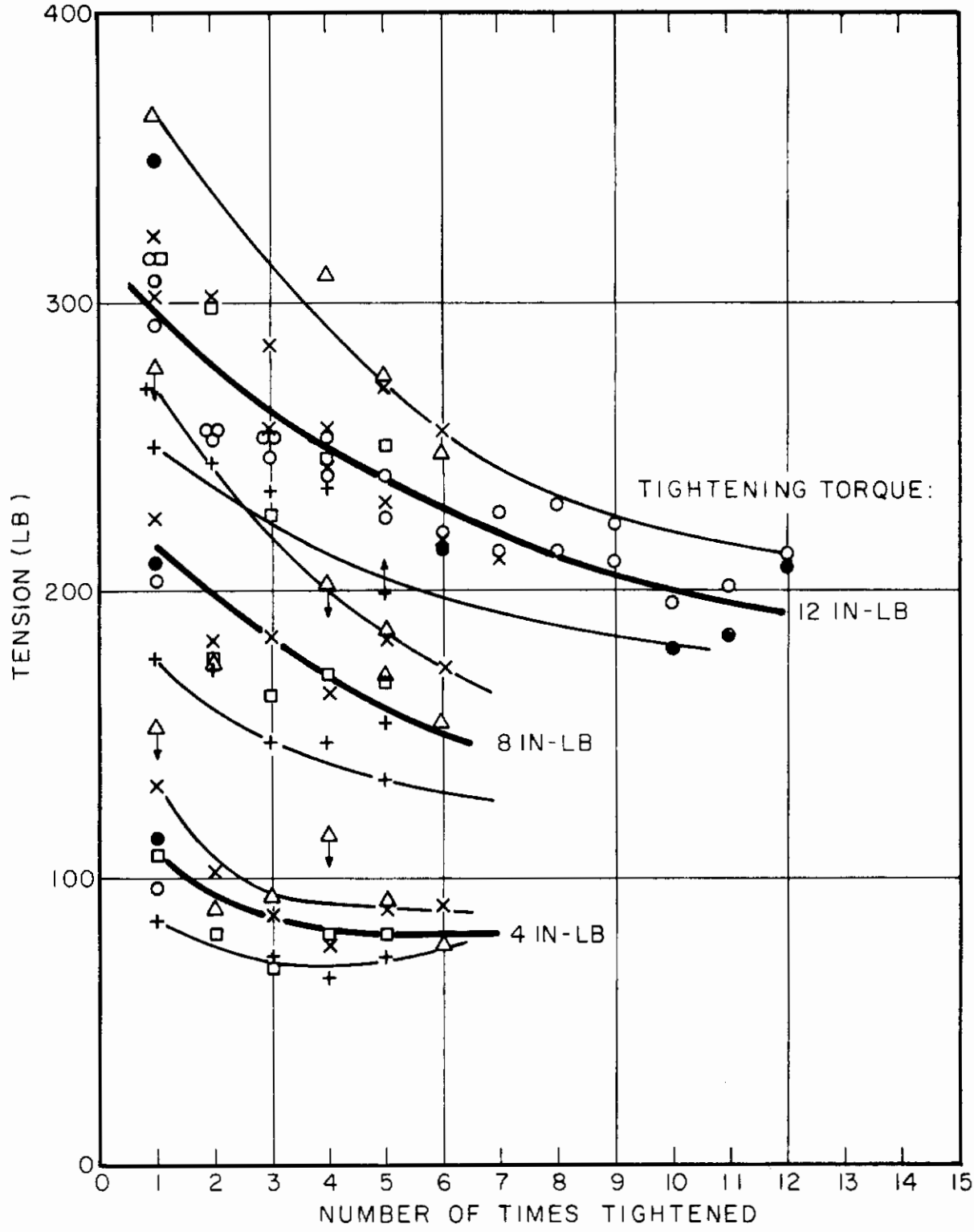

FIG. 38 TENSION IN #6-32 SS BOLTS (1/4" SS NUTS AND STEEL WASHERS) VS. NUMBER OF TIMES TIGHTENED

APPENDIX III

ON THE MOTION OF A PLATE RELATIVE TO A BEAM ATTACHED WITH UNIFORMLY SPACED POINT-FASTENERS

The motion of those plate portions near an attached beam relative to this beam must be understood before one can hope to analyze the damping due to any mechanism associated with such relative motions. The present appendix is a step toward the calculation of the normal motions of the plate portions between fasteners relative to an attached beam and toward the evaluation of the effects of frequency and other important parameters.

Under realistic conditions (and in the beam-plate experiments discussed in this report) the plate is generally driven at a point or points far from the attached beam, so that a diffuse flexural wave field is set up on the plate. This field interacts with the beam, primarily at the fastening points. These plate motions may be reasonably represented by superposition of 1) the diffuse plate motion in absence of an attached beam, and 2) the plate response to excitation at the fastening points, of proper phase and magnitude so that these points remain fixed in space. (This fixity requirement essentially assumes that the beam motion is very small compared to the plate motion - a condition which one may expect to encounter generally in practice.) One cannot prescribe truly realistic driving point phases and magnitudes, however, without a great deal of mathematical complexity. In order to arrive at some understanding of the phenomena involved it seems sensible to deal first with a simpler mathematical formulation which bypasses this complexity and which hopefully will retain the essential features of a more realistic formulation.

Accordingly, the following pages deal with a study of the plate responses to in-phase forces of equal amplitude, applied at points spaced uniformly along a line. (This arrangement also corresponds to the plate being driven via a rigid beam, with forces transmitted only at the joining points.)

PLATE DRIVEN AT A SINGLE POINT

The deflection w of an infinite plate due to an oscillating point force* F_o applied at the origin is given by[1]

$$w = w_1(0)\left[H_o^{(2)}(kr) - H_o^{(2)}(-ikr)\right] \equiv w_1(0)\, G(kr) \quad , \qquad (15)$$

where

$$w_1(0) = \frac{v_o}{i\omega} = \frac{F_o}{i\omega Z_o} \quad , \quad Z_o = 8\sqrt{Dm} \quad . \qquad (16)$$

Here r denotes a radial coordinate within the plane of the plate and t denotes time. Also, $w_1(0)$ and v_o denote driving point displacement and velocity phasors, respectively, and Z_o denotes the classical driving point impedance (expressed in terms of flexural rigidity D and mass per unit surface area m). The symbol k denotes the flexural wave number; it obeys

$$k^4 = \omega^2\, m/D \quad . \qquad (17)$$

The function $H_o^{(2)}$ is the zero order Hankel function of the second kind, which is related to the zero order Bessel function J_o, the zero order Neumann function N_o, and the zero order Hankel function of the first kind H_o. For purposes of computation it is convenient to introduce these latter functions. One finds[1,2]

---

*The usual complex notation convention is employed here. Steady-state sinusoidal motion is implied; the time-dependent function $\alpha(t)$ corresponding to a complex variable (i.e."phasor") α is obtained from

$$\alpha(t) \equiv \mathrm{Re}\left\{\alpha\, e^{i\omega t}\right\} \quad .$$

1/ L. Cremer, "The Propagation of Structure-borne Sound". Sponsored Research (Germany) Report No. 1 (Series B). (British) Dept. of Scientific and Industrial Research. Circa 1948, pp 56-59.

2/ E. Jahnke and F. Emde, Tables of Functions, Dover Publications, New York, 4th Ed., 1945, pp 133-138.

$$G(kr) = J_o(kr) - i[N_o(kr) + iH_o(ikr)] \quad . \tag{18}$$

For small arguments[2,3], i.e. for $|x|<<1$,

$$J_o(x) \approx 1 - \left(\frac{x}{2}\right)^2 + \frac{1}{4}\left(\frac{x}{2}\right)^4 - \cdots$$

$$N_o(x) \approx \frac{2}{\pi} \ell n \frac{\gamma x}{2} \quad , \tag{19}$$

$$iH_o(ix) \approx - \frac{2}{\pi} \ell n \frac{\gamma x}{2} \quad ,$$

where $\gamma = 1.781072$ is Euler's constant.

For large arguments,[2,3] i.e. for $|x|>>1$,

$$J_o(x) \approx \sqrt{\frac{2}{\pi x}} \cos(x-\pi/4)$$

$$N_o(x) \approx \sqrt{\frac{2}{\pi x}} \sin(x-\pi/4) \tag{20}$$

$$iH_o(ix) \approx \sqrt{\frac{2}{\pi x}} e^{-x} \quad .$$

One thus finds that

$$\left.\begin{aligned} G(x) &\approx 1 - \left(\frac{x}{2}\right)^2 \qquad\qquad \text{for } |x|<<1 \\ G(x) &\approx \sqrt{\frac{2}{\pi x}} \left[\cos(x-\pi/4) - i\left\{\sin(x-\pi/4) + e^{-x}\right\}\right] \\ &\approx \sqrt{\frac{2}{\pi x}} e^{-i(x-\pi/4)} \end{aligned}\right\} \text{for } |x|>>1 \tag{21}$$

3/ P. M. Morse and H. Feshbach, Methods of Theoretical Physics, McGraw-Hill Book Company, Inc., New York, 1953. Part II, pp 1321-1323.

Figure 39 is a complex-plane plot of G(kr) similar to Cremer's.[1] It shows that $|G(kr)|$ decreases and approaches zero as kr increases, the decrease being rather rapid for small kr and slow for large kr.

PLATE DRIVEN AT TWO POINTS

Absolute Motion of Driving Points

Before considering the response of a plate driven at many points one may do well to study the behavior of a plate being driven at two points by equal forces of magnitude F_o acting in phase. The deflection $w_2(0)$ of the plate at either of the two driving points (by symmetry, the two respond identically) may be determined by superposition. If d denotes the distance between the two driving points, then one may write

$$w_2(0)/w_1(0) = G(0) + G(kd) = 1 + G(kd) \quad , \tag{22}$$

where $w_1(0)$ denotes the driving point deflection amplitude obtained with only a single force F_o acting.

A complex plane presentation of 1+G(kd) appears exactly like that of G, except that the 1+G curve is one unit further in the positive real axis direction than the G curve. (Alternately, if the curve is kept fixed, the coordinate system may be translated one unit in the negative real axis direction, as indicated in Fig. 39.)

Figure 40 shows how the amplitude ratio $|w_2(0)/w_1(0)|$ varies with kd. As also evident from Fig. 39, this amplitude ratio is 2.0 for small kd, exhibits a generally oscillatory nature, and approaches 1.0 for large kd. At small kd the two forces act essentially as a single one of double magnitude, hence produce twice as much deflection as a single force. At large kd the deflection due to the second force produced at the driving point of the first is negligible, hence the driving point of each force responds essentially only to its own force, independently of the other.

The foregoing observation may have some interesting practical applications. If one is required to apply an oscillating force of given magnitude to a plate, it may be advantageous to distribute this force to two (or more, say n) driving points spaced a suitable distance d apart, via a rigid bracket or platelet. At low frequencies (small kd) essentially nothing will be changed relative to single-point application of the

force, but at high frequencies (large kd) the applied force will "see" twice (or n times) the single-point impedance and its point of application will therefore move with only 1/2 (or 1/n) of the single-point amplitude.

Relative Motions of Plate Between Driving Points

If one considers a rigid beam driving a plate only via a number of discrete fastening points (with excitation applied to the beam so that its rotational motion is suppressed), then the forces at all points act in phase. The relative motion of the plate with respect to the beam is then the same as that with respect to the driving points.

With two driving points a distance d apart the relative motion of the plate between the driving points is given by

$$\begin{aligned} w_{2rel}(kr)/w_1(0) &= G(kr) + G(kd-kr) - w_2(0)/w_1(0) \\ &= G(kr) + G(kd-kr) - [1 + G(kd)] \end{aligned} \tag{23}$$

where r is measured from any one of the driving points.

By specializing Eq. (23) for r=d/2 one finds that the relative motion of the point midway between the driving points is described by

$$w_{2rel}(kd/2)/w_1(0) = 2G(kd/2) - [1 + G(kd)] \quad . \tag{24}$$

Amplitudes calculated from this equation are also plotted in Fig. 40. If one is interested in the relative motion produced by a given driving point motion rather than in that produced by a given driving force, one may obtain the desired information by dividing Eq. (24) by the driving point amplitude, as given by Eq. (22), and obtain

$$\frac{w_{2rel}(kd/2)/w_1(0)}{w_2(0)/w_1(0)} = \frac{w_{2rel}(kd/2)}{w_2(0)} = \frac{2G(kd/2)}{1 + G(kd)} - 1 \quad . \tag{25}$$

The absolute value of this expression is also plotted in Fig. 40.

For damping calculations it may turn out that the space-wise average relative deflection is desired, and not merely the relative deflection of the mid-point. This average value for a given kd may be computed from Eq. (23); the results of such calculations are shown in Fig. 40. From the similarity of the pertinent curves in this figure one may conclude that the mid-point amplitude is a good measure of the average amplitude, at least up to values of kd of about 8.0.

PLATE DRIVEN AT INFINITE NUMBER OF EVENLY SPACED POINTS

Absolute Motion of Driving Points

By extending the previous analysis to an infinite number of driving points equally spaced along a straight line one finds that the deflection of the driving points is given by

$$w_\infty(0)/w_1(0) = G(0) + 2 \sum_{n=1}^{\infty} G(nkd) \quad . \tag{26}$$

The factor 2 here is required to account for contributions of forces on both sides of a given point. Here again, $w_1(0)$ denotes the deflection obtained at a single driving point when no forces are acting elsewhere.

Relative Motion of Points Midway Between Driving Points

The (absolute) deflection at a point half-way between any two driving points is given by

$$w_\infty(kd/2)/w_1(0) = 2 \sum_{n=0}^{\infty} G\left[kd\left(n + \tfrac{1}{2}\right)\right] \quad , \tag{27}$$

whereas the deflection of this point relative to the driving point obeys

$$w_{\infty rel}(kd/2)/w_1(0) = w_\infty(kd/2)/w_1(0) - w_\infty(0)/w_1(0) \quad . \tag{28}$$

Convergence; Calculations

The foregoing expressions, although simple in form, may pose formidable computational difficulties. Convergence of the various foregoing series is a problem that must be considered among others. It may best be approached by using the large parameter approximation of Eq. (21), which indicates that $|G(nkd)|$ decreases monotonically as n increases. If Eq. (21) is a good approximation for $nkd > n_o kd$ where n_o is a suitably chosen integer, then one may rewrite Eq. (26) as

$$w_\infty(0)/w_1(0) \approx G(0) + 2\sum_{n=1}^{n_o} G(nkd) + 2\sigma e^{i\pi/4} \qquad (29)$$

where, in view of Eq. (21)

$$\sigma \equiv \sum_{n=n_o+1}^{\infty} \left[\frac{\cos(nkd)}{\sqrt{nkd}} - i\,\frac{\sin(nkd)}{\sqrt{nkd}} \right] . \qquad (30)$$

One may then investigate the convergence of Eq. (26) by studying the convergence of Eq. (30).

For values of kd that are odd multiples of π one finds that the real and imaginary parts of σ are alternating series whose terms decrease in absolute value, and the series σ converges. [4/] For values of kd that are even multiples of π, the two component series are of the form $\Sigma\, n^{-1/2}$, which is known to diverge.

For small values of kd, say $kd \ll \pi/2$, one may replace the summation of Eq. (30) by an integral and write

$$\sigma = \sum_{\substack{n=n_o+1 \\ \Delta n=1}}^{\infty} \frac{e^{-inkd}}{\sqrt{nkd}}\,\Delta n \approx \frac{1}{kd}\int_{x_o}^{\infty} \frac{e^{-ix}}{\sqrt{x}}\,dx \qquad (31)$$

4/ H. W. Reddick and F. H. Miller, Advanced Mathematics for Engineers, 2nd Ed. John Wiley and Sons, Inc., New York, 1948, Chapter IV.

where x is a dummy variable which replaces nkd in the integration, and

$$x_o \equiv (n_o + 1/2)kd \quad . \tag{32}$$

In order to evaluate the right-hand side of Eq. (31) one may note that it is simply related to the Fresnel integral

$$C(x_o) - iS(x_o) \equiv \frac{1}{\sqrt{2\pi}} \int_o^{x_o} \frac{e^{-ix}}{\sqrt{x}}\, dx \tag{33}$$

whose real and imaginary parts, C and S, are tabulated.[5/] One finds that

$$\begin{aligned} \sigma &= [C(\infty) - iS(\infty) - C(x_o) + iS(x_o)]\ \sqrt{2\pi}/kd \\ &= \left[\frac{1-i}{2} - C(x_o) + iS(x_o)\right] \sqrt{2\pi}/kd \quad . \end{aligned} \tag{34}$$

Obviously, the series of Eq. (30) converges for $0<kd<<\pi/2$ although it diverges for kd=0.

One finds similarly that the series of Eq. (27) also converges if kd is equal to odd multiples of π and diverges for kd values that are even multiples of π.

The results of some relatively rough calculations based on the equations and approximations discussed in this subsection are summarized in Fig. 41. These calculations were carried out "by hand", and thus account for only a very limited number of terms for infinite series (for which good approximations are not available). Although a high-speed computer can undoubtedly be used to advantage to obtain more extensive and more precise results, the results shown in Fig. 41 do illustrate the behavior of the various functions adequately for the present purpose.

Figure 41 is analogous to Fig. 40; Fig. 41 pertains to an infinite number of driving points, Fig. 40 to only two. A marked similarity of these two figures is evident. A major difference between them is the tending towards infinity of some of the curves of Fig. 41 at d/λ values of 0, and 2π, compared to the appearance of peaks in the corresponding curves of Fig. 40.

5/ Jahnke and Ende, pp 35, 36.

RESULTS

As evident from the curves for $|w_{2rel}(kd/2)/w_2(0)|$ and $|w_{\infty rel}(kd/2)/w_\infty(0)|$ shown in Figs. 40 and 41, the maximum relative motions of the points on plates midway between fasteners (relative to attached beams) corresponds to values of d/λ that are somewhat greater than 1/2. Here, as previously, λ denotes the plate flexural wavelength.

These mid-point motions appear to be representative of space-wise average motions of the plate portions between fasteners, for values of d/λ up to about 1.2. Figure 40 also indicates the occurrence of secondary relative motion maxima near $d/\lambda \approx 1.5$; Fig. 41 is not sufficiently complete to show any corresponding maxima that might occur in the case of plates driven at an infinite number of points.

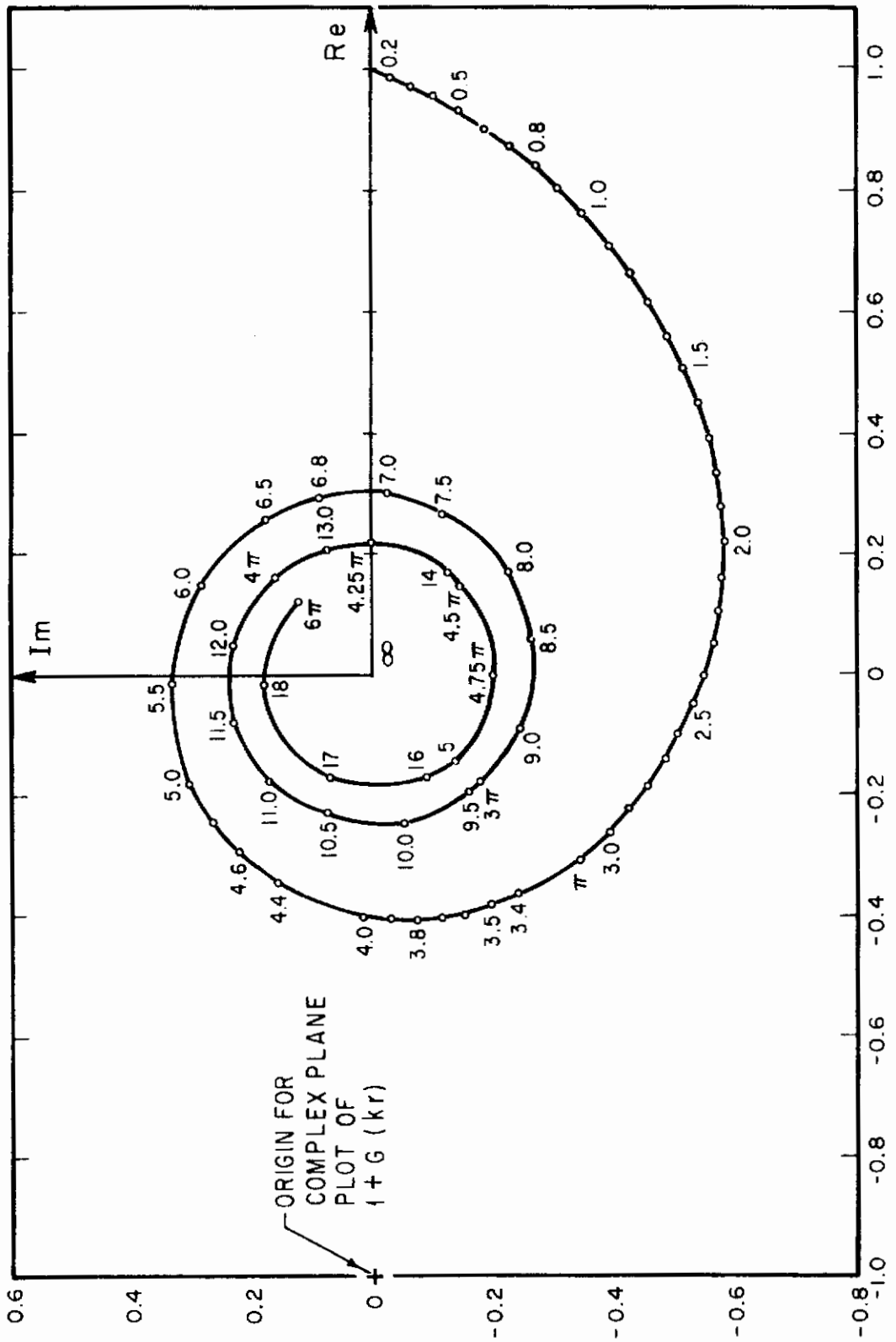

FIG. 39 COMPLEX PLANE PLOT OF PLATE DEFLECTION FUNCTION G(kr)

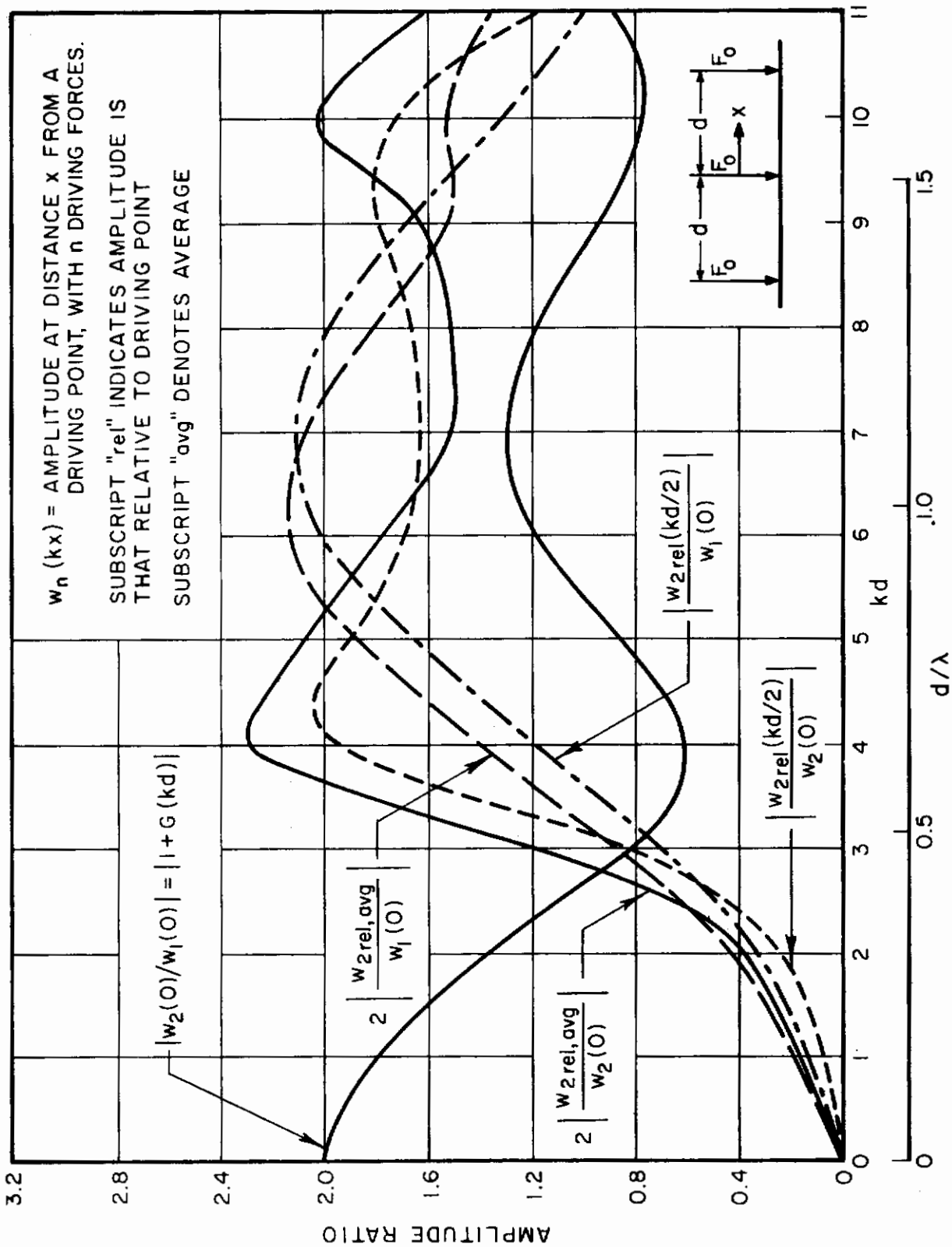

FIG. 40 DEFLECTION AMPLITUDES OF PLATES DRIVEN AT TWO POINTS

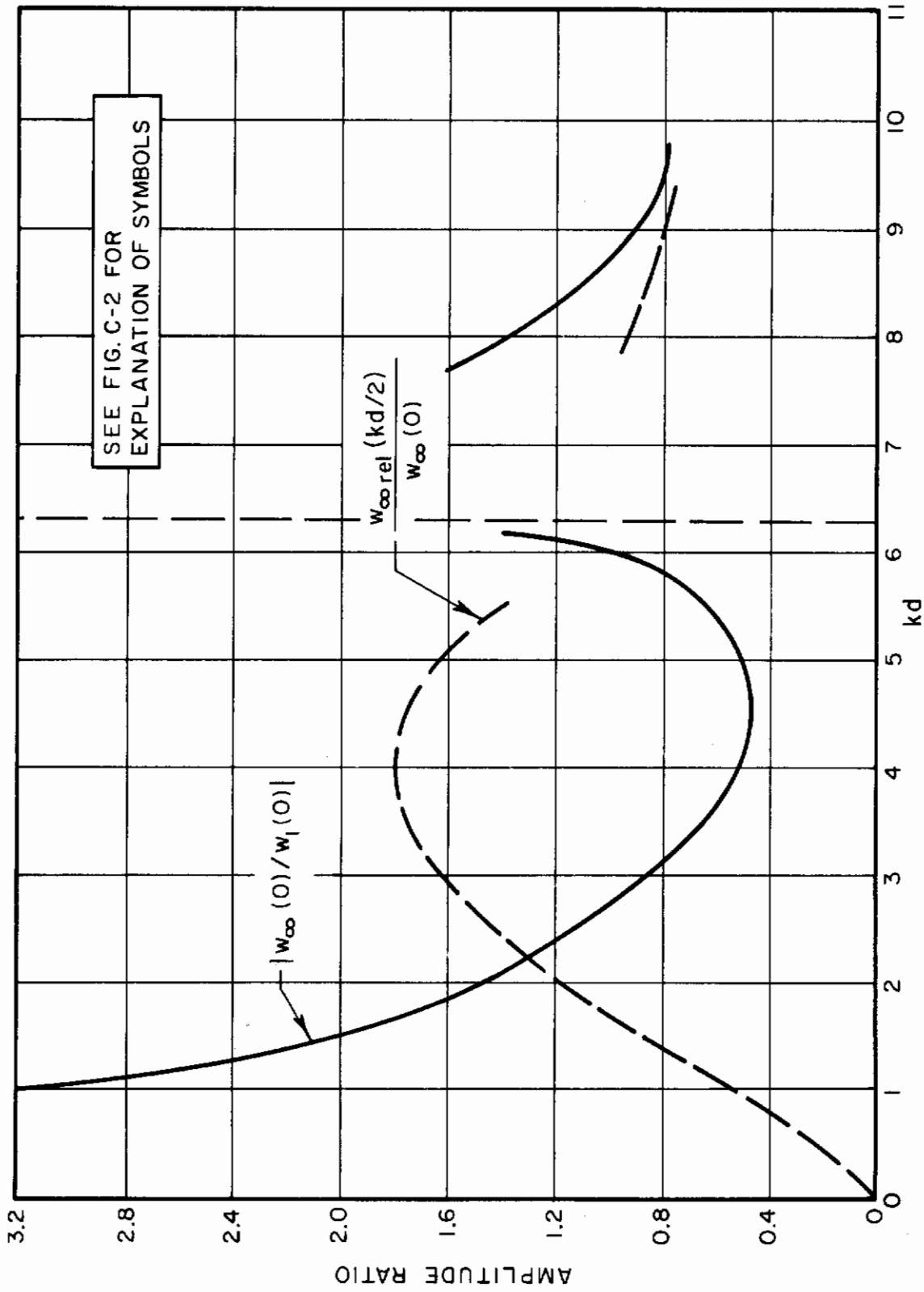

FIG. 41 APPROXIMATE DEFLECTION AMPLITUDES OF PLATES DRIVEN AT INFINITE NUMBER OF POINTS

APPENDIX IV

CHARACTERISTICS OF BEAM DAMPING DUE TO SOME POSTULATED ENERGY DISSIPATION MECHANISMS AT SUPPORTS

I. INTRODUCTION

In the following pages are summarized analyses pertaining to several energy dissipation mechanisms that one can visualize as possibly acting at structural joints. These analyses are concerned with a configuration consisting essentially of a long narrow plate whose short edges are fastened to rigid supports, and which is driven by a sinusoidal force (of adjustable frequency and amplitude) applied to the plate center. The analyses seek to develop relations between the rms force, driving point velocity, and the steady-state average power dissipation one would measure at the central driving point for the various mechanisms considered.

II. DAMPING MECHANISMS ASSOCIATED WITH LONGITUDINAL RELATIVE MOTION

It has been suggested[1/*] that damping at support junctions may be due to relative shearing motions associated with effective shortening of a beam span resulting when the beam is deflected laterally. The present section deals with the power dissipation one may expect to observe for various assumed friction processes acting in conjunction with the longitudinal relative motion induced by this foreshortening.

A. Uniform Coulomb Friction; Inextensible Overlap

Consider a beam attached to rigid supports, as sketched in Fig. 42, to be driven laterally. Longitudinal motion of the beam portions overlapping the supports will result relative to these supports due to this lateral motion, and friction at the interfaces will produce energy losses. One of the simplest loss mechanisms one may postulate is that of Coulomb friction. This mechanism consists of a friction force which is of constant magnitude whenever relative motion occurs, but which has a direction which

---

*Superscript numbers and the symbol shown here refer to the list of references for Appendix IV, page 125.

always opposes the motion. In the following paragraphs the damping due to such Coulomb forces is analyzed, subject to the additional assumption that the overlap portions of the beam do not deform (axially) due to the friction forces. However, effects of elastic restoring forces, as perhaps provided by bolts or rivets, and elastic deformation of the free length of the beam are taken into account.

A problem related to the one outlined here has been approached by Mentel[1], but for a different purpose. The following analysis leans somewhat on Mentel's work, at least in its initial stages, and consists to some extent of a reinterpretation and of extensions of it.

The change in projected length (on the x-axis of Fig. 42) of a beam in absence of axial forces is given by[2]

$$\Delta(2L)_1 = \frac{1}{2}\int_0^{2L} (\partial y/\partial x)^2 \, dx \equiv 2C \, y_o^2 \quad , \tag{35}$$

according to classical small-deflection beam theory. Here $y(x)$ denotes the deflection shape, y_o the central deflection of the beam. C is defined by Eq. (35) as a coefficient which depends on the deformation curve of the beam and which expresses the relation between $\Delta(2L)_1$ and y_o. Note that L is defined as half the total beam length, as indicated in the figure.*

An axial force N acting on the beam will cause it to stretch by an amount

$$\Delta(2L)_2 = N(2L)/EA \quad , \tag{36}$$

where A denotes the cross-sectional area and E the Young's modulus of the beam. This stretching reduces the axial displacement (compared to the inextensible case) resulting in a net axial displacement on each side of the beam of Fig. 42, (assuming symmetric behavior) given by

$$s \equiv \Delta L_1 - \Delta L_2 = C \, y_o^2 - \frac{NL}{EA} \quad . \tag{37}$$

---

*A list of symbols for Appendix IV also appears on page 126.

Let us assume that the overlapping beam portion itself is rigid and that it is elastically restrained by a stiffness K (representing all elastic restoring forces, such as those associated with bolt deformations and shear of asperities at the interface) and subject also to an ideal Coulomb friction force of magnitude μ. If longitudinal inertia effects are neglected, one finds (see diagram, Fig. 42b) that

$$N = Ks + \mu \operatorname{sgn} \dot{s} \quad . \tag{38}$$

Equation (38) is represented by the two slanting straight lines of Fig. 42c. Since the Coulomb friction force may vary between $+\mu$ and $-\mu$ if no slippage occurs (that is, for $\dot{s} = 0$), the N-s curve one obtains as s traverses a complete cycle is a parallelogram, as shown. One may note that for the beam under discussion $s \geq 0$ at all times, and that the foregoing derivation assumes that N is sufficiently large to overcome the friction initially. The parallelogram thus may be considered to correspond to conditions after the vibratory steady state is reached.

Substitution of Eq. (38) into (37) and subsequent solution for s yields

$$s = \frac{Cy_o^2 - (L\mu/EA)\operatorname{sgn}(\dot{s})}{1 + KL/EA} \tag{39}$$

from which one may readily calculate the maximum and minimum overlap displacements s_{max} and s_{min}.

The energy dissipated by one end of the beam in one cycle of overlap displacement s (or for one half-cycle of lateral beam displacement y) is represented by the area of the parallelogram. Thus, the energy U dissipated by the beam (both supports) per cycle of lateral beam displacement is given by

$$U = 4(s_{max} - s_{min})(2\mu) = \frac{8\mu}{1 + KL/EA}\left(Cy_{max}^2 - 2L\mu/EA\right) \tag{40}$$

where y_{max} denotes the (time-wise) maximum value of y_o.

Again, Eq. (40) is valid only for $Cy_{max}^2 > 2L\mu/EA$. One may readily verify that no slip at all occurs if $Cy_{max}^2 < L\mu/EA$, whereas if $2L\mu/EA > Cy_{max}^2 > L\mu/EA$ slip occurs only until steady-state conditions are established.

Equation (40) establishes the amplitude dependence of cyclic energy dissipation one would expect to observe if Coulomb friction associated with longitudinal slip is the dominant energy dissipation mechanism. Although Eq. (40) exhibits no explicit frequency dependence of U, one must recall that the coefficient C depends on the beam deflection shape, which does depend on frequency. (The frequency-dependence of the parameter C is discussed subsequently.) Of course, it is possible that the friction force μ may also be frequency-dependent in actuality.

B. Nonuniform Coulomb Friction; Elastic Overlap and Partial Slip

The previous analysis of energy dissipation due to Coulomb damping in the configuration of Fig. 42 neglects stretching of the overlapped portion of the beam and thus pertains only to the case where relative motion occurs at once over the entire interface. This sort of behavior is likely to be approximated at rather large (beam lateral motion) amplitudes, but probably not at relatively small amplitudes. The present section deals with an analysis that takes stretching of the overlap into account and also considers nonuniform friction force distributions.

1. General Analysis

For the present analysis the beam support is still considered rigid; i.e., much stiffer than the beam itself, and the beam overlap is assumed to act in extension like a one-dimensional elastic continuum. It is postulated that the friction force distribution may be expressed in terms of a function $\bar{\mu}(x)$ of axial position (Fig. 43b) which may, for example, account for the distribution of normal pressure, for the axial distribution of friction area (such as around a bolt), and/or for variations in the friction coefficient. (Note that $\bar{\mu}$ here has dimensions of force/length, whereas the previously used μ denotes a force.) If an axial force P is applied to the end of the overlapped beam portion then it will stretch, and slippage of a part of the overlap with respect to its support will occur. If the applied force is opposed only by the friction forces, i.e. if external elastic restoring forces and inertia effects may be neglected, then the distance d over which slip occurs for a given value P=F of the applied force may be calculated from the equilibrium requirement

$$F = I(d) \tag{41}$$

where

$$I(x) \equiv \int_0^x \bar{\mu}(x)\, dx \tag{42}$$

and the origin of the x coordinate is at the outermost edge of the friction (or interface contact) area as indicated in Fig. 43.

The axial force in the beam will then be zero where no slip has occurred ($x>d$) and will be equal to the applied force F outside of the friction region ($x<0$). Within the slipped region equilibrium requires that the axial force N(x) obey

$$N(x) = F - \int_0^x \bar{\mu}\, dx = F - I(x) \quad , \quad 0 \leq x \leq d \quad . \tag{43}$$

This axial force distribution permits one to calculate the strain distribution, and from this one may in turn readily determine the displacement u of the point on the beam at the edge of the friction area. One finds

$$uAE = \int_0^d N\, dx \quad , \tag{44}$$

where A denotes the area of the beam cross section and E the Young's modulus of the beam material, as before.

If after application of the force F the applied force is reduced to a new value G, the beam may be expected to contract. This contraction can occur only in conjunction with some interface slippage, this time in the direction opposite to that in which slippage occurred during the initial load application. This reversed slippage causes reversed friction forces to act on the bar, resulting in a friction force distribution like that represented by the solid curves of Fig. 43d.

The new axial force distribution N(x) and the extent of the reversed slip region $x=b$ may again be determined from equilibrium requirements. One finds

$$N(x) = \begin{cases} F-I(x) & b \leq x \leq d \\ F-2I(b) + I(x) & 0 \leq x \leq b \end{cases} \tag{45}$$

$$G = F-2I(b) \quad . \tag{46}$$

N=G for x<0, N=0 for x>d is again implied; the new corresponding displacement u may now be calculated by substituting Eq. (45) into (44).

If after reduction to G the load is increased to a new value ($H \leq F$), this load increase produces extension of the bar and slippage in the initial direction, so that the friction force distribution appears like that of Fig. 43e. One may find the corresponding new axial force distribution and the extent x=c of the newly "re-slipped" region from

$$N(x) = \begin{cases} F - I(x) & b \leq x \leq d \\ F - 2I(b) + I(x) & c \leq x \leq b \\ F - 2I(b) + 2I(c) - I(x) & 0 \leq x \leq c \end{cases} \qquad (47)$$

$$H = I(d) - 2I(b) + 2I(c) \quad . \qquad (48)$$

The displacements u_F, u_G, u_H, obtained at the force values F, G, H, respectively, may be found to be given by

$$\begin{aligned} AE\, u_F &= Fd - M(d) \\ AE(u_G - u_F) &= 2M(b) - 2bI(b) \\ AE(u_H - u_G) &= -2M(c) + 2cI(c) \end{aligned} \qquad (49)$$

where

$$M(x) \equiv \int_0^x I(x)\, dx \quad . \qquad (50)$$

For the case where H=F one may conclude from comparison of Eqs. (41) and (48) that I(b) = I(c), or that b=c. [If the original $\mu(x)$ is everywhere positive, then I(x) is monotonic, and I(b) = I(c) implies b=c uniquely.] But Eqs. (49) show that then $u_F = u_H$. One may easily convince oneself that further load cycles between F and G will result in repeated tracing of the same force-displacement curves; i.e. of the loop sketched in Fig. 43f.

The energy U_c dissipated per cycle* is proportional to the area of this loop and may be determined most readily from $U_c = -\oint u dP$. One finds, after some manipulation, that

$$\frac{AEU_c}{2} = (F-G)\,[(F-G)b - 3M(b)] - 2\int_0^b I^2(x)\,dx \qquad (51)$$

where b must be obtained from Eq. (46).

2. Special Cases

a) Uniformly distributed friction force

For $\bar{\mu}(x) = \mu_o$ = constant one obtains the particularly simple result

$$U = 4U_c = (F-G)^3/3AE\mu_o \quad , \qquad (52)$$

which agrees with a result readily deducible from the work of Goodman[6]. As also was noted by him, the cyclic energy dissipation in this case is dependent on the third power of the load range, but independent of the average load level.

b) Circular friction area

For a bolted joint one may assume the friction area to be circular. If this area has a radius a and if the interface pressure and friction coefficient are uniform, then one may set

$$\bar{\mu} = \mu_1 \sqrt{2ax-x^2} \qquad (53)$$

to account for the circular geometry. The appropriate integrations can be carried out in closed form, but the results are lengthy and so cumbersome that they cannot readily be interpreted without considerable numerical work. Hence they are omitted here. However, for $b \ll a$ [noting that all integrations implied in Eq. (51) extend no further than to x=b] one may take

---

*U_c denotes the energy dissipated at one support of the beam of Fig. 42 per cycle of the variable u (or s). The total energy dissipated per cycle of beam lateral motion is $U=4U_c$.

$$\bar{\mu} = \mu_1 \sqrt{2a}\ \sqrt{x} \tag{54}$$

and obtain the following from Eqs. (51) and (46):

$$AEU_c = (11/20)(9/32)^{1/3}\ (F-G)^{8/3}\ (\mu_1 \sqrt{a})^{-2/3}\ . \tag{55}$$

One notes that here U_c varies as the 8/3-power of load range, but is again independent of average load level.

c) Exponential friction distribution

If one postulates a more general exponential dependence of the friction distribution by setting

$$\bar{\mu}(x) = \mu_a (x/a)^n\ . \tag{56}$$

One then obtains

$$AEU_c = (F-G)^{\frac{2n+3}{n+1}} \left[\frac{(n+1)\ a^n}{2\mu_a}\right]^{\frac{1}{n+1}} \left[\frac{4n^2 + 7n + 1}{2n^2 + 7n + 6}\right]\ . \tag{57}$$

For n=0, corresponding to constant μ, this reduces to the previously found 3rd power dependence on load range; for n=1/2 this reduces to Eq. (55) if the coefficients are properly matched (i.e. if $\mu_a = \mu_1 a \sqrt{2}$). As n increases the exponent on (F-G) approaches 2. For an exponential friction distribution the cyclic energy dissipation therefore varies as some power between the second and third of the load range.

3. Expressions in Terms of Beam Lateral Deflection

In the beam set-up sketched in Fig. 42 one may measure the maximum lateral beam deflection y_{max} at the beam center more readily than the axial load range (F-G), hence it is of interest to re-cast the previously established relations in terms of y_{max}.

One notes that in the assumed absence of axial inertis and viscous phase lag effects the maximum axial deflection occurs when the axial force is maximum, and that this maximum force F occurs when the beam lateral deflection is greatest. Similarly, the minimum axial deflection occurs when the axial force is minimum (equal to G), which occurs when the beam lateral deflection is zero. Thus, from Eq. (37),

$$u_{max} = u_F = Cy_{max}^2 - FL/EA$$
$$u_{min} = u_G = - GL/EA \quad . \tag{58}$$

With these and Eqs. (49) and (46) one finds

$$\frac{AEC}{L} y_{max}^2 = (F-G) \left(1 + \frac{b}{L}\right) - \frac{2}{L} M(b) \quad . \tag{59}$$

By use of Eq. (46) one may also write

$$\frac{2M(b)}{L} = \frac{(F-G)}{LI(b)} \int_0^b I \, dx = (F-G) \frac{\langle I \rangle b}{I(b)L} \tag{60}$$

where $\langle I \rangle$ denotes the mean value of I between x=0 and x=b. Then one may rewrite Eq. (59) as

$$\frac{AECy_{max}^2}{L} = (F-G) \left[1 + \frac{b}{L} \left(1 - \frac{\langle I \rangle}{I(b)}\right)\right] \quad . \tag{61}$$

Since I(x) increases monotonically, $\langle I \rangle$ is always less than I(b) and the parentheses multiplying b/L in the above expression always have a value less than unity. In most practical configurations the slip length is much less than the beam length, b/L<<1, so that

$$y_{max}^2 \approx L(F-G)/AEC \quad . \tag{62}$$

Equation (51) may similarly be rewritten as

$$\frac{AEU_c}{2} = (F-G)^2 b \left[1 - \frac{3}{2} \frac{\langle I \rangle}{I(b)} - \frac{1}{2} \frac{\langle I^2 \rangle}{I^2(b)}\right] \quad . \tag{63}$$

The terms in the right hand bracket are generally not negligible relative to unity. They involve b, and b depends on (F-G). Hence, one cannot readily set down a simple general expression for U_c in terms of y_{max}^2 which involves no implicit dependence on (F-G).

However, one may treat various special cases. For $\bar{\mu}=\mu_o$ one finds from Eqs. (52) and (62) that*

$$U_c \approx \frac{(AE)^2}{12\,\mu_o}\left(\frac{y_{max}^2\,C}{L}\right)^3 \quad . \tag{64}$$

Similarly, from Eq. (55) one finds that for $\bar{\mu}=\mu_1\sqrt{2a}\sqrt{x}$,

$$U_c \approx \frac{11}{20}\left(\frac{9}{32}\right)^{1/3}(\mu_1\sqrt{a})^{-2/3}\left(\frac{y_{max}^2 AEC}{L}\right)^{8/3} \tag{65}$$

and, from Eq. (57), for $\bar{\mu}=\mu_a(x/a)^n$,

$$U_c \approx \left[\frac{(n+1)a^n}{2\mu_a}\right]^{\frac{1}{n+1}}\left[\frac{4n^2+7n+1}{2n^2+7n+8}\right]\left[\frac{AECy_{max}^2}{L}\right]^{\frac{2n+3}{n+1}} \quad . \tag{66}$$

---

*For $\bar{\mu}=\mu_o$ one may carry out an exact analysis, based directly on Eq. (59), and find

$$U_c = \frac{(2\mu_o L)^3}{12AE\mu_o}\left[\sqrt{1+\frac{AEC\,y_{max}^2}{\mu_o L^2}}-1\right]^3$$

which reduces to Eq. (64) for $AECy_{max}^2/\mu_o L^2 \ll 1$. However, for $AECy_{max}^2/\mu_o L^2 \gg 1$,

$$U_c \approx \frac{(2\mu_o L)^3}{12AE\,\mu_o}\left(\frac{AEC}{\mu_o}\right)^{3/2}\left(\frac{y_{max}}{L}\right)^3 \approx \frac{2}{3}(\mu_o AE)^{1/2}\,C^{3/2}\,y_{max}^3 \quad .$$

C. Purely Viscous Friction

If the damping at the interface is assumed to be of purely viscous character, then the axial force-displacement relation may be written

$$N = Ks + c_v\dot{s} \tag{67}$$

where c_v is a "viscous damping coefficient". Substitution of Eq.(67) into Eq. (37) leads to the differential equation

$$(1 + KL/AE)s + (Lc_v/AE)\dot{s} = Cy_o^2 \quad . \tag{68}$$

If y_o varies sinusoidally with frequency ω_o, then one may write

$$y_o^2 = y_{max}^2 \sin^2\omega_o t = \tfrac{1}{2}y^2(1-\cos\omega t) \quad , \quad \omega \equiv 2\omega_o \quad . \tag{69}$$

After substitution of Eq. (69) into (68) one may solve the resulting inhomogeneous differential equation to obtain

$$\frac{s(\omega^2+\nu^2)}{J\nu} = \left(\frac{\omega}{\nu}\right)^2(1-e^{-\nu t}) + 1-\cos\omega t - \left(\frac{\omega}{\nu}\right)\sin\omega t$$

$$J \equiv Cy_{max}^2\, AE/2Lc_v \tag{70}$$

$$c_v\nu \equiv K + AE/L$$

if one assumes also that the system is initially at rest at zero displacement.

The "steady state" is approached as νt becomes $\gg 1$. The motion described by Eq. (70) then approaches a pure sinusoid and the corresponding steady state cyclic energy dissipation may be calculated from

$$U_c = \tfrac{1}{4}U = \oint N\, ds = \oint N\,\dot{s}\, dt = \frac{1}{\omega}\int_o^{2\pi} N\,\dot{s}\, d(\omega t) \quad . \tag{71}$$

With $\dot{s}$ determined from Eq. (70) and N given by (67) one finds

$$U = \frac{4\pi J^2 c_v \omega}{\omega^2 + \nu^2} = \pi y_{max}^4 \left(\frac{CAE}{L}\right)^2 \frac{2c_v\omega_o}{(2c_v\omega_o)^2 + (K+AE/L)^2} \quad , \qquad (72)$$

where ω_o is the previously introduced frequency of the lateral motion of the beam.

D. Shear of Viscoelastic Layer

Consider a thin viscoelastic layer interposed between the rigid support and the beam. Let the thickness of this layer be denoted by h and its area (perpendicular to h) by A_σ. If the complex shear modulus of the viscoelastic material is $G=G_1+iG_2$ at frequency $\omega=2\omega_o$ then the axial force is given by

$$N = (G_1+iG_2)\, A_\sigma\, s/h \quad . \qquad (73)$$

This is analogous to Eq. (67), with

$$K = G_1 A_\sigma/h \quad , \qquad c_v = G_2 A_\sigma/h\omega \quad . \qquad (74)$$

Hence, one may simply substitute (74) into (68) to obtain

$$U = \pi y_{max}^4 \left(\frac{CAE}{L}\right)^2 \frac{G_2 A_\sigma/h}{(G_2 A_\sigma/h)^2 + (G_1 A_\sigma/h + AE/L)^2} \quad . \qquad (75)$$

E. Plastic Flow of Interface Asperities in Shear

One may visualize that energy at the joints of Fig. 42 may be dissipated due to yielding and subsequent plastic flow (in shear) of asperities bridging the two structures at the interface. If these asperities are considered rigid-plastic and non-work-hardening, then the axial force-displacement relation may be written as

$$N = Ks + F_y \operatorname{sgn} \dot{s} \qquad (76)$$

where F_y denotes the force required to produce yielding. Since Eq. (76) is identical to Eq. (38) except for the substitution of F_y for μ, the analysis for the present case is identical to that for Coulomb friction. Hence the result applicable here is described by Eq. (40) with μ replaced by F_y.

III. DAMPING MECHANISMS ASSOCIATED WITH ROTATION AT SUPPORTS

Since longitudinal motion of supported beam ends is a second order effect of the lateral motion of a beam, it is likely that equally significant damping contributions may be made by mechanisms that are associated with other types of relative motion, e.g., with rotation of the beam ends with respect to their supports. The next few paragraphs present a brief analysis of some such mechanisms and draw some conclusions concerning their energy dissipation properties.

A. Compression of Viscoelastic Asperities; Rigid Overlap

One may visualize that asperities of the support and beam overlap-surfaces become in effect welded together at their points of contact by the action of interface pressure, such as that generated by the action of a tight bolt. Thus, one might expect to find a thin layer of welded asperities in which even slight motion (perpendicular to the interface) can induce high stresses (in view of the thinness of the layer and the small welded areas) and thus produce damping.

As a first approximation one might consider the portion of the beam that overlaps the support to be rigid. If one neglects its inertia, as one may do in view of the extremely small expected amplitudes, then one finds that the motion of this overlapped portion is fully determined by the shear force Q and moment M_b acting at its edge (see Fig. 44b) and by p(z), the support load distribution (force/unit length) change measured from the condition where $Q=M_b=0$, i.e. from the condition where the beam is undeflected from its equilibrium position.

Equilibrium of the overlapped portion demands

$$M_b = \int_0^w p(z)\, z\, dz \quad , \qquad Q = \int_0^w p(z)\, dz \quad , \tag{77}$$

where the z-axis is that indicated in Fig. 44b and w denotes the total length of overlap. The edge force Q and moment M are applied to the overlap by the adjacent beam and may be approximated by the corresponding quantities acting at the support of

a clamped-clamped beam, since the deflections of the overlap are very small in general. Thus, if the beam deflections y(x) are given in terms of the x-y axis system shown in Fig. 44b, one may write

$$M_b = EI_b[\partial^2 y/\partial x^2]_{x=0} \equiv C_M y_o \quad , \quad Q = EI_b[\partial^3 y/\partial x^3]_{x=0} \equiv C_F y_o \qquad (78)$$

where y_o denotes the deflection of the beam center and C_M and C_Q are coefficients that depend only on the deflection shape of the beam and on its flexural rigidity EI_b. These coefficients are discussed further in Section IV of this appendix.

If it may be assumed that the asperities produce an elastic restoring force, then

$$p(z) = k(K_1 z + K_2) \quad , \qquad (79)$$

where k denotes the stiffness per unit length of the layer of asperities and K_1 and K_2 are constants. Then, from Eqs. (77)-(79) one finds

$$\begin{aligned} C_Q\, y_o &= wk\left(K_1 \frac{w}{2} + K_2\right) \\ C_M\, y_o &= w^2 k\left(K_1 \frac{w}{3} + \frac{K_2}{2}\right) \quad , \end{aligned} \qquad (80)$$

which one may readily solve to obtain

$$kK_1 = \frac{6y_o}{w^2}\left(\frac{2C_M}{w} - C_Q\right) \quad , \quad kK_2 = \frac{2y_o}{w}\left(2C_Q - \frac{3C_M}{w}\right) \quad . \qquad (81)$$

The total energy stored in the layer of asperities then is given by

$$\begin{aligned} W &= \tfrac{1}{2}k \int_o^w (K_1 z + K_2)^2\, dz = \frac{k}{2}\left[K_1^2 \frac{w^3}{3} + K_1 K_2 w^2 + k_2^2 w\right] \\ &= \frac{2y_o^2}{kw}\left[3\left(\frac{C_M}{w}\right)^2 - 3\left(\frac{C_M}{w}\right)C_Q + C_Q^2\right] \quad . \end{aligned} \qquad (82)$$

If this layer is considered as viscoelastic, with loss factor η, then the energy U_c dissipated (at one support) per cycle, in view of the definition of loss factor, is given by

$$U_c = 2\pi W\eta = 4\pi\eta \frac{y_o^2}{kw}\left[3\left(\frac{C_M}{w}\right)^2 - 3\left(\frac{C_M}{w}\right)C_Q + C_Q^2\right] \quad . \tag{83}$$

The total cyclic energy dissipation U for one support is twice this value, of course.

B. Compression of Viscoelastic Asperities; Flexible Overlap

Under some circumstances it may be more reasonable to assume (in view of the possibly great relative stiffness of the layer of asperities) that the behavior of the overlap may be comparable to that of a semi-infinite beam on an elastic foundation, as sketched in Fig. 44b.

The deflection y of the overlap then is given by[2/]

$$y = \frac{-e^{\alpha x}}{2\alpha^3 EI_b}\left[Q\cos\alpha x - \alpha M_b(\cos\alpha x + \sin\alpha x)\right] \quad ,$$
$$\alpha^4 \equiv k/4EI_b \quad , \tag{84}$$

in terms of the coordinate system of Fig. 44b. One may then calculate the energy storage in the layer of asperities analogous to Eq. (82), and from it determine the cyclic energy dissipation U_c (for one support) to be

$$U_c \approx \pi\eta k \int_{-\infty}^{o} y^2\,dx = \frac{\pi\eta\alpha}{2k} y_o^2\left[3C_Q^2 + 6\alpha^2 C_M^2 - 8\alpha C_M C_Q\right] \quad . \tag{85}$$

For the odd resonant modes of a clamped-clamped beam one finds (see next section) that

$$C_Q \approx -p_n C_M \quad , \qquad C_M \approx \pm\sqrt{2}\, EI_b p_n^2 \quad , \tag{86}$$

where p_n denotes the wave number pertinent to the n^{th} mode.

With the aid of this one may rewrite the result of Eq. (83) as

$$U_c = \frac{4\pi\eta\ y_o^2}{kw^3} C_M^2\left[3 + 3p_n w + (p_n w)^2\right] \approx \frac{24EI_b}{w^3}\left(\frac{\omega_n}{\omega_o}\right)^2 \quad , \qquad (87)$$

where ω_n denotes the n^{th} natural (radian) frequency. The latter approximate equality holds as long as the flexural wavelength on the beam is much greater than the overlap width w, which may be expected to apply at least for the lowest few modes of practical systems. Here

$$\omega_o \equiv \sqrt{k/m} \qquad (88)$$

represents the natural frequency of the overlap mass on a spring having the stiffness of the layer of asperities; m denotes the beam mass per unit length. One would expect $\omega_o >> \omega_n$ for the lowest few modes.

Similarly, one may rewrite Eq. (85) as

$$U_c \approx \frac{\pi\eta\ y_o^2}{2k} \alpha^3 C_M^2\left[3\left(\frac{p_n}{\alpha}\right)^2 + 8\left(\frac{p_n}{\alpha}\right) + 6\right] \approx \frac{3\pi\eta\ y_o^2\ \omega_n^2 m}{2\alpha} \qquad (89)$$

where the approximate equality applies for $p_n/\alpha = \sqrt{2\omega_n/\omega} << 1$.

IV. BEAM RESPONSE PARAMETERS

A. Beam Deflection Shape

It is well known[3,4] that the deflection shape of a uniform beam that is driven laterally at (circular) frequency ω_o may be expressed as

$$y = (B_1 \sin px + B_2 \cos px + B_3 \sinh px + B_4 \cosh px)e^{i\omega_o t} \qquad (90)$$

where t denotes time, the B's are constants that depend on boundary conditions; and p is the wave number and is given by

$$p^4 = \omega_o^2 m/EI_b \quad . \qquad (91)$$

Here m is the beam mass per unit length, I_b the moment of inertia of the beam cross section, and E the modulus of elasticity of the beam material.

In view of the symmetry of the beam under consideration one may confine his attention to only one half of it, say the left half of Fig. 42a. If the origin of the x-axis is taken at the left support and if this support is assumed "clamped", then appropriate boundary conditions are

$$y(0) = y'(0) = y'(L) = 0 \quad , \qquad y(L) = y_o \quad , \tag{92}$$

where the prime denotes differentiation with respect to x. Application of these conditions to Eq. (90) permits one to find

$$B_1 = -B_3 = y_o X_1/Y$$
$$B_2 = -B_4 = y_o X_2/Y \tag{93}$$

where $X_1 \equiv \sin\beta + \sinh\beta$

$X_2 \equiv \cos\beta - \cosh\beta$

$Y \equiv 2(1-\cos\beta\cosh\beta)$

$\beta \equiv pL$.

B. Parameter C of Eq. (35) for Non-resonant Conditions

By substituting Eqs. (93) into (90), introducing the result into Eq. (35) and carrying out the indicated integration, one finds that

$$4Y^2C/p = 2X_1(X_2^3 + \beta X_1) + (X_1^2 - X_2^2)(X_2 - \cosh\beta)\sin\beta$$
$$- (X_1^2 + X_2^2)(X_2 + \cos\beta)\sinh\beta \quad . \tag{94}$$

At resonances of the beam one finds that Y=0 and that C according to the previous equation then takes on an infinite value. This result is not surprizing, since the classical theory of undamped beam vibrations implies that at resonance infinite deformations occur at locations where no restraints are prescribed. In actuality, of course, the beam deformations at resonance are limited

by damping and generally also by nonlinearities (particularly if damping is small). The foregoing analysis of this section thus cannot be applied to the calculation of C or ΔL_1 for resonant conditions.

At frequencies not too near a resonance, Eq. (94) should, however, still provide a good estimate of C. For frequencies below the fundamental resonance one may obtain a useful approximation by substituting into Eq. (94) the various series expansions of the hyperbolic and circular functions. Then, for $\beta^4 \ll 1$ one may reduce the result to

$$C/p = 3/5\beta \qquad \text{or} \qquad C = 3/5L \quad . \tag{95}$$

The beam motion somewhat below the fundamental frequency takes place quasi-statically; i.e., inertia effects are negligible. Indeed, if one computes C from the static deflection[2] one obtains precisely the previous result.

Although Eq. (94) permits one in theory to evaluate C for any off-resonance frequency, such calculations for higher frequencies may be of little value, since there the assumed boundary conditions may be rather poor representations of reality, and other uncertainties (e.g. in material properties) may lead to considerable error.

C. Parameter C of Eq. (35) for Resonances

In order to evaluate C at resonances one may take an alternate approach and assume that the deflection shapes obtained are the resonant mode shapes of a clamped-clamped beam. Then the deflection shape associated with the n^{th} mode may be written (within an arbitrary multiplicative constant) as [5]

$$y_n = \cosh p_n x - \cos p_n x - \sigma_n(\sinh p_n x - \sin p_n x) \tag{96}$$

where

$$\sigma_n = \frac{\cosh(2\beta_n) - \cos(2\beta_n)}{\sinh(2\beta_n) - \sin(2\beta_n)} \quad , \qquad \beta_n \equiv p_n L \tag{97}$$

and the wave numbers p_n are solutions of the "frequency equation"

$$\cos(2\beta_n)\cosh(2\beta_n) = 1 \quad . \tag{98}$$

For the odd-numbered modes (which are the symmetric ones and hence the only ones of interest here) the maximum beam deflection y_n occurs at the beam center x=L and may be readily evaluated from Eq. (96). By substitution of Eq. (96) into (35) one finds that C_n, the value of C for the n^{th} mode, may be expressed as

$$C_n = \beta_n R_n / 4 y_{on}^2 L \quad , \tag{99}$$

where

$$\begin{aligned} R_n = {} & (1+\sigma_n^2)(\cosh \beta_n - 2\cos \beta_n) \sinh \beta_n \\ & + (1-\sigma_n^2)(2\cosh \beta_n - \cos \beta_n) \sin \beta_n \\ & - 2\sigma_n(\cosh \beta_n - \cos \beta_n)^2 + 2\sigma_n^2 \beta_n \quad , \end{aligned} \tag{100}$$

$$y_{on} = \cosh \beta_n - \cos \beta_n - \sigma_n(\sinh \beta_n - \sin \beta_n) \quad .$$

By substitution of Eq. (98) into (97) and using both of these to simplify Eqs. (100) one finds that

$$\begin{aligned} R_n &= \frac{2 \sinh(2\beta_n)}{\cosh(2\beta_n)[\cosh(2\beta_n) + 1]} [\beta_n \sinh(2\beta_n) - \cosh(2\beta_n)] \\ y_{on} &= \frac{1 + \sqrt{\cosh(2\beta_n)}}{\cosh \beta_n} \quad . \end{aligned} \tag{101}$$

For $\beta_n \gg 1$, therefore,

$$\begin{aligned} R_n &\approx 2(\beta_n - 1) \quad , \qquad y_{on} \approx \sqrt{2} \\ C_n L &\approx \frac{\beta_n}{4}(\beta_n - 1) \quad . \end{aligned} \tag{102}$$

Values of C_nL for the first few odd (symmetric) modes are tabulated below*

n	1	3	5	7	9
β_n	2.365	5.50	8.64	11.78	14.9
C_nL	0.61	6.25	16.6	31.6	51.8

D. Parameters C_M and C_Q of Eqs. (78), for Resonances

By direct substitution of Eq. (96) into Eqs. (78) one obtains

$$C_M = 2EI\, p_n^2/y_{on} \quad , \qquad C_Q = -\sigma_n p_n C_M \tag{103}$$

where σ_n is given by Eq. (97) and y_{on} by Eq. (100). Some values calculated for the odd-numbered modes of a clamped-clamped beam with the aid of the tables of Bishop and Johnson[2] are tabulated below. The approximations given in Eqs. (86) follow at once from these values.

n	1	3	5	n>5
y_{on}	1.588	-1.406	1.415	$(-1)^{\frac{n-1}{2}}\sqrt{2}$
$\sigma_n = -C_Q/p_nC_M$	.982	1.000	1.000	1.000
$C_M/\sqrt{2EI}\, p_n^2 = \sqrt{2}/y_{on}$	.892	-1.006	.999	$(-1)^{\frac{n-1}{2}}$

*For n>5, $\beta_n \approx (2n+1)\pi/4$. For n up to 5 one may calculate C_nL directly from Bishop and Johnson's Tables.[2] The values for n=1,3,5 shown here were obtained in this manner; use of Eq. (102) gives, respectively C_nL=0.81, 6.17, 16.5. The approximation of Eq. (102) improves with increasing n.

E. Relation Between Loss Factor and Power Dissipation

The loss factor η_s of a structure may be defined as

$$\eta_s = U/2\pi W \quad , \tag{104}$$

where U denotes the energy dissipated per cycle and W the "energy of vibration", which may be taken as the (time-wise) maximum kinetic energy of the structure as long as η_s is not too large[7].

If a beam vibrates sinusoidally in time, its deflection may be expressed in terms of $y\, e^{i\omega_o t}$, where y denotes the deflection shape. A general deflection shape may be expressed[4] in terms of the normal mode shapes $y_n(x)$ as

$$y = \Sigma\, Y_n y_n \quad , \tag{105}$$

where the Y_n are constants and the summation is taken over all integers. The velocity of the structure is given by $(d/dt)(ye^{i\omega_o t}) = i\omega_o y e^{i\omega_o t}$, to which corresponds an amplitude (time-wise maximum) given by $\omega_o y$. The maximum kinetic energy then may be expressed as

$$W = \frac{m}{2}\int_\ell \omega_o^2 y^2\, dx = \frac{m}{2}\,\omega_o^2 \sum_n Y_n^2 \int_\ell y_n^2\, dx \tag{106}$$

where m denotes the mass per unit length and ℓ the total length of the beam.* The last form of Eq. (106) follows from the orthogonality of normal modes.

At ω_r, the resonance frequency of the r^{th} mode, the r^{th} mode response predominates and

$$W_r = \frac{m}{2}\,\omega_r^2\, Y_r^2\, \Phi_{r\ell} \quad ; \qquad \Phi_{r\ell} \equiv \int_\ell y_n^2\, dx \quad . \tag{107}$$

---

*The discussion here applies also for two dimensional structures, e.g. plates, if the mode shapes are taken as two-dimensional and the beam length ℓ is replaced by plate area.

Φ_r is a dimensionless constant that depends on the shape of the r^{th} mode and on the normalization one imposes on the normal mode functions. If one follows Bishop and Johnson[5], and chooses the y_n so that $\int_\ell y_n^2\, dx = \ell$, then $\Phi_n=1$ and one may simplify Eq. (107) accordingly.

The average rate of energy dissipation, i.e. the power dissipation P_d, is given by

$$P_d = Uf = U\omega_o/2\pi \quad , \tag{108}$$

where f denotes the (cyclic) frequency. From Eq. (104) one then obtains that the power dissipated at resonances of the r^{th} mode is related to the loss factor η_s as

$$P_d = \eta_s W_r \omega_r = \frac{m_T}{2}\eta_s \omega_r^3 Y_r^2 \quad , \tag{109}$$

where $m_T=m\ell$ denotes the total mass of the beam.

The deflection amplitude at the beam center is given by $y(L)=Y_r y_r(L)$, so that Eq. (109) may be rewritten as

$$\frac{4P_d}{m_T\eta_s} = \frac{2}{\pi}\frac{U\omega_r}{m_T\eta_s} = \gamma_r\omega_r^3 X_o^2 = \gamma_r\omega_r V_o^2 = \gamma_r \frac{A_o^2}{\omega_r} \quad , \tag{110}$$

where $X_o=y(L)$ has been introduced for the deflection amplitude at the beam center, and where $V_o=\omega_r X_o$ and $A_o=\omega_r V_o$ denote the corresponding velocity and acceleration amplitudes. The parameter γ_r, which was introduced in Eq. (110) for the sake of simplicity, is given by

$$\gamma_r \equiv 2/y_r^2(L) \tag{111}$$

if the aforementioned normalization is used. γ_r is found to have a value which is very nearly unity in all cases of interest. In fact, for all odd modes of simply supported beams $\gamma=1$ exactly. For built-in beams one may determine that $\gamma_r=1.000$ for $r\geq 5$ ($\gamma_1\approx 0.795$ for the first mode, $\gamma_3\approx 1.014$ for the third mode).

F. Comparison of Energy Dissipation in Supports of Cantilever and Clamped-Clamped Beams

Before one can deduce the energy dissipated in support joints from loss-factor measurements carried out on beams, one must know the energy of vibration W, as apparent from Eq. (104). If the loss factor measurements are carried out at the r^{th} beam resonance, then the appropriate energy W_r is given by Eq. (107). With the previously indicated normalization of the mode shapes

$$\int_0^{\ell} y_n^2 \, dx = \ell \quad , \tag{112}$$

one finds from Eqs. (104) and (107) that the total energy dissipated per cycle is given by

$$U = \pi \eta_s m_T \omega_r^2 Y_r^2 \quad . \tag{113}$$

The energy dissipated per cycle per support may then be calculated simply by dividing Eq. (113) by the number of supports. Some attention must be paid to the selection of properly corresponding modal amplitudes Y_r if one wishes to use Eq. (112) to compare the energies dissipated in supports of beams with different end conditions (or mode shapes). By substitution of the deflection shape $y=Y_r y_r(x)$ into the expressions of Eqs. (78) for the bending moment M_b and shear force Q acting at a clamped support one may obtain

$$\begin{aligned} M_b &= EI_b \, Y_r \, p_r^2 \, \phi_o'' \\ Q &= EI_b \, Y_r \, p_r^3 \, \phi_o''' \end{aligned} \tag{114}$$

where

$$\phi_o'' \equiv [\partial^2 y_r / \partial (p_r x)^2]_{x=0} \quad , \quad \phi''' \equiv [\partial^3 y_r / \partial (p_r x)^3]_{x=0} \tag{115}$$

p_r is the wave number corresponding to the r^{th} resonance and is related to the frequency ω_r as given in Eq. (91).

For cantilevers and clamped-clamped beams one finds that $\phi_o''=2$ (exactly) for all modes[5] if the normalization (111) is used.

Similarly, $\phi'''_o \approx 2$ within 2% for all but the first modes. ($\phi'''_o = 1.468°$ for the first mode of a cantilever; $\phi'''_o = 1.965$ for that of a clamped-clamped beam.) By combining Eqs. (91), (114), (103) one may establish that

$$U = \frac{\pi}{(\phi''_o)^2} \frac{\ell \eta_s}{EI_b} M_b^2 = \frac{\pi}{(\phi'''_o)^2} \frac{\ell \eta_s}{\sqrt{mEI_b}\ \omega_r} Q^2 \quad . \tag{116}$$

As has been pointed out previously, ϕ''_o and ϕ'''_o are insensitive to mode number and to whether one or two beam ends are clamped. Thus, the same value of cyclic energy dissipation U applies for a given measured loss factor η_s at a given frequency and for given moment and shear force amplitudes, for all modes (except one*) of a beam with either clamped-clamped or clamped-free ends. In other words, no mode shape correction need be introduced in comparisons of clamped-clamped and cantilever beam damping data, with one exception.*

---

*The exception is the first cantilever mode. For this mode

$$\frac{U_{1\ \text{cant}}/Q^2}{U_{\text{others}}/Q^2} \approx \frac{1.8(\eta_s/\omega_r)_{1\ \text{cant}}}{(\eta_s/\omega_r)_{\text{others}}} \quad .$$

REFERENCE LIST FOR APPENDIX IV

1. T. J. Mentel, "Vibrational Energy Dissipation at Structural Support Junctions," Sec. 4 of Structural Damping, J. Ruzicka, Ed.; ASME, New York, 1959.

2. R. J. Roark, Formulas for Stress and Strain, McGraw-Hill Book Company, Inc., New York, 3rd Ed.; 1954.

3. P. M. Morse, Vibration and Sound, McGraw-Hill Book Company, Inc.; 1948.

4. K. N. Tong, Theory of Mechanical Vibration, John Wiley and Sons, Inc.; New York, 1960.

5. R. E. D. Bishop and D. C. Johnson, Vibration Analysis Tables, Cambridge University Press; Cambridge, 1956.

6. L. E. Goodman, "A Review of Progress in Analysis of Interfacial Slip Damping," Sec. 2 of Structural Damping, J. Ruzicka, Ed.; ASME, New York, 1959.

7. E. E. Ungar and E. M. Kerwin, Jr., "Loss Factors of Viscoelastic Systems in Terms of Energy Concepts," J. Acoust. Soc. Am. 34 (July 1962) pp 954-957.

LIST OF SYMBOLS FOR APPENDIX IV

A	cross-sectional area of beam
A_o	acceleration amplitude at beam center
A_σ	area of layer between support and beam
B_1, B_2, B_3, B_4	constants
C	coefficient defined in Eq. (35)
C_M, C_Q	coefficients defined in Eq. (78)
C_n	value of C for n^{th} mode
E	Young's modulus
F, G, H	specific values of P
F_y	yield force
G^*	complex shear modulus
G_1	real part of G^*
G_2	imaginary part of G^*
I	integral defined in Eq. (42)
I_b	beam cross-sectional moment of inertia
J	parameter defined in Eq. (70)
K	stiffness
K_1, K_2	constants
L	half-length of beam
M	integral defined in Eq. (50)
M_b	bending moment
N	axial force
P	axial force, variable
P_d	power dissipation
R_n, y_{on}	parameters defined in Eq. (100)
U	energy dissipated by total beam per cycle of lateral deflection
U_c	energy dissipated at one beam support per cycle of axial motion
V_o	velocity amplitude at beam center
W	total stored (strain) energy or energy of vibration

X_o	deflection amplitude at beam center
X_1, X_2	parameters defined in Eq. (93)
Y	parameter defined in Eq. (93)
Y_n	coefficients in modal expansion, Eq. (105)
a	radius of circular friction area
b	extent of reversed slip region (see Fig. 43)
c	extent of re-slipped region (see Fig. 43)
c_v	viscous damping coefficient
d	distance over which slip occurs initially (see Fig. 43)
f	frequency
h	thickness of layer between support and beam
k	compressional stiffness per unit length of asperities layer
ℓ	total beam length, 2L
m	beam mass per unit length
m_T	total beam mass
n	exponent, defined in Eq. (56)
p	wave number, see Eq. (91)
p_n	wave number corresponding to n^{th} beam mode
p(z)	distribution of supporting force per unit length
s	axial displacement of beam ends
t	time
u	relative displacement at edge of overlap
u_F, u_G, u_H	values of u obtained with forces F,G,H
w	total length of overlap
w_r	w at response of r^{th} mode
x	coordinate measured along (undeflected) beam length
y	lateral deflection of beam
y_{max}	time-wise maximum value of y_o
y_o	value of y at beam center
$y_n(x)$	mode shapes
z	axial coordinate

α	parameter defined in Eq. (84)
β	parameter defined in Eq. (93)
γ	parameter defined by Eq. (101)
$\Delta(2L)$	change in total beam projected length
η	loss factor of layer of asperities
η_s	loss factor of structure
μ	Coulomb friction force
μ_a	constant coefficient, used in Eq. (56) to describe exponential friction force distribution
μ_o	constant value of $\bar{\mu}(x)$, for uniformly distributed friction force
$\bar{\mu}(x)$	Coulomb friction force per unit length
μ_1	constant coefficient, used in Eq. (53) to describe friction force distributed over circle
σ_n, β_n	parameters defined in Eq. (97)
ν	parameter defined in Eq. (36); has dimensions of frequency
Φ_r	mode parameter defined in Eq. (107)
ω	$2\omega_o$
ω_n	n^{th} natural frequency of beam, radians/unit time
ω_o	radian frequency of lateral motion

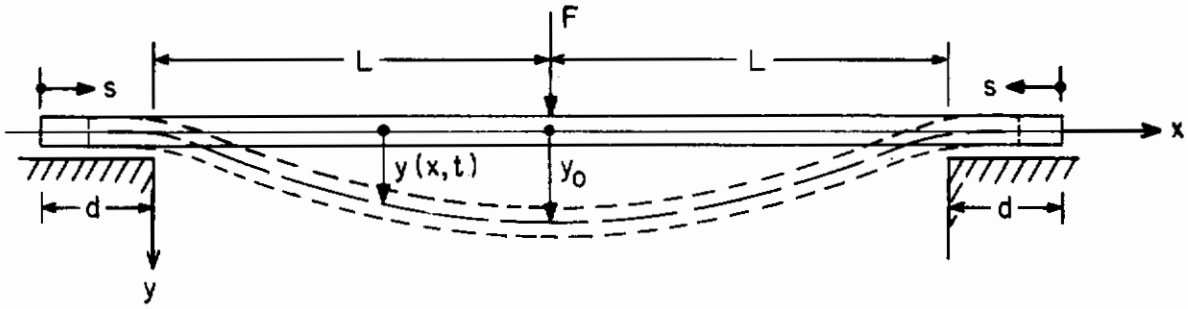

a. GENERAL ARRANGEMENT

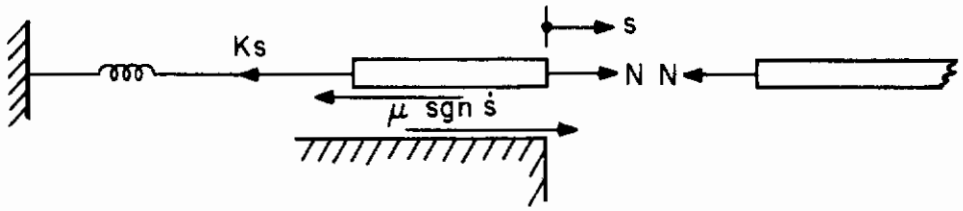

b. FORCES ON OVERLAPPING PART (COULOMB FRICTION)

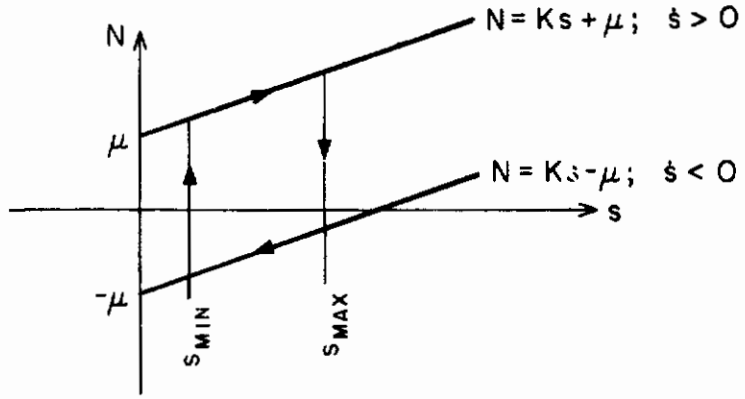

c. FORCE DISPLACEMENT RELATION FOR RIGID OVERLAP (COULOMB FRICTION)

FIG. 42 BEAM ON RIGID END-SUPPORTS

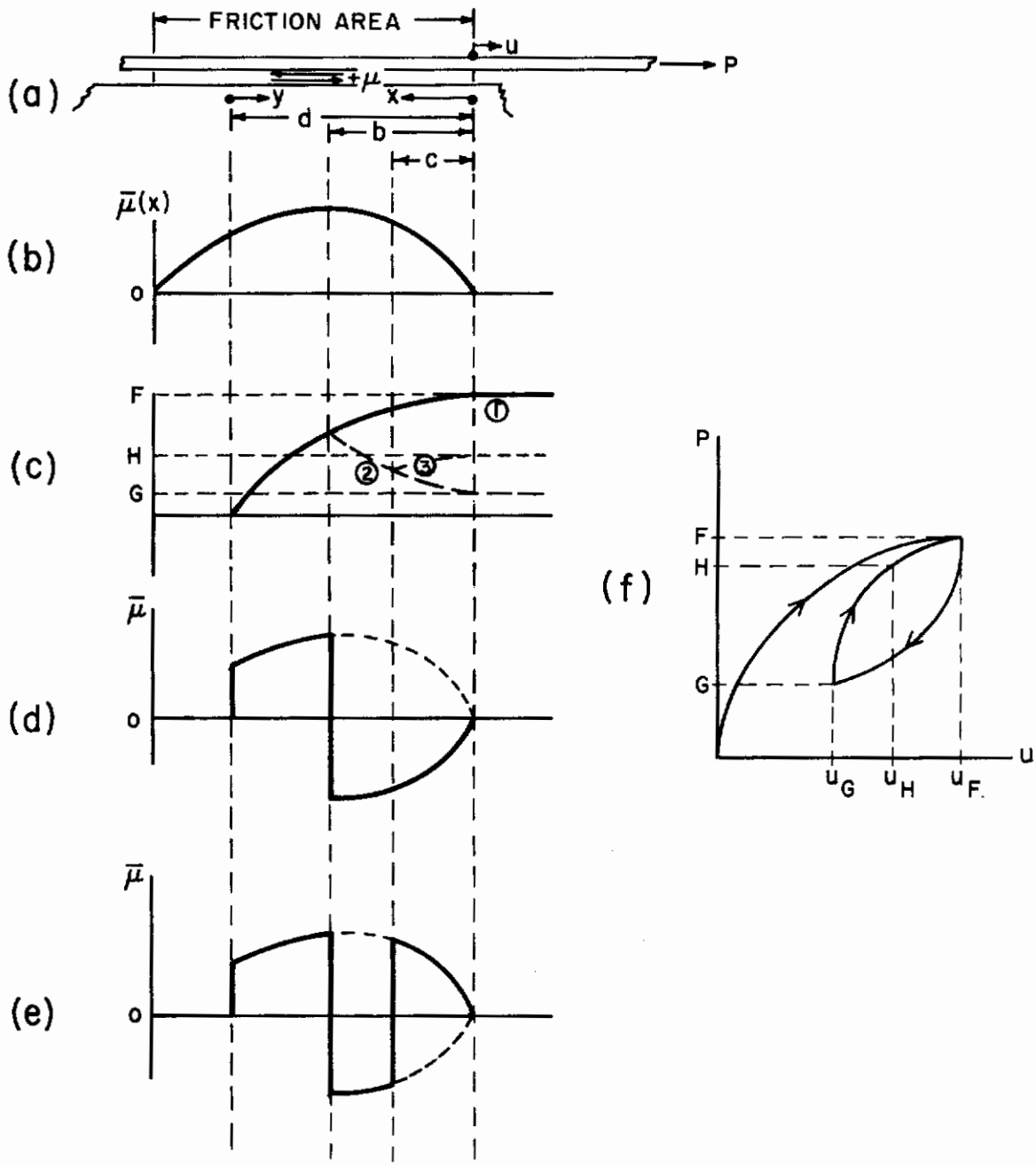

FIG. 43 SLIP WITH GENERAL FRICTION DISTRIBUTION

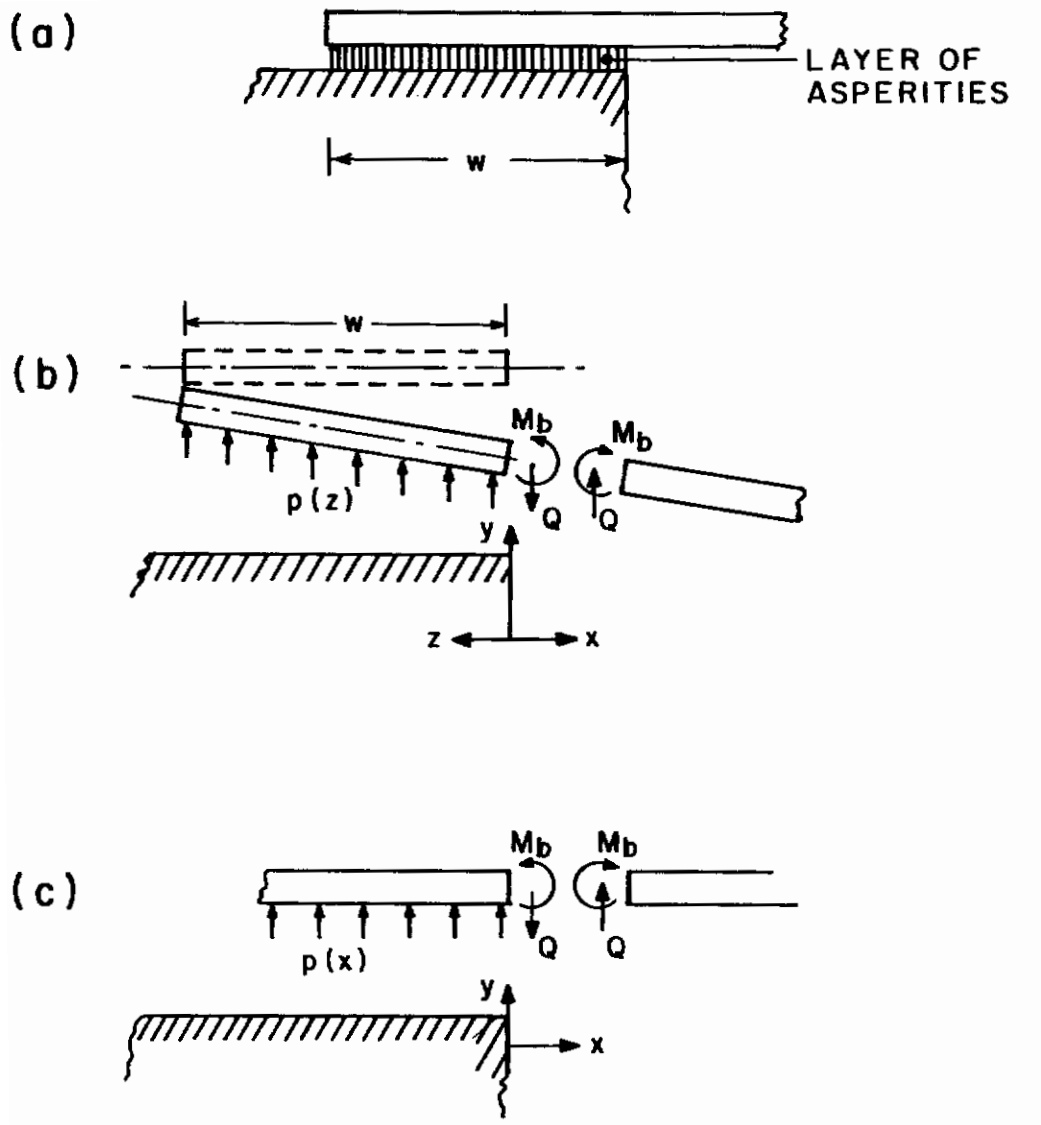

FIG. 44 COMPRESSION OF LAYER OF ASPERITIES AT BEAM SUPPORTS